Tectonic-climatic Interactions and Glacial History within the Chugach and Kenai Mountains, Alaska

Joshua David Valentino

Dissertation submitted to the faculty of the Virginia Polytechnic Institute and State University in partial fulfillment of the requirements for the degree of

Doctor of Philosophy

In

Geosciences

James A. Spotila, Chair

Lewis A. Owen

Ken A. Eriksson

Brian W. Romans

Rick D. Law

February, 9th 2017

Blacksburg, Virginia

Keywords: Glaciers, Alaska, Thermochronology, Exhumation, Topography

Tectonic-climatic Interactions and Glacial History within the Chugach and Kenai Mountains, Alaska

Joshua David Valentino

ABSTRACT

The architecture and morphology of a mountain range is fundamentally controlled by the combination of rock uplift and distribution of precipitation. This relationship attributes fluctuations in climate to the erosion of orogens, sedimentation rates, and geodynamics of the crust. Glaciers are the most effective climate driven erosive processes, where the frequency of glacial periods has a direct impact on the structure of mountain ranges through time. The late Cenozoic global cooling period was the beginning of a series of many glaciations which increased erosion in orogens experiencing fast rock uplift. We characterize the threshold for the onset of effective glacial erosion and record the increase in erosion rate during the late Cenozoic in the Chugach and Kenai Mountains of Alaska. We utilized low temperature thermochronometry and cosmogenic dating to constrain the spatial and temporal distribution of exhumation and glacial history in order to characterize the net effect of glaciers on an orogen that experiences slow rock uplift. We constrain the spatial distribution of exhumation and characterize the landscape along the Kenai Peninsula, underlain by the transition from flat slab to normal subduction. The region is characterized by old AHe ages which mimic the subduction angle of the down going plate and decrease away from an exhumational hotspot at a syntax in the Chugach Mountains. We attribute the long term exhumational characteristic of the Kenai Peninsula to subduction and underplating of sediment shed from the accreting Yakutat microplate to the east. A delineation of the glacial history using ^{10}Be cosmogenic dating depict a series of glacial advances which date to the early and late Wisconsin. We find that the asynchronuity of glaciation across maritime and continental Alaska is controlled by steep

orographic precipitation gradients which result from upper plate deformation. Finally, we observe an increase in erosion since the late Cenozoic using both AHe and cosmogenic dating and conclude that it is possible for the onset of effective glacial erosion in regions that experience slow to moderate rock uplift and that climate drives erosion rates in these regions.

Tectonic-climatic Interactions and Glacial History within the Chugach and Kenai Mountains, Alaska

Joshua David Valentino

GENERAL AUDIENCE ABSTRACT

The formation of mountain ranges is controlled by how fast they grow and the precipitation they receive. Fluctuations in climate change influence the architecture and erosion of the crust, especially in regions where there are glaciers. The beginning of global glacial activity approximately five million years ago, increased erosion in mountain ranges that experience fast growing rates. We characterize the effect of glaciers on mountain growth and record the related erosion in the Chugach and Kenai Mountains of Alaska. We used dating techniques to measure the spatial and temporal distribution of erosion in mountain ranges that grow slowly. We measured erosion rate variations in the Kenai Mountains, and discovered that erosion rate mimics the change in tectonic morphology along the subduction zone. The glacial history of the Chugach Mountains was delineated and shows a series of glacial advances from 50-14 thousand years ago. We found that the characteristics of the glacial advances were dependent upon the distribution of precipitation along the mountain ranges, and that the latest glacial ice age was dryer than older events. Finally, we observed an increase in erosion in the mountain ranges and concluded that it is possible for glaciers to effectively erode slowly growing mountains.

ACKNOWLEDGMENTS

The completion of this degree would not be possible without the encouragement and love of my friends and family. First and foremost, I want to thank my fiancé and soon to be wife Lindsay Bartz for everything that she has done for me during this chapter in my life. She is a fantastic woman and I consider myself incredibly lucky to have her in my life. I am thankful for her encouraging words and hardball common sense during the long and hard times of the degree. I appreciate her patience as we lived four hours apart for almost five years as I finished. I consider it a bonus that we are both geologist and could discuss my studies, ideas, and conclusions throughout the years.

I am very grateful for my family full of geologist who had inspired me from a young age to appreciate rocks. Thank you to my mother (Karen Valentino) for teaching me the fundamentals and math and more math, for twelve years around our dining room table. Thank you to my Dad (David Valentino) for inspiring work ethic and teaching me almost everything I know about geology. I was also inspired by my Uncle Rick who taught geology at Temple University. He was a badass and I miss him every single day since his passing. My brother is also a geologist and the classes that we took together and field trips that we went on were some of the best times of my life. My sister went against the grain and did not become a geologist but is instead pursuing a PhD across the drill field in biochemistry at Virginia Tech!

Jim Spotila was my advisor and mentor during this endeavor, and I want to thank him for providing guidance, insight, and expertise during my work with him. He helped me mature into the scientist that I am today through patient teaching and plenty of rewriting my work. I am thankful that I had the chance to work on such exciting projects with him. I also want to thank Lewis Owen who was my advisor at University of Cincinnati who educated me on the

cosmogenic work, provided a tour of the scotches of the United Kingdom, and raced me up every mountain that we hiked together in Alaska. I also want to thank my other committee members Brian Romans, Ken Eriksson, and Rick Law for providing helpful insight and commentary during our annual meetings and when I had questions.

Finally, I want to thank my office mates and colleagues Michelle Fame, Phillip Prince, and Joe Cochran for engaging in helpful and entertaining discussion of geology and our projects. Michelle and I had many adventures together either in the lab at Virginia Tech and University of Cincinnati or in the field. One of the best moments out of many was in the Presidential Range in New Hampshire where a racoon began to accidentally brush against and play my guitar at 2 AM in the tent adjacent to where we were sleeping. After much crashing and yelling the racoon made it out of the tent and nothing was miraculously damaged (aside from our nerves), and we continue to talk about the story to this day.

ATTRIBUTIONS

Chapter 2 was submitted to the journal of *Tectonophysics* as "Valentino, J. D., Spotila, J. A., Owen, L. A., and Buscher, J. T., Rock Uplift at the Transition from Flat-slab to Normal Subduction: The Kenai Mountains, Southeast Alaska." Valentino collected and prepared the samples which were dated using (U-Th)/He thermochronometry, and wrote the rough draft for the manuscript. James Spotila aided by processing the samples for ^{4}He in his lab at Virginia Tech and aided in the multiple revisions of the manuscript. Lewis Owen and Jamie Buscher provided helpful insight and corrections for the manuscript.

Valentino, J. D., Spotila, J. A., Owen, L. A., & Buscher, J. T. (2016). Rock uplift at the transition from flat-slab to normal subduction: The Kenai Mountains, Southeast Alaska. *Tectonophysics*, *671*, 63-75.

TABLE OF CONTENTS

LIST OF FIGURES

Chapter 1

Chapter 2

Chapter 3

Chapter 4

LIST OF TABLES

Chapter 2

Chapter 3

Chapter 4

GRANTS AND FUNDING

Funding for this research was provided by the National Science Foundation grant numbers EAR-1123688 and 1123643 and SEED funding through PRIME Laboratories at Purdue (for ^{10}Be and ^{36}Cl AMS analysis). Additional funding was provided by the department of Geosciences at Virginia Tech through teaching and research assistantships.

CHAPTER 1

INTRODUCTION

Joshua D. Valentino

Department of Geosciences, Virginia Tech, Blacksburg, Virginia 24061, USA

The development of mountain range morphology and geodynamics is fundamentally driven by a combination of tectonic activity and the distribution of climate driven erosion (Montgomery et al., 2001). Climatic patterns are most commonly heterogeneous across mountain ranges, resulting in focused regions of erosion, which influence the geodynamics, distribution of deformation, and fault geometry through the life of an orogen. This relationship has been observed in mountain ranges throughout the world (Montgomery et al., 2001; Berger et al., 2008) and successfully portrayed via modeling (West et al., 2005; Roe et al., 2006; Whipple, 2009), yet empirical details of the process through time are still limited. The impact of long term climate fluctuations and transitions can have dramatic influences on the architecture and deformation of tectonic plate boundaries. The Late Cenozoic climate transition from warm to cold increased the magnitude and frequency of glaciations, which impacted orogens globally through focused erosion via glaciers (Raymo and Ruddiman, 1991; Herman and Champagnac, 2016). Glaciers are both sensitive to climate fluctuations and are highly effective erosion agents which under the right conditions, can match the rock uplift rate with erosion rate, limiting topography (e.g. glacial buzz-saw hypothesis) (Brozovic et al., 1997; Egholm et al., 2009). Although observed throughout the world, the set of conditions and thresholds necessary for the onset of effective glacial erosion is not quantitatively well constrained. The spatial and temporal variation of rock uplift rate, exhumation rate, and glacial presence in an orogen are measurable responses to the interaction of tectonic activity and climate. The Chugach and Kenai Mountains of southern Alaska are prime locations to empirically measure the response of exhumation, topography, and precipitation to rock uplift and glacial erosion.

The Chugach and Kenai Mountains constitute a glaciated forearc, which transitions across the Yakutat microplate and the Aleutian subduction zone (Fig. 1.1). The mountain ranges are a product of accretion in the Late Cretaceous and oblique collision and flat slab subduction of the Yakutat microplate from the Oligocene to present (Plafker, 1987; Fuis et al., 2008; Haeussler et al., 2008). The Chugach and Kenai Mountains have been periodically glaciated through the Quaternary, and fluctuated from complete coverage to valley glaciers emanating from ice fields throughout the center region of the ranges. Today, the region is dominated by alpine glaciers, ice fields, and extensive valley glaciers that are actively eroding the topography through headwall erosion and valley glacier down cutting. The diverse distribution of complex tectonic systems and glacial history in the Chugach and Kenai Mountains provide an excellent location to constrain the thresholds that control the onset of effective glacial erosion through time. Low temperature thermochronology (U-Th)/He (AHe) and terrestrial cosmogenic nuclide (TCN) dating were used to constrain lateral variations of exhumation, establish a new glacial history chronology, and measure exhumation on multiple timescales. These empirical measurements resulted in a regional characterization of the impact of both tectonic activity and climate fluctuations on the development of the landscape of the southern margin of Alaska through the Late Cenozoic.

Our first project addressed the characteristics of upper plate deformation through analysis of exhumation across the transition from flat slab to normal subduction. In southern Alaska, the Kenai Peninsula is an extension of the forearc along the Aleutian megathrust which spans the transition of the flat slab Yakutat microplate and the normally subducting Pacific plate. Prior work has shown that there are zones of very high exhumation rates (2-4 mm/yr) associated with upper plate deformation above the subducted Yakutat, but no previous work has characterized

how exhumation changes on the edges and away from the flat slab. We utilized AHe dating to constrain the lateral variations of exhumation across this unique transition. Our 17 new ages show some of the oldest results (40-50 Ma) along the forearc and depict a sharp transition from high exhumation along the edge of the Yakutat plate which quickly decreases with distance from the boundary. These findings show that exhumation has been limited on the Kenai Peninsula, while in contrast the topography depicts deeply incised valleys and an uplifted dome like structure. The conflict with topography and AHe ages implies that the uplift of the Kenai Peninsula is significantly younger than the surrounding ranges because aerial exposure of the landscape for an extended period of time would have removed the older material. Our results support the current model that underplating of the submarine fan deposits related to the uplift and erosion of the Chugach and Saint Elias Mountains directly above the Yakutat plate is driving continued growth of the Kenai Peninsula.

We characterized and developed a new chronology of Holocene, late Wisconsin, and early Wisconsin glacial events in the Chugach Mountains of Alaska. Alaska hosts one of the best documented glacial history records in the world, preserving glacial evidence from the late Cenozoic and parts of the Pleistocene through the Holocene, yet absolute dating is sparse in regions such as the Chugach Mountains. We utilized ^{10}Be and ^{36}Cl TCN dating to constrain the ages of glacial moraines and polished surfaces throughout the Chugach Mountains. We completed 40 cosmogenic ages which characterize one early Wisconsin event, and five late Wisconsin moraines. The results of the cosmogenic ages roughly correlate with the old chronology of Karlstrom (1964) and improve the timing of deglaciation in the region. The architecture of each moraine was mapped and used to reconstruct the glacial equilibrium line (ELA) altitude of each event. The distribution of ELAs through the Quaternary revealed that

erosion had been focused at an elevation of ~ 1000 meters throughout the late Wisconsin and support the model of a precipitation deficit during that time period.

The characterization of rock uplift, precipitation, and exhumation through time can shed light on whether erosion rates increase with the presence of glaciers in orogens with slow to moderate rock uplift as compared to orogens that have accelerated rock uplift. We measured exhumation rates over multiple timescales throughout the Chugach Mountains utilizing AHe (10^6-10^7 yr) and catchment-wide TCN (10^3-10^4 yr) dating. The AHe dating provides and average exhumation rate which includes the transition from hotter to colder climate during the late Cenozoic. The basinwide TCN dating produces much shorter exhumation rates on a catchment scale, spanning the Pleistocene to present. Comparing the exhumation rates with these two techniques allow for a characterization of the change in exhumation with the dramatic increase in glacial presence during the late Cenozoic. If the short-term erosion rates are faster than the long-term erosion rates, then it is implied that where tectonic uplift is minimal, the presence of glaciers increase erosion rates. In contrast, if the short-term erosion rate is similar in age or varied across the Chugach Mountains from basin to basin, then we can constrain the degree to which precipitation and rock uplift serve as thresholds for the onset of accelerated glacial erosion. Our exhumation rates show that both high and low rates in individual catchments, implying that a specific distribution of precipitation and rock uplift in the Chugach Mountains may control the effectiveness of glacial erosion.

The completion of the research in this dissertation has answered some of our original questions and has opened up several possible avenues of future study. The most pertinent continuation would be to collect and process more AHe ages along the southern section of the Kenai Peninsula. The single young age of 9.5 Ma contrast with the much older ages in the

region implying that there may be complex tectonic activity driving higher exhumation. Complete sample coverage of the area focusing on the fault bound sections of the mountain range could result in an interesting story of the young growth and development of the southern Kenai Peninsula. Another interesting area are the Amatuli and Ushagat islands which are situated roughly halfway between the Kenain Peninsula and Kodiak Island. Formation of these islands may be driven by underplating or faulting and constraining the exhumation history using AHe could result in an interesting story and shed light on whether there is continued southern growth of the Kenai Peninsula into the region.

REFERENCES

Arkle, J., Armstrong, P., Haeussler, P., Prior, M., Hartman, S., Sendziak, K., Brush, J., 2013. Focused exhumation in the syntaxis of the western Chugach Mountains and Prince William Sound, Alaska. Geol. Soc. Am. Bull. 125 (5–6), 776–793. http://dx.doi.org/10.1130/b30738.1.

Berger, A. L., Gulick, S. P., Spotila, J. A., Upton, P., Jaeger, J. M., Chapman, J. B., ... & McAleer, R. J. (2008). Quaternary tectonic response to intensified glacial erosion in an orogenic wedge. *Nature Geoscience*, *1*(11), 793-799.

Brozović, N., Burbank, D. W., & Meigs, A. J. (1997). Climatic limits on landscape development in the northwestern Himalaya. *Science*, *276*(5312), 571-574.

Buscher, J.T., Berger, A.L., Spotila, J.A., 2008. Exhumation in the Chugach–Kenai Mountain Belt above the Aleutian Subduction Zone, Southern Alaska. Active Tectonics and Seismic Potential of Alaska vol. 179. American Geophysical Union Monograph Series, pp. 151–166.

Egholm, D. L., Nielsen, S. B., Pedersen, V. K., & Lesemann, J. E. (2009). Glacial effects limiting mountain height. *Nature*, *460*(7257), 884-887.

Fuis, G., Moore, T., Plafker, G., Brocher, T., Fisher, M., Mooney, W., Nokleberg, W., Page, R., Beaudoin, B., Christensen, N., Levander, A., Lutter, W., Saltus, R., Ruppert, N., 2008. Trans-Alaska Crustal Transect and continental evolution involving subduction underplating and synchronous foreland thrusting. Geology 36 (3), 267–270. http://dx.doi.org/10.1130/g24257a.1.

Haeussler, P.J., 2008. An overview of the Neotectonics of interior Alaska: far-field deformation from the Yakutat microplate collision. Active Tectonics and Seismic

Potential of Alaska. American Geophysical Union Geophysics Monograph Series 179, pp. 83–108.

Herman, F., & Champagnac, J. D. (2016). Plio-Pleistocene increase of erosion rates in mountain belts in response to climate change. *Terra Nova*, *28*(1), 2-10.

Plafker, G., 1987. Regional geology and petroleum potential of the northern Gulf of Alaska continental margin. In: Scholl, D.W., Grantz, A., Vedder, J.G. (Eds.), Geology and Resource Potential of the Continental Margin of Western North America and Adjacent Ocean Basins—Beaufort Sea to Baja California: Circum-Pacific Council for Energy and Mineral Resources. Earth Sciences Series, 6, 299–268.

Roe, G.H., Stolar, D.B., Willett, S.D., 2006, Response of a steady-state critical wedge orogen to changes in climate and tectonic forcing: Geological Society of America Special Paper 398, p. 227-239.

West, A. J., Galy, A., & Bickle, M. (2005). Tectonic and climatic controls on silicate weathering. *Earth and Planetary Science Letters*, *235*(1), 211-228.

Whipple, K. X. (2009). The influence of climate on the tectonic evolution of mountain belts. *Nature Geoscience*, *2*(2), 97-104.

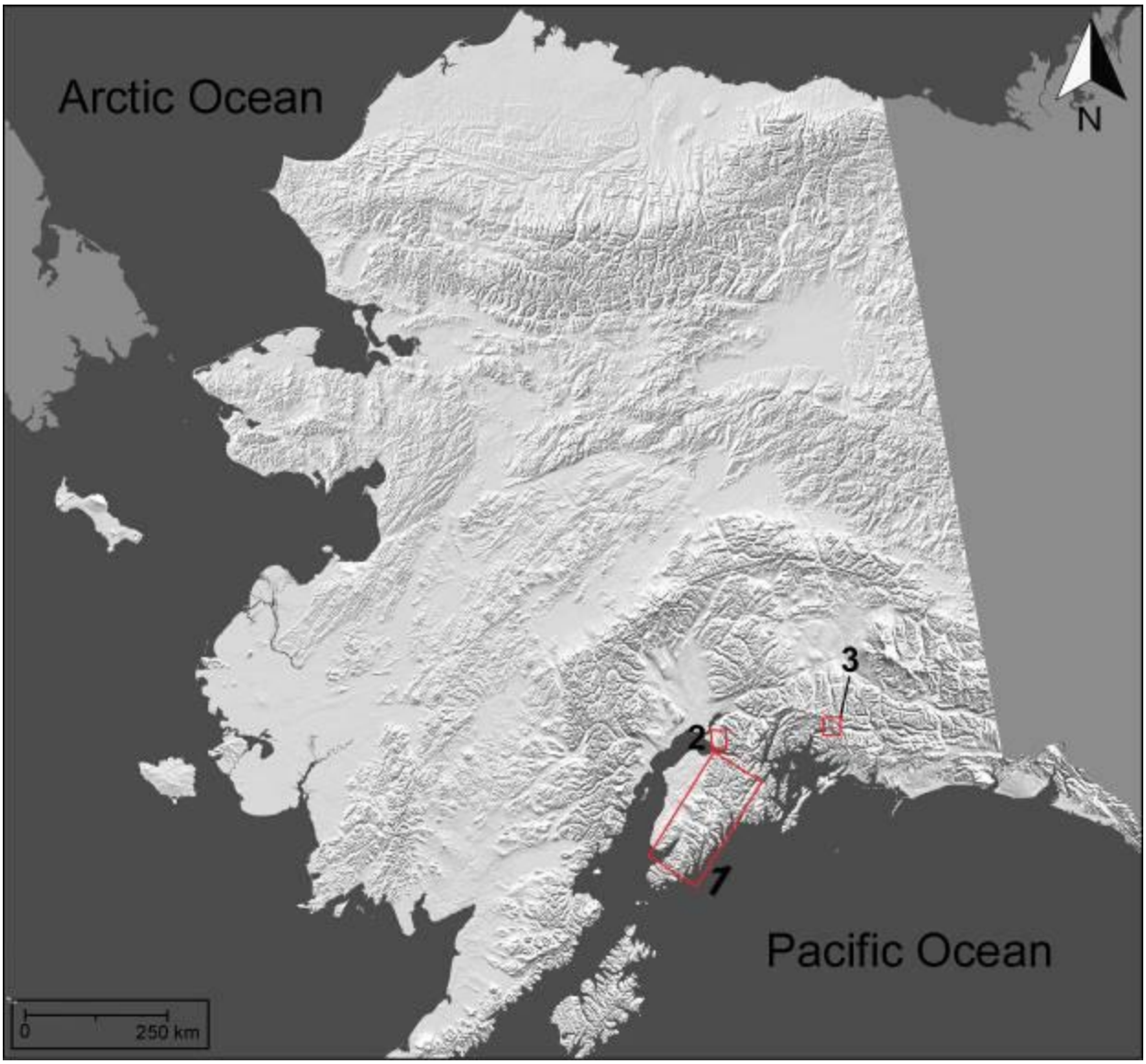

Figure 1.1: A shaded relief map of Alaska (Riehle et al., 1997) showing the field area locations for this study. Area 1 corresponds with the Kenai Mountains which are the focus of the 2nd chapter. The 3rd and 4th chapters include area 2 which is the westernmost extent of the Chugach Mountains adjacent to Anchorage and area 3 which is Thompson Pass east of Valdez.

CHAPTER 2

Rock Uplift at the Transition from Flat-slab to Normal Subduction: The Kenai Mountains, Southeast Alaska

Joshua D. Valentino, James Spotila, Lewis Owen, Jamie Buscher

Department of Geosciences, Virginia Tech, Blacksburg, Virginia 24061, USA

Department of Geology, University of Cincinnati, Cincinnati, OH 45221, USA

Andean Geothermal Center of Excellence (CEGA), Universidad de Chile, Plaza Ercilla 803, Santiago, Chile

Department of Geology, Facultad de Ciencias Fisicas y Matematicas, Universidad de Chile, Plaza Ercilla 803, Santiago, Chile

ABSTRACT

The process of flat-slab subduction results in complex deformation of overlying forearcs, yet how this deformation decays with distance away from the zone of underthrusting is not well understood. In south central Alaska, flat-slab subduction of the Yakutat microplate drives shortening and rock uplift in a broad coastal orogenic belt. Defined limits of the zone of underthrusting allow testing how orogenesis responds to the transition from flat-slab to normal subduction. To better understand forearc deformation across this transition, apatite (U–Th)/He low temperature thermochronometry is used to quantify the exhumation history of the Kenai Mountains that are within this transition zone. Measured ages in the northern Kenai Mountains vary from 10–20 Ma and merge with the exhumation pattern in the Chugach Mountains to the northeast, where high exhumation occurs due to flat-slab-related deformation. In the southern Kenai Mountains, however, ages increase to 30–50 Ma across a transition near Seward, Alaska, above the zone from flat-slab to normal subduction. These ages are relatively old in comparison to ages determined in other studies in southern Alaska and suggest minimal exhumation. Furthermore, transitions in topographic expression of the coastal orogen also occur at the margin of Yakutat underthrusting. These observations suggest that either deformation associated with flat-slab subduction requires tens of kilometers to decay with distance away from the zone of underthrusting, or that orogenesis in the Kenai Mountains is driven by a distinct tectonic cause. A potential driver of deformation is underplating of thick sediments, specifically the Surveyor Submarine Fan, along the Aleutian Megathrust, analogous to the tectonic mechanism responsible for the emergence of the Kodiak Island forearc. If correct, this may represent a recent tectonic transition in the region, given the minimal exhumation of the rugged Kenai Mountains despite the presence of an erosion-conducive glacial climate.

INTRODUCTION

Deformation in the upper plate of subduction zones relates to the orientation and morphology of the down-going plate (Fisher et al., 1998, Brandon et al., 1998 and Dominguez et al., 2000). Lateral transitions in slab dip and morphology along a trench can lead to complex patterns of forearc development and uplift. For example, a change in subduction angle from steep to flat-slab may cause a gradual increase in upper plate shortening and rock uplift (Gutscher et al., 2000). Instances of flat-slab subduction in Central America and the Andes show that widespread deformation and uplift above the flat section decreases in intensity with gradual increase in subduction angle (Gutscher et al., 2000 and Ramos et al., 2002). How upper plates respond along sharp transitions in slab subduction and geometry is less well known.

The Kenai Peninsula is part of a ~ 2000 km long exhumed accretionary prism and forearc along the southern margin of Alaska (Fig. 2.1) (Plafker et al., 1989). The region undergoes active rock uplift related to flat slab subduction, oblique collision, and accretion of the Yakutat microplate (Plafker and Berg, 1994 and Haeussler et al., 2000). Intense deformation and exhumation occurs in the Wrangellia–St. Elias and Chugach Mountains, which are undergoing accretion directly related to Yakutat collision (Spotila and Berger, 2010, Arkle et al., 2013 and Enkelmann et al., 2015). The mountainous forearc continues beyond the Yakutat microplate to where normal subduction of the Pacific plate occurs along the Aleutian Megathrust. The coastal mountains are rugged, have high topography (mean elevation 1000 m above sea level [asl]), and are deeply incised by glaciers (Buscher et al., 2008). The Kenai Mountains span both the western limit of the Yakutat plate and normal Pacific plate subduction, providing a unique opportunity to study deformation across a sharp transition in down going slab geometry and morphology.

The approach of this study is to provide a first order constraint on the timing and magnitude of exhumation across the Kenai Mountains from which no previous thermochronometry has been documented. We measured apatite (U–Th)/He ages (AHe) across the Kenai Peninsula to test the effect of the slab transition on deformation of the forearc. Specifically, we sought to test whether a localized zone of rapid rock uplift occurred outside of the lateral transition zone away from the Yakutat plate, as suggested by the distribution of rugged topography. Our results using difficult lithologies provide the first quantitative values for exhumation associated with the unique tectonic transition.

BACKGROUND

Flat slab subduction drives upper plate deformation and orogenesis that can penetrate hundreds of kilometers into overriding continental lithosphere (English et al., 2003, Li and Li, 2007 and Ramos et al., 2002). The common view is that flat slab subduction is linked to buoyant oceanic crust associated with thickened oceanic plateaus, hot-spot trails, or rapidly subducting, young slabs. After onset of flat slab subduction, upper plate shortening propagates landward and drives exhumation and broad surface uplift of the forearc, magmatic arc, and back arc basin, development of fold-thrust belts with widespread fault reactivation, and migration of arc volcanism (Little and Naeser, 1989, Berger et al., 2008, Gutscher et al., 2000, Ramos et al., 2002, Finzel et al., 2011 and Gardner et al., 2013). Tectonic underplating of the slab and overlying off-scraped sediments may also contribute to uplift and exhumation (Fuis et al., 2008 and Ducea et al., 2009).

Flat slab subduction is hypothesized to be the primary cause of modern orogenesis in southern Alaska (Plafker, 1987, Bruhn et al., 2004, Abers, 2008, Haeussler, 2008 and Riccio et al., 2014). The driver for flat slab subduction is considered to be the Yakutat microplate, an exotic terrain consisting of an over-thickened (11–22 km) oceanic plateau that collides at 50 mm/yr into and subducts at a low angle beneath the North American plate (Figs. 2.1, 2.3; Plafker and Berg, 1994, Fletcher and Freymueller, 1999, Haeussler et al., 2003, Freymueller et al., 2008, Christeson et al., 2010, Elliott et al., 2010 and Worthington et al., 2012). Flat slab subduction and associated collision in the St. Elias orogen initiated in the Middle Miocene (Plafker and Berg, 1994, Perry et al., 2009 and Enkelmann et al., 2010). The leading edge of the Yakutat plate is now located ~ 250 km northwest of the subduction zone at ~ 150 km depth under central Alaska (Ferris et al., 2003). The western trailing edge of the Yakutat plate is situated underneath northern Kenai Peninsula today and bends alongside the down going Pacific plate (Figs. 2.1, 2.3; Eberhart-Phillips et al., 2006 and Fuis et al., 2008). Flat subduction of the Yakutat plate drives convergent deformation and orogenesis for hundreds of kilometers throughout the overriding plate (Mazzotti and Hyndman, 2002 and Bruhn et al., 2004). The effect of this deformation includes widespread acceleration of exhumation (Enkelmann et al., 2010 and Spotila and Berger, 2010), basin inversion (Finzel et al., 2011 and Ridgway et al., 2011), and cessation of subduction related volcanism since the Eocene (Pavlis and Roeske, 2007).

Although the effects of Yakutat subduction are clearly expressed in the central and southern Alaska mountain ranges that lie directly above it, including the St. Elias, Chugach, Tordrillo, Talkeetna, and Alaska Ranges (Spotila and Berger, 2010, Arkle et al., 2013 and Haeussler, 2008), the spatial and temporal characteristics of the transition to areas

beyond the leading edge of the subducting microplate are not clear. Deformation related to the Yakutat plate has been suggested to penetrate 600–800 km northeast and 150–200 km northwest of the collision zone (Fig. 2.1; Mazzotti and Hyndman, 2002 and Finzel et al., 2011). Evidence for this deformation is seen in basin inversion and faulting away from the immediate zone of Yakutat subduction (Pavlis and Roeske, 2007, Ridgway et al., 2007, Finzel et al., 2011 and Haeussler and Saltus, 2011), but it is not fully understood how upper plate deformation decreases with distance from the subducting slab or what transitions occur at the margin of the slab. The Kenai Peninsula is an example of such a location that lies at the transitional zone just outside of Yakutat flat slab subduction.

The Kenai Peninsula is a northeast trending forearc high situated along the transition from flat slab subduction of the Yakutat plate to normal subduction of the Pacific plate beneath southern Alaska (Fig. 2.1). The peninsula forms the westernmost component of a continuous arc of mountainous topography that extends as far east as the Fairweather Range (Buscher et al., 2008). The rugged Kenai Mountains are located along the peninsula south of the Turnagain Arm, and is the southwestern continuation of the Chugach Mountains to the northeast. Although the Kenai Mountains are situated to record the changes in deformation and rock uplift that occur at the edge of flat subduction, little is known about its recent deformational and denudational history.

The Kenai Peninsula is composed of the Cretaceous and early Tertiary Chugach and Prince William terranes and associated Tertiary–Neogene cover over the Jurassic terrane underlying the Kenai lowlands (Fig. 2.2). These terranes were accreted to the forearc in the Late Cretaceous to early Tertiary via motion on the Border Ranges and Contact faults (Freeland and Dietz, 1973, Plafker et al., 1989, Plafker and Berg, 1994, Haeussler et al., 2003 and Fuis et al.,

2008). The terranes were metamorphosed and intruded due to subduction of the Kula-Resurrection ridge from 57–52 Ma (Haeussler et al., 2003 and Bradley et al., 2000). The Yakutat plate began subducting beneath the southern margin of Alaska by 32–23 Ma, and reached the forearc by Late Oligocene and Early Miocene (Plafker and Berg, 1994, Haeussler et al., 2003 and Finzel et al., 2011). The uplift of the Kenai Peninsula may have been related to passage of the Yakutat plate beneath it. Sedimentary and stratigraphic relationships in Cook Inlet suggest that emergence and erosion of the Kenai Mountains began during the Miocene and became the predominant source of sediment by the Late Miocene (Kirschner and Lyon, 1973). The Beluga formation records the onset of widespread deposition from the Kenai Mountains and is characterized by conglomeratic sandstones and the presence of epidote which is uniquely characteristic of the Chugach terrane (Kirschner and Lyon, 1973). This timing roughly matches when the Yakutat microplate passed underneath the peninsula. The EDGE seismic transect between the Kenai Peninsula and Kodiak Island revealed an erosional backstop, where the accretionary prism is absent and older Eocene strata occur (Ye et al., 1997, Von Huene et al., 1998 and von Huene and Klaeschen, 1999). This unconformity is interpreted to be related to the passage of the trailing edge or southwest margin of the Yakutat plate beneath the region, and stratigraphic relationships place the timing of this event at 3.5 Ma (Von Huene et al., 1998). The orientations and movements of the Yakutat and Pacific plates since 3.5 Ma have caused the trailing edge to migrate to the northeast underneath the Kenai Peninsula until it reached the present position under northernmost Kenai Peninsula and Sargent Ice field (Von Huene et al., 1998, Pavlis et al., 2004 and Eberhart-Phillips et al., 2006).

Modern deformation of the Kenai Peninsula is associated with the Yakutat collision and Pacific Plate subduction (Haeussler et al., 2003). The axis of the peninsula lies ~ 250 km from

the modern trench (Fig. 2.1). Farther north in the Chugach Mountains, which lie directly above the subducting Yakutat microplate, convergence is thought to have been primarily accommodated via thrusting and rock uplift on the Contact fault since the Mid-Miocene (Arkle et al., 2013). The role of the Contact fault in deformation along the Kenai Peninsula has not yet been defined. The Border Ranges fault is the other major fault in the region and is thought to act as the modern backstop to forearc deformation in the Chugach and Kenai Mountains (Plafker et al., 1989, Plafker and Berg, 1994 and Arkle et al., 2013). The Border Ranges fault experienced dextral and contractional reactivation in the Neogene, but is buried by undeformed late Tertiary glacial deposits along the Kenai Mountains (Pavlis and Bruhn, 1983, Little and Naeser, 1989, Plafker et al., 1989 and Plafker and Berg, 1994). Contractional deformation also occurs west of the Kenai Peninsula in the Cook Inlet. This forearc basin consists of a succession of Mesozoic and Cenozoic sediment, sourced from the surrounding mountains, that are 12 km- and 7 km-thick, respectively (Fisher and Magoon, 1978 and Bruhn and Haeussler, 2006). Active shortening in the basin due to coupling along the megathrust ranges from 0.3 to 2.7 mm/yr and is manifest as a series of Pliocene to Quaternary anticlines and several mm/yr dextral and reverse slip along the Castle Mountain and Bruin Bay faults (Hartman et al., 1974, Cohen and Freymueller, 1997, Haeussler et al., 2000, Parry et al., 2001, Bruhn and Haeussler, 2006 and Willis et al., 2007) (Fig. 2.3). This recent deformation has been attributed to a combination of the Yakutat collision to the east and subduction of the Pacific plate below the region (Haeussler et al., 2000).

Although sedimentary records in Cook Inlet suggest that the Kenai Mountains began eroding during the Late Miocene, the spatial pattern, magnitude, and rate of uplift and erosion are not constrained. The Kenai Mountains consists of a 150-km-long elliptical mountainous

region that is the southern continuation of the coastal orogen (Fig. 2.3). The Kenai Mountains have an average height of ~ 2000 m asl and tapers gradually to the west, where it is juxtaposed by the Border Ranges fault, causing an abrupt linear trend against the Cenozoic fill of Cook Inlet. On the east the range is dissected by glacial fjords, where cirques are submerged below sea level. The apparent subsidence on the east flank of the mountains is estimated to be ~ 100–300 m (Plafker, 1969) which may have been caused by a combination of rising sea level, climate changes during the LGM, and dynamic subsidence. The summits of the Kenai Mountains are heavily glaciated, capped by the Sargent and Harding icefields. These icefields give the range a welt-like appearance, as an elliptical concentration of high elevation that tapers off radially before merging with the Chugach Mountains (Fig. 2.4). Because of the presence of glaciers, mean slopes for Alaska mountain ranges are lower than expected based on the steepness of bare bedrock surfaces (Buscher et al., 2008). In the Kenai Mountains, for example, unglaciated surfaces above modern glacial trimline tend to be at or beyond the angle of repose. Nonetheless, the average slope in the Kenai Mountains (17°) is comparable to that observed in both the Chugach (19°) and St. Elias (16°) ranges, both of which lie directly over the Yakutat slab (Buscher et al., 2008 and Arkle et al., 2013). The welt-like nature of the Kenai Mountains is also apparent in the geometry of drainage basins (Fig. 2.5). North of the Kenai Mountains, the main divide occurs near the eastern edge of the peninsula, whereas in the Kenai Mountains the divide steps west to the central axis of the peninsula and separates much smaller basins. The concentration of high elevation, relief, and glacial coverage into a welt in the Kenai Mountains suggests it may be a locus of rock uplift, similar to the bull's eye of rock uplift in the comparably rugged western syntaxis of the Chugach Mountains at the north end of Prince William Sound (Arkle et al., 2013).

Glacial climate and associated glacial and periglacial processes are probably a contributing factor to the ruggedness of the Kenai Mountains. The eastern side of the Kenai Peninsula experiences a wet maritime climate with ~ 180 cm/yr precipitation, whereas the western side experiences a colder continental interior climate with only ~ 50 cm/yr precipitation (National Climate Data Center, 2005 and National Climate Data Center, 2007). A result of this orographic gradient is heavier glaciation of the eastern flank, where glacial equilibrium line altitude (ELA) drops to ~ 800 m asl, whereas on the western flank ELA is above 1200 m asl (Péwé, 1975, Mann and Peteet, 1994 and Wiles et al., 1995). During the local last glacial maximum, estimated to have been ~ 23 ka for this region (Karlstrom, 1961), the ELA was 300–500 m lower and glaciers covered the majority of the peninsula (Wiles et al., 1995). Based on the warm maritime setting, glaciers throughout the Quaternary on the Kenai Peninsula are likely to have been wet-based and therefore highly erosive (Péwé, 1975).

The exhumation history of the Kenai Mountains has not yet been documented because of a lack of previous low temperature thermochronometry in the coastal orogen (Fig. 2.1). However, previous work has defined the exhumation pattern of neighboring ranges. Apatite fission-track and (U–Th)/He ages from the Chugach and St. Elias ranges reveal rapid exhumation of > 1 mm/yr and up to 5 mm/yr in the core of the Yakutat collision zone, tapering away to < 0.1 mm/yr to the north and west (Spotila et al., 2004, Enkelmann et al., 2010 and Spotila and Berger, 2010). Local concentrations of late Cenozoic exhumation of 0.4–0.5 mm/yr occur in a bull's eye of the western Chugach syntaxis at Mount Marcus Baker and along splay faults in Prince William Sound, including on the Patton Bay fault on Montague Island (Arkle et al., 2013, Ferguson et al., 2015 and Haeussler et al., 2015). These exhumation hotspots decay to average rates of < 0.05 mm/yr in the Chugach Mountains and northern portion of the Kenai

Peninsula (Buscher et al., 2008). Testing whether a hotspot of exhumation occurs in the Kenai Mountains and relating this exhumation to regional tectonics are the main goals of this study.

METHODS

Low temperature thermochronometry was used to constrain the exhumation history of the Kenai Mountains. We obtained seventeen new apatite AHe ages across the region, where no previous low temperature thermochronometry had been completed. Sample locations were broadly distributed to provide regional spatial coverage, although locally samples were clustered to provide a range of elevation. However, rugged terrain prevented the collection of good vertical sample profiles. Samples were collected via helicopter and where trail access was possible. AHe ages are based on the radiogenic production and thermal diffusion of ^{4}He and record cooling from closure temperatures of ~ 50–70 °C, or exhumation from ~ 2–3 km depth for typical geothermal gradient (i.e. 25 °C) (Farley, 2000 and Ehlers and Farley, 2003). Closure temperatures for AHe are dependent on multiple factors, however, including cooling history, crystal grain size, and radiation damage (Farley, 2000, Ehlers and Farley, 2003, Flowers et al., 2009 and Brown et al., 2013).

AHe ages were measured at Virginia Tech on both single and multigrain aliquots. Dated apatite grains were generally > 70 μm in diameter and were selected under 100 × magnification based on distinct crystal habit, birefringence, relief, and lack of obvious microinclusions or fractures. Aliquots were outgassed in Pt tubes in a resistance furnace at 950 °C for 20 min and analyzed for ^{4}He by ^{3}He spike and quadrupole mass spectrometry. Radiogenic parent isotopes were measured at the University of Arizona using isotope dilution and ICP mass spectrometry. Predicted age uncertainty is ~ 5% (1σ), based on instrument precision and *FT* calculations

(Farley, 2000). However, average observed standard deviation of measured ages was 19.5% (1σ) (Table 2.1). In addition, 19 outlier age determinations (17% of total) were culled from the data set prior to the calculation of mean ages, on the basis that they were more than double the mean age and thus likely anomalous (Table 2.1). Comparably large uncertainties have been observed in other nearby studies (11–17%, 1σ) (Buscher et al., 2008, Arkle et al., 2013 and Ferguson et al., 2015), suggesting that local lithologies (graywacke, metaflysch) are problematic for AHe dating. For this reason, we took the approach of Berger et al. (2008) and measured a high number of replicate analyses per sample (~ 6, but as high as n = 13) to improve reproducibility.

Several samples (12Kn7, 12Kn8, 12Kn12) had particularly poor reproducibility that seems to relate to poor apatite quality, crystal grain size, and abundance. Fig. 2.6 shows example apatite grains and lithologies that are representative of these samples. Reasonable quality apatite occurred in some samples that are typical of other studies (A and B in Fig. 2.6). In contrast, many of the apatites were opaque, broken along their basal cleavage, i.e., parallel to 001 plane, or fractured (C–G in Fig. 2.6). The surfaces of many grains were also frosted, etched, or rounded, possibly associated with sedimentary transport and post-burial alteration. Anomalously old ages may result from the presence of radiogenic microinclusions that went undetected in these visually imperfect grains. Observed age dispersion may also result from the occurrence of fractures or other crystal imperfections, which introduce the possibility for loss of ^{4}He, loss of parent radiogenic material, and complications in correctly measuring *FT* values (Brown et al., 2013). Differences in chemistry, parent atom zonation, and radiation damage are other potential causes of age dispersion (Flowers et al., 2009), particularly given that our samples are sedimentary or metasedimentary in origin and thus consist of multi-sourced detrital apatite. Rough positive correlations between eU and AHe age for several samples suggest that radiation

damage could be a contributing factor to the observed age dispersion. However, a surprising result of this study is that measured ages on large, fractured, opaque single grain with microinclusions, which traditionally would have been avoided, reproduced reasonably well (H and I in Fig. 2.6).

RESULTS

The range of measured AHe ages in the Kenai Mountains is ~ 10–58 Ma (Fig. 2.2). These ages are relatively old in comparison to other studies in southern Alaska (e.g. Spotila and Berger, 2010, Arkle et al., 2013 and Ferguson et al., 2015) and are not indicative of recent, rapid exhumation. The “bull's eye” of young (< 5 Ma) AHe ages identified north of Prince William Sound (Arkle et al., 2013), for example, does not extend southwards into the Kenai Mountains, despite the rugged topography of the range that would suggest recent uplift and erosion.
Ages in the north, closest to the Chugach Mountains, are the youngest measured (10–20 Ma). These ages overlap with those determined by Buscher et al. (2008); Arkle et al. (2013) and are relatively consistent across the entire Chugach Mountains from the Cook Inlet to Prince William Sound. Ages increase to 30–50 Ma in the central and southern Kenai Mountains. The ages are generally 40–50 Ma on the west and ~ 25 Ma on the Pacific coast (Fig. 2.7A). This trend is consistent with observations by Buscher et al. (2008) farther north in the Chugach Mountains, which are interpreted to represent an AHe partial retention zone that was tilted up on the east via greater exhumation along the Pacific coast. However, existing sample coverage does not permit a unique characterization of AHe isochron geometry. Likewise, sample coverage does not permit determination of age-elevation relationships. The few samples that do span a range of relief in close proximity to each other do not indicate an obvious age-elevation trend.

Although measured ages become younger to the southeast towards the Contact fault, they do not bear any other obvious relationship to mapped faults. However, one measured age may require a local tectonic explanation. Sample 12Kn13 from the southern part of the peninsula produced a younger age (9.5 Ma) that does not fit with the regional pattern (Fig. 2.2). Given that only one sample in the region shows this young age, however, we consider it to be an unexplained local phenomenon and additional data would be required to understand its significance.

The old AHe ages measured in this study are older than any ages previously measured in southern Alaska. The older ages measured in this study roughly correlate with the early Cenozoic ages measured previously in the Tordrillo Mountains (Haeussler, 2008). The three oldest ages in the Tordrillo Mountains (39, 48, and 74 Ma) were shown to be affected by apatite zonation, but these ages may also represent a slow background exhumation rate, similar to the older ages in the Kenai Mountains. The older AHe ages from the Kenai Mountains overlap with higher temperature cooling ages that suggest widespread rapid cooling post ~ 52 Ma (Helwig and Emmet, 1981 and Bradley et al., 2000). This cooling event corresponds to a subduction of a slab window around ~ 55 Ma (Bradley et al., 2000). Our ages suggest that cooling to apatite closure temperatures must have been very rapid following this event. Since this cooling event, the upper crust must have been relatively stable and only slowly exhumed, allowing formation of a partial retention zone (PRZ).

DISCUSSION

Despite its rugged topography, the Kenai Mountains do not appear to contain a locus of recent, rapid exhumation. Measured AHe cooling ages of 40–55 Ma are the oldest that have been measured along the coastal orogen of south-central Alaska. These ages imply that rocks of the Kenai Peninsula must have cooled quickly after passage of a slab window in early Cenozoic (Bradley et al., 2000), but subsequently experienced minimal exhumation and prolonged crustal stasis. Based on the oldest cooling age, a calculated closure temperature of ~ 58 °C, and an assumed geothermal gradient of ~ 22 °C/km calculated from the temperature logs of COST No. 1 well in Cook Inlet (Magoon, 1986), the average exhumation rate since 50 Ma has only been ~ 0.05 mm/yr, although we do not expect that exhumation would have been constant throughout the Cenozoic. An alternative explanation for the observed AHe ages is that the geothermal gradient in the forearc is lower than implied by Magoon (1986). Subduction refrigeration can accompany flat slab subduction, in which the cold down-going slab cools the overlying mantle wedge and decreases geothermal gradient by as much as 10–15 °C/km (Dumitru et al., 1991, Peacock, 1996 and Westaway, 2006). If the geothermal gradient was much reduced following passage of a slab window beneath the Kenai Mountains, this could have rendered the AHe system insensitive to subsequent exhumation of even several kilometers. Without independent constraints on the mid to late Cenozoic geothermal gradient, however, this possibility is difficult to assess. We therefore elect to interpret our data using the best known estimate of current geothermal gradient (Magoon, 1986), while acknowledging the caveat that a lower than expected geothermal gradient could account for some of the spatial variation and great antiquity of the observed ages.

Although future work will be required to better determine age-elevation relationships in the area, the high variation in old AHe ages across minimal elevation range implies the

occurrence of an AHe PRZ in the Kenai Mountains. The spatial variation in ages can be loosely fit by closely stacked isochrons of a PRZ that is tilted gently down to the west away from the windward side of the range (Fig. 2.7B). The orientation and location of the isochrons are difficult to define and non-unique, due to differences in sample elevation and scatter in the AHe ages. The crustal section containing this potential PRZ is less deeply eroded than the PRZ in the Chugach Mountains in the vicinity of Turnagain Arm, where ages are slightly younger (10–20 Ma) (Buscher et al., 2008). In regional context, it therefore appears that the locus of rapid exhumation in the Chugach Mountains north of Prince William Sound identified by Arkle et al. (2013) transitions gradually to a zone of moderate exhumation in the westernmost Chugach Mountains and to a zone of minimal exhumation farther southwest into the Kenai Mountains (Fig. 2.8). The transition from moderate to minimal exhumation near Seward is sharp and may represent the progressive change from the trailing edge of the Yakutat plate to the Pacific plate.

If the crest of the Kenai Mountains has experienced minimal erosion, the shape of the topography itself should represent the geometry of surface uplift responsible for creating the range. Topographic profiles show that the Kenai Mountains are a broad dome (Fig. 2.4). The dome has a sharp, fault-bounded western margin. Total recent exhumation into this dome has been limited to valley incision, without lowering of upper ridge surfaces. In the northern Kenai Mountains, the dome is deeply incised, whereas in the south the dome is capped by the Harding Icefield. Across the dome the elevation of peaks and ridges are somewhat concordant and can be used to define an imaginary surface that represents the limit of recent rock uplift (Fig. 2.4) (Buscher et al., 2008). This dome could be produced as doubly-plunging antiformal arc of rock uplift. If correct, this interpretation suggests that the Kenai Mountains are a transient landform with erosion that lags behind surface uplift and creation of topographic potential energy

(e.g. Ouimet et al., 2009 and Oskin and Burbank, 2005). The Kenai Mountains may thus provide an example of a range in the early stage of orogenesis that is in a state of disequilibrium with the local erosional setting. A minor influence of climate on exhumation pattern may be apparent in the Kenai Mountains, however. The decrease in AHe age to the southeast and implied greater depth of erosion into the PRZ of ~ 0.5–1.0 km may be due to heavier precipitation and lower glacial ELA on the Pacific Coast (Fig. 2.7B).

Several lines of evidence combine with the relatively old AHe ages of the Kenai Mountains to suggest that they are kinematically distinct from the Chugach Mountains to the north. The gross topography of the Kenai Mountains appears disconnected and offset from the core of the Chugach Mountains at the southern margin of the underthrusting Yakutat microplate. The main drainage divide and axis of highest topography in the Kenai Mountains are situated in the center of the peninsula, whereas north of Seward in the Chugach Mountains the divide and topographic axis are located near the eastern margin of the mountains close to Prince William Sound, corresponding to much larger western catchments and glacial valleys (Fig. 2.3 and Fig. 2.5). The topographic crest jumps approximately 30 km to the west south of Seward and also changes orientation from north-south in the Chugach Mountains to NE–SW in the Kenai Mountains (Fig. 2.3). Greater erosion in the Chugach Mountains may have pushed the regional drainage divide to an axis of uplift in Prince William Sound near active faults like the Contact fault (Arkle et al., 2013). The locus of rock uplift in the Kenai Mountains may instead be focused in the middle of the peninsula, or a lower degree of erosion may have so far left the master divide in the Kenai Mountains immune to lateral shifts related to faulting, precipitation gradient, or glacier headward retreat. These transitions correspond to physical trends in the neighboring Cook Inlet. A shallowing of basin thickness to the south and increase in gravity anomalies roughly

coincides with where AHe ages increase to the southwest of Seward (Mankhemthong et al., 2013). This suggests the tectonic rock uplift of the Kenai Mountains and deformation and subsidence in Cook Inlet may be related to each other, yet distinct from the deformation and uplift of the Chugach Mountains to the north.

Although it is possible that the deformation associated with flat slab subduction that is observed in the Chugach Mountains (Arkle et al., 2013) gradually tapers off with distance from the underthrusting plate, the transitions in exhumation and topography around Seward (Fig. 2.3), within the transition zone of slab dip from flat to normal subduction, suggest a fundamental change in tectonic origin of forearc deformation. An alternative explanation for uplift of the Kenai Mountains other than from the underthrusting Yakutat microplate is underplating along the Aleutian megathrust. Underplating along a subduction zone occurs when subducting sediment and oceanic crust adhere to the upper plate, because of down going plate roughness, over-thickened sedimentary cover, or mantle wedge melting (Zhou and Li, 2000 and Ducea et al., 2009). The subducting Pacific plate is covered by thick deposits derived from the surrounding orogens, which could inhibit subduction and lead to underplating (Pavlis and Bruhn, 1983). Surveyor submarine fan deposits are up to 4 km thick offshore the Kenai Peninsula and stretch from the St. Elias orogen to the southern edge of Kodiak Island (Reece et al., 2011; Fig. 2.1). The associated accretionary prism offshore of the Kenai Peninsula has a broad mid-slope terrace unlike the surrounding region along the Aleutian trench, which is indicative of being influenced by a region of a rough down-going plate (Fruehn et al., 1999 and von Huene and Klaeschen, 1999). Ye et al. (1997) identified a low velocity zone along the seismic EDGE transect which was interpreted as underplated sediments. In addition, a mid to upper plate discontinuity dipping ~ 20° to the northwest underneath the Kenai Peninsula was previously

discovered by Stephens et al. (1990). Underplating on Kodiak Island is thought to occur near the brittle-ductile transition (~ 10 km depth) and result in widespread penetrative shortening and exhumation (Clendenen et al., 2003 and Carver and Plafker, 2008). Our results imply that the Kenai Mountains are experiencing rock uplift due to forearc growth associated with underplating processes that are comparable to those inferred for the longer history of deformation on Kodiak Island (Pavlis and Bruhn, 1983).

If underplating has been responsible in part for rock uplift of the Kenai Mountains, it is unclear when this process began and what fraction of uplift it is responsible for. Stratigraphic and provenance relationships in Cook Inlet imply that the Kenai Peninsula became emergent in the Late Miocene (Kirschner and Lyon, 1973 and Finzel et al., 2011), although it is not clear how high or widespread the mountainous topography was at this time. In contrast, the low exhumation implied by our data suggests that surface uplift has outpaced rock uplift, which we expect should require a recent pulse of surface uplift given the highly erosive nature of the temperate maritime glacial setting. Erosion rates in this setting could easily be > 1 km/Ma (Riihimaki et al., 2005, Koppes and Hallet, 2006 and Headley et al., 2013), which would have resulted in reset AHe cooling ages and removal of the PRZ in only a few million years. It is thus possible that the Late Miocene emergence of the peninsula involved minimal topographic growth, and that the majority of the Kenai Mountain relief has been produced only in the last few million years. One possible explanation is that the Late Miocene uplift of the Kenai Peninsula resulted from passage of the Yakutat microplate below it. Based on tectonic models, the trailing edge of the microplate should have passed between Kodiak Island and the tip of the Kenai Peninsula at about 3.5 Ma, and subsequently would have tracked north under the Kenai Mountains to its present position (Fig. 2.1) (DeMets et al., 1990, Von Huene et al., 1998, von

Huene and Klaeschen, 1999, Fruehn et al., 1999 and Pavlis et al., 2004). Significant underplating may have then begun in the absence of the microplate and arrival of the thickly blanketed subducting slab, resulting in a renewed phase of rock uplift for the Kenai Mountains. If underplating is indeed active beneath the Kenai Mountains, it is possible that continued rock uplift will eventually grow the Kenai Peninsula southwards to eventually connect with Kodiak Island.

CONCLUSION

Although the topography of the Kenai Mountains is rugged, suggesting rapid exhumation, measured AHe ages are older here than in other southern Alaska mountain ranges. These results were only obtainable via extensive replicate dating of sub-optimal apatite grains, given the challenging nature of the local bedrock. The old AHe ages indicate that the Kenai Mountains have not experienced recent, rapid exhumation of sufficient magnitude to reset the AHe thermochronometer (~ 1–2 km). The Kenai Mountains are therefore distinct from the locus of sustained concentrated rock uplift that has been identified in the Chugach Mountains north of Prince William Sound (Arkle et al., 2013). The minimal exhumation and topographic character suggest that the Kenai Mountains have distinct uplift kinematics from the rest of the coastal orogenic belt to the north and east. We hypothesize that early emergence of the Kenai Peninsula was driven by flat slab subduction, as the trailing edge of the subducting Yakutat plate passed northeastwards below it between the Late Miocene and Pliocene. We further hypothesize that a subsequent, localized pulse of rock uplift has occurred recently in the area of the Kenai Mountains due to underplating associated with thick sediments that sit atop the subducting Pacific Plate. This would make the modern Kenai Mountains analogous to the forearc

deformation that has produced Kodiak Island. These findings illustrate the dynamic, localized complexity of emergent forearc deformation in response to the variation in orientation and character of subducting slabs. The results also suggest that the Kenai Mountains are an unusual orogen that is in disequilibrium with the local erosional setting, presumably due to recent onset or acceleration of surface uplift. Despite the potential for aggressive glacial erosion given the local climate, erosion significantly lags behind rock uplift.

REFERENCES

Abers, G.A., 2008. Orogenesis from subducting thick crust and evidence from Alaska. Active Tectonics and Seismic Potential of Alaska vol. 179. American Geophysical Union Monograph Series, pp. 337–349.

Arkle, J., Armstrong, P., Haeussler, P., Prior, M., Hartman, S., Sendziak, K., Brush, J., 2013. Focused exhumation in the syntaxis of the western Chugach Mountains and Prince William Sound, Alaska. Geol. Soc. Am. Bull. 125 (5–6), 776–793. http://dx.doi.org/10.1130/b30738.1.

Berger, A.L., Spotila, J.A., Chapman, J.B., Pavlis, T.L., Enkelmann, E., Ruppert, N.A., Buscher, J.T., 2008. Architecture, kinematics, and exhumation of a convergent orogenic wedge: a thermochronological investigation of tectonic–climatic interactions within the central St. Elias Orogen, Alaska. Earth Planet. Sci. Lett. 270 (1–2), 13–24. http://dx.doi.org/10.1016/j.epsl.2008.02.034.

Bol, A.J., Roeske, S., 1993. Strike–slip faulting and block rotation along the Contact fault system, Prince William sound Alaska. Tectonics 12 (1), 49–62.

Bradley, D.C., Parrish, R., Clendenen, W., Lux, D., Layer, P., Heizler, M., Donley, D.T., 2000. New geochronological evidence for the timing of early Tertiary ridge subduction in southern Alaska. US Geol. Surv. Prof. Pap. 1615, 5–21.

Brandon, M.T., Roden-Tice, M.K., Garver, J.I., 1998. Late Cenozoic exhumation of the Cascadia accretionary wedge in the Olympic Mountains, northwest Washington State. Geol. Soc. Am. Bull. 110 (8), 985–1009.

Brown, R.W., Beucher, R., Roper, S., Persano, C., Stuart, F., Fitzgerald, P., 2013. Natural age

dispersion arising from the analysis of broken crystals. Part I: theoretical basis and implications for the apatite (U–Th)/He thermochronometer. Geochim. Cosmochim. Acta 122 (0), 478–497. http://dx.doi.org/10.1016/j.gca.2013.05.041.

Bruhn, R., Haeussler, P., 2006. Deformation driven by subduction and microplate collision: geodynamics of Cook Inlet basin, Alaska. Geol. Soc. Am. Bull. 118 (3–4), 289–303. http://dx.doi.org/10.1130/b25672.1.

Bruhn, R., Pavlis, T., Plafker, G., Serpa, L., 2004. Deformation during terrane accretion in the Saint Elias orogen, Alaska. Geol. Soc. Am. Bull. 116 (7–8), 771–787. http://dx.doi.org/10.1130/b25182.1.

Buscher, J.T., Berger, A.L., Spotila, J.A., 2008. Exhumation in the Chugach–Kenai Mountain Belt above the Aleutian Subduction Zone, Southern Alaska. Active Tectonics and Seismic Potential of Alaska vol. 179. American Geophysical Union Monograph Series, pp. 151–166.

Carver, G., Plafker, G., 2008. Paleoseismicity and neotectonics of the Aleutian subduction zone—An overview. Active Tectonics and Seismic Potential of Alaska, pp. 43–63.

Christeson, G., Gulick, S., van Avendonk, H., Worthington, L., Reece, R., Pavlis, T., 2010. The Yakutat terrane: dramatic change in crustal thickness across the Transition fault, Alaska. Geology 38 (10), 895–898. http://dx.doi.org/10.1130/g31170.1.

Clendenen, W.S., Fisher, D., Byrne, T., 2003. Cooling and Exhumation History of the Kodiak Accretionary Prism, Southwest Alaska. Special Papers, Geological Society of America, pp. 71–88.

Cohen, S.C., Freymueller, J.T., 1997. Deformation of the Kenai Peninsula, Alaska. J. Geophys. Res. 102 (B9), 20479–20487. http://dx.doi.org/10.1029/97JB01513.

DeMets, C., Gordon, R.G., Argus, D.F., Stein, S., 1990. Current plate motions. Geophys. J. Int. 101, 425–478.

Dominguez, S., Malavieille, J., Lallemand, S.E., 2000. Deformation of accretionary wedges in response to seamount subduction: insights from sandbox experiments. Tectonics 19 (1), 182–196.

Ducea, M., Kidder, S., Chesley, J., Saleeby, J., 2009. Tectonic underplating of trench sediments beneath magmatic arcs: the central California example. Int. Geol. Rev. 51 (1), 1–26. http://dx.doi.org/10.1080/00206810802602767.

Dumitru, T.A., Gans, P.B., Foster, D.A., Miller, E.L., 1991. Refrigeration of the western Cordilleran lithosphere during Laramide shallow-angle subduction. Geology 19 (11), 1145–1148.

Eberhart-Phillips, D., Christensen, D.H., Brocher, T.M., Hansen, R., Ruppert, N.A., Haeussler, P.J., Abers, G.A., 2006. Imaging the transition from Aleutian subduction to Yakutat collision in central Alaska, with local earthquakes and active source data. J. Geophys. Res. Solid Earth 111 (B11). http://dx.doi.org/10.1029/2005JB004240.

Ehlers, T.A., Farley, K.A., 2003. Apatite (U–Th)/He thermochronometry: methods and applications to problems in tectonic and surface processes. Earth Planet. Sci. Lett. 206 (1–2), 1–14. http://dx.doi.org/10.1016/S0012-821X(02)01069-5.

Elliott, J.L., Larsen, C.F., Freymueller, J.T., Motyka, R.J., 2010. Tectonic block motion and glacial isostatic adjustment in southeast Alaska and adjacent Canada constrained by

GPS measurements. J. Geophys. Res. 115, B09407. http://dx.doi.org/10.1029/2009 JB007139.

English, J.M., Johnston, S.T., Wang, K., 2003. Thermal modelling of the Laramide orogeny: testing the flat-slab subduction hypothesis. Earth Planet. Sci. Lett. 214 (3–4), 619–632. http://dx.doi.org/10.1016/S0012-821X(03)00399-6.

Enkelmann, E., Zeitler, P.K., Garver, J.I., Pavlis, T.L., Hooks, B.P., 2010. The thermochronological record of tectonic and surface process interaction at the Yakutat–North American collision zone in Southeast Alaska. Am. J. Sci. 310 (4), 231–260.

Enkelmann, E., Koons, P.O., Pavlis, T.L., Hallet, B., Barker, A., Elliott, J., Garver, J.I., Gulick, S.P.S., Headley, R.M., Pavlis, G.L., et al., 2015. Cooperation among tectonic and surface processes in the St. Elias Range, Earth's highest coastal mountains. Geophys. Res. Lett. 42, 5838–5846. http://dx.doi.org/10.1002/2015GL064727.

Farley, K.A., 2000. Helium diffusion from apatite: General behavior as illustrated by Durango fluorapatite. J. Geophys. Res. 105 (B2), 2903–2914. http://dx.doi.org/10. 1029/1999JB900348.

Ferguson, K., Armstrong, P., Arkle, J., Haeussler, P., 2015. Focused rock uplift above the subduction décollement at Montague and Hinchinbrook Islands, Prince William Sound, Alaska. Geosphere 11 (1), 144–159. http://dx.doi.org/10.1130/ges01036.1.

Ferris, A., Abers, G.A., Christensen, D.H., Veenstra, E., 2003. High resolution image of the subducted Pacific (?) plate beneath central Alaska, 50–150 km depth. Earth Planet. Sci. Lett. 214 (3–4), 575–588. http://dx.doi.org/10.1016/S0012-821X(03)00403-5.

Finzel, E.S., Trop, J.M., Ridgway, K.D., Enkelmann, E., 2011. Upper plate proxies for flat-slab subduction processes in southern Alaska. Earth Planet. Sci. Lett. 303 (3–4), 348–360. http://dx.doi.org/10.1016/j.epsl.2011.01.014.

Fisher, M.A., Magoon, L.B., 1978. Geologic framework of lower Cook inlet, Alaska. AAPG Bull. 62 (3), 373–402.

Fisher, D.M., Gardner, T.W., Marshall, J.S., Sak, P.B., Protti, M., 1998. Effect of subducting sea-floor roughness on fore-arc kinematics, Pacific coast, Costa Rica. Geology 26 (5), 467–470.

Fletcher, H.J., Freymueller, J.T., 1999. New GPS constraints on the motion of the Yakutat block. Geophys. Res. Lett. 26 (19), 3029–3032.

Flowers, R.M., Ketcham, R.A., Shuster, D.L., Farley, K.A., 2009. Apatite (U–Th)/He thermochronometry using a radiation damage accumulation and annealing model. Geochim. Cosmochim. Acta 73 (8), 2347–2365. http://dx.doi.org/10.1016/j.gca. 2009.01.015.

Freeland, G.L., Dietz, R.S., 1973. Rotation history of Alaskan tectonic blocks. Tectonophysics 18 (3–4), 379–389. http://dx.doi.org/10.1016/0040-1951(73)90054-1.

Freymueller, J.T., Woodard, H., Cohen, S.C., Cross, R., Elliott, J., Larsen, C.F., Hreinsdóttir, S., Zweck, C., 2008. Active deformation processes in Alaska, based on 15 years of GPS measurements. Active Tectonics and Seismic Potential of Alaska, (pp. 1–42). American Geophysical Union Geophysics Monograph Series 179.

Fruehn, J., von Huene, R., Fisher, M.A., 1999. Accretion in the wake of terrane collision: the

Neogene accretionary wedge off Kenai Peninsula, Alaska. Tectonics 18 (2), 263–277. http://dx.doi.org/10.1029/1998TC900021.

Fuis, G., Moore, T., Plafker, G., Brocher, T., Fisher, M., Mooney, W., Nokleberg, W., Page, R., Beaudoin, B., Christensen, N., Levander, A., Lutter, W., Saltus, R., Ruppert, N., 2008. Trans-Alaska Crustal Transect and continental evolution involving subduction underplating and synchronous foreland thrusting. Geology 36 (3), 267–270. http://dx.doi.org/10.1130/g24257a.1.

Gardner, T., Fisher, D., Morell, K., Cupper, M., 2013. Upper-plate deformation in response to flat slab subduction inboard of the aseismic Cocos Ridge, Osa Peninsula, Costa Rica. Lithosphere 5 (3), 247–264. http://dx.doi.org/10.1130/l251.1.

Gutscher, M.A., Maury, R., Eissen, J.P., Bourdon, E., 2000. Can slab melting be caused by flat subduction? Geology 28 (6), 535–538. http://dx.doi.org/10.1130/0091-7613(2000)28<535:csmbcb>2.0.co;2.

Haeussler, P.J., 2008. An overview of the Neotectonics of interior Alaska: far-field deformation from the Yakutat microplate collision. Active Tectonics and Seismic Potential of Alaska. American Geophysical Union Geophysics Monograph Series 179, pp. 83–108.

Haeussler, P.J., Saltus, R.W., 2011. Location and Extent of Tertiary Structures in Cook Inlet Basin, Alaska, and Mantle Dynamics that Focus Deformation and Subsidence (No. 1776-D, pp. i-26). US Geological Survey.

Haeussler, P., Bruhn, R., Pratt, T., 2000. Potential seismic hazards and tectonics of the upper Cook Inlet basin, Alaska, based on analysis of Pliocene and younger deformation.

Geol. Soc. Am. Bull. 112 (9), 1414–1429. http://dx.doi.org/10.1130/0016-7606(2000)112<1414:pshato>2.0.co;2.

Haeussler, P., Bradley, D., Wells, R., Miller, M., 2003. Life and death of the Resurrection plate: evidence for its existence and subduction in the northeastern Pacific in Paleocene–Eocene time. Geol. Soc. Am. Bull. 115 (7), 867–880. http://dx.doi.org/10.1130/0016-7606(2003)115<0867:ladotr>2.0.co;2.

Haeussler, P.J., Armstrong, P.A., Liberty, L.M., Ferguson, K.M., Finn, S.P., Arkle, J.C., Pratt, T.L.,2015. Focused exhumation along megathrust splay faults in Prince William Sound, Alaska. Quat. Sci. Rev. 113, 8–22.

Hartman, D.C., Pessel, G.H., McGee, D.L., 1974. Stratigraphy of the Kenai Group, Cook Inlet. Alaska Division of Geological and Geophysical Surveys. Alaska Open File Report 49.

Headley, R.M., Enkelmann, E., Hallet, B., 2013. Examination of the interplay between glacial processes and exhumation in the Saint Elias Mountains, Alaska. Geosphere 9 (2), 229–241.

Helwig, J., Emmet, P., 1981. Structure of the Early Tertiary Orca Group in Prince William Sound and some implications for the plate tectonic history of southern Alaska. J. Alaska Geol. Soc. 1, 12–35.

Karlstrom, T.N.V., 1961. The glacial history of Alaska: it's bearing on paleoclimatic history. Ann. N. Y. Acad. Sci. 95 (1), 290–340. http://dx.doi.org/10.1111/j.1749-6632.1961.tb50040.x.

Kirschner, C.E., Lyon, C.A., 1973. Stratigraphic and Tectonic Development of Cook Inlet

Petroleum Province. Regional Arctic Geology of Alaska, pp. 396–407.

Koppes, M., Hallet, B., 2006. Erosion rates during rapid deglaciation in Icy Bay, Alaska. J. Geophys. Res. Earth Surf. 111 (F2).

Li, Z.X., Li, X.H., 2007. Formation of the 1300-km-wide intracontinentalorogen and postorogenic magmatic province in Mesozoic South China: a flat-slab subduction model. Geology 35 (2), 179–182. http://dx.doi.org/10.1130/g23193a.1.

Little, T.A., Naeser, C.W., 1989. Tertiary tectonics of the Border Ranges Fault System, Chugach Mountains, Alaska: deformation and uplift in a forearc setting. J. Geophys. Res. 94 (B4), 4333–4359. http://dx.doi.org/10.1029/JB094iB04p0433.

Magoon, L.B., 1986. Present-day geothermal gradient. U.S. Geol. Surv. Bull. (B-1596), 41–46.

Mankhemthong, N., Doser, D.I., Pavlis, T.L., 2013. Interpretation of gravity and magnetic data and development of two-dimensional cross-sectional models for the Border Ranges fault system, south-central Alaska. Geosphere 9 (2), 242–259.

Mann, D.H., Peteet, D.M., 1994. Extent and timing of the Last Glacial Maximum in Southwestern Alaska. Quat. Res. 42 (2), 136–148. http://dx.doi.org/10.1006/qres.1994.1063.

Mazzotti, S., Hyndman, R., 2002. Yakutat collision and strain transfer across the northern Canadian Cordillera. Geology 30 (6), 495–498. http://dx.doi.org/10.1130/0091-7613(2002)030<0495:ycasta>2.0.co;2.

National Climate Data Center, 2005. Kenai municipal airport weather station data. [online]. Available from http://www.ncdc.noaa.gov/cdo-web/quickdata ([cited 16December

2015]).

National Climate Data Center, 2007. Seward meteorological station. [online]. Available from http://www.ncdc.noaa.gov/cdo-web/quickdata ([cited 16 December 2015]).

Oskin, M., Burbank, D.W., 2005. Alpine landscape evolution dominated by cirque retreat. Geology 33 (12), 933–936. 74 J.D. Valentino et al. / Tectonophysics 671 (2016) 63–75

Ouimet, W.B., Whipple, K.X., Granger, D.E., 2009. Beyond threshold hillslopes: channel adjustment to base-level fall in tectonically active mountain ranges. Geology 37 (7), 579–582.

Parry, W.T., Bunds, M.P., Bruhn, R.L., Hall, C.M., Murphy, J.M., 2001. Mineralogy, 40Ar/39Ar dating and apatite fission track dating of rocks along the Castle Mountain fault, Alaska. Tectonophysics 337 (3–4), 149–172. http://dx.doi.org/10.1016/S0040-1951(01)00117-2.

Pavlis, T.L., Bruhn, R.L., 1983. Deep-seated flow as a mechanism for the uplift of broad forearc ridges and its role in the exposure of high P/T metamorphicterranes. Tectonics 2 (5), 473–497. http://dx.doi.org/10.1029/TC002i005p00473.

Pavlis, T.L., Roeske, S.M., 2007. The Border Ranges fault system, southern Alaska. Geol. Soc. Am. Spec. Pap. 431, 95–127.

Pavlis, T.L., Picornell, C., Serpa, L., Bruhn, R.L., Plafker, G., 2004. Tectonic processes during oblique collision: insights from the St. Elias orogen, northern North American Cordillera. Tectonics 23 (3).

Peacock, S.M., 1996. Thermal and petrologic structure of subduction zones. Subduction:

Top to Bottom. AGU Geophysical Monograph 96, Washington, D.C., pp. 119–133.

Perry, S.E., Garver, J.I., Ridgway, K.D., 2009. Transport of the Yakutat Terrane, Southern Alaska: evidence from sediment petrology and detrital zircon fission-track and U/Pb double dating. J. Geol. 117 (2), 156–173. http://dx.doi.org/10.1086/596302.

Péwé, T.L., 1975. Quaternary Geology of Alaska. U.S. Geological Survey Professional Paper 835, p. 145.

Plafker, G., 1969. Tectonics of the March 27, 1964, Alaska Earthquake. US Government Printing Office, p. 74.

Plafker, G., 1987. Regional geology and petroleum potential of the northern Gulf of Alaska continental margin. In: Scholl, D.W., Grantz, A., Vedder, J.G. (Eds.), Geology and Resource Potential of the Continental Margin of Western North America and Adjacent Ocean Basins—Beaufort Sea to Baja California: Circum-Pacific Council for Energy and Mineral Resources. Earth Sciences Series, 6, 299–268.

Plafker, G., Berg, H.C., 1994. Overview of the geology and tectonic evolution of Alaska. In: Plafker, G., Berg, H.C. (Eds.), The Geology of Alaska vol. G-1. Geological Society of America, Geology of North America, Boulder, Colorado, pp. 989–1021.

Plafker, G., Nokleberg, W.J., Lull, J.S., 1989. Bedrock geology and tectonic evolution of the Wrangellia, Peninsular, and Chugach Terranes along the Trans-Alaska Crustal Transect in the Chugach Mountains and Southern Copper River Basin, Alaska. J. Geophys. Res. 94 (B4), 4255–4295. http://dx.doi.org/10.1029/JB094iB04p04255.

Plattner, C., Malservisi, R., Dixon, T.H., LaFemina, P., Sella, G.F., Fletcher, J., Suarez-Vidal, F.,

2007. New constraints on relative motion between the Pacific Plate and Baja California microplate (Mexico) from GPS measurements. Geophys. J. Int. 170 (3), 1373–1380. http://dx.doi.org/10.1111/j.1365-246x.2007.03494.x.

Ramos, V.A., Cristallini, E.O., Pérez, D.J., 2002. The Pampean flat-slab of the Central Andes. J. S. Am. Earth Sci. 15 (1), 59–78. http://dx.doi.org/10.1016/S0895-9811(02)00006-8.

Reece, R.S., Gulick, S.P., Horton, B.K., Christeson, G.L., Worthington, L.L., 2011. Tectonic and climatic influence on the evolution of the Surveyor Fan and Channel system, Gulf of Alaska. Geosphere 7 (4), 830–844.

Riccio, S.J., Fitzgerald, P.G., Benowitz, J.A., Roeske, S.M., 2014. The role of thrust faulting in the formation of the eastern Alaska Range: thermochronological constraints from the Susitna Glacier Thrust Fault region of the intracontinental strike–slip Denali Fault system. Tectonics 33, 2195–2217. http://dx.doi.org/10.1002/2014TC003646.

Ridgway, K., Thoms, E., Layer, P., Lesh, M., White, J., Smith, S., 2007. Neogene transpressional foreland basin development on the north side of the central Alaska Range, Usibelli Group and Nenana Gravel, Tanana basin. Geol. Soc. Am. Spec. Pap. 431, 507–547. http://dx.doi.org/10.1130/2007.2431(20).

Ridgway, K.D., Trop, J.M., Finzel, E.S., 2011. Modification of continental forearc basins by flat-slab subduction processes: a case study from Southern Alaska. Tectonics of Sedimentary Basins. John Wiley & Sons, Ltd, pp. 327–346.

Riihimaki, C.A., MacGregor, K.R., Anderson, R.S., Anderson, S.P., Loso, M.G., 2005. Sediment evacuation and glacial erosion rates at a small alpine glacier. J. Geophys. Res. Earth Surf. 110 (F3).

Spotila, J.A., Berger, A.L., 2010. Exhumation at orogenic indentor corners under long-term glacial conditions: example of the St. Elias orogen, Southern Alaska. Tectonophysics 490 (3–4), 241–256. http://dx.doi.org/10.1016/j.tecto.2010.05.015.

Spotila, J.A., Buscher, J.T., Meigs, A.J., Reiners, P.W., 2004. Long-term glacial erosion of active mountain belts: example of the Chugach–St. Elias Range, Alaska. Geology 32 (6), 501–504.

Stephens, C.D., Page, R.A., Lahr, J.C., 1990. Reflected and mode-converted seismic waves within the shallow Aleutian Subduction Zone, Southern Kenai Peninsula, Alaska. J. Geophys. Res. Solid Earth 95 (B5), 6883–6897. http://dx.doi.org/10.1029/JB095iB05p06883.

von Huene, R.V., Klaeschen, D., 1999. Opposing gradients of permanent strain in the aseismic zone and elastic strain across the seismogenic zone of the Kodiak shelf and slope, Alaska. Tectonics 18 (2), 248–262.

Von Huene, R., Klaeschen, D., Gutscher, M., Fruehn, J., 1998. Mass and fluid flux during accretion at the Alaskan margin. Geol. Soc. Am. Bull. 110 (4), 468–482.

Westaway, R., 2006. Cenozoic cooling histories in the Menderes Massif, western Turkey, may be caused by erosion and flat subduction, not low-angle normal faulting. Tectonophysics 412 (1), 1–25.

Wiles, G.C., Calkin, P.E., Post, A., 1995. Glacier fluctuations in the Kenai Fjords, Alaska, U.S.A.: an evaluation of controls on iceberg-calving glaciers. Arct. Alp. Res. 27 (3), 234–245. http://dx.doi.org/10.2307/1551954.

Willis, J.B., Haeussler, P.J., Bruhn, R.L., Willis, G.C., 2007. Holocene slip rate for the western segment of the Castle Mountain fault, Alaska. Bull. Seismol. Soc. Am. 97 (3), 1019–1024.

Worthington, L.L., Van Avendonk, H.J.A., Gulick, S.P.S., Christeson, G.L., Pavlis, T.L., 2012. Crustal structure of the Yakutat terrane and the evolution of subduction and collision in southern Alaska. J. Geophys. Res. 117, B01102. http://dx.doi.org/10.1029/2011JB008493.

Ye, S., Flueh, E.R., Kaeschen, D., Von Huene, R., 1997. Crustal structure along the EDGE transect beneath the Kodiak Shelf off Alaska derived from OBH seismic refraction data. Geophys. J. Int. 130, 283–302. http://dx.doi.org/10.1111/j.1365-246X.1997.tb05648.x.

Zhou, X.M., Li, W.X., 2000. Origin of Late Mesozoic igneous rocks in Southeastern China: implications for lithosphere subduction and underplating of mafic magmas. Tectonophysics 326 (3), 269–287.

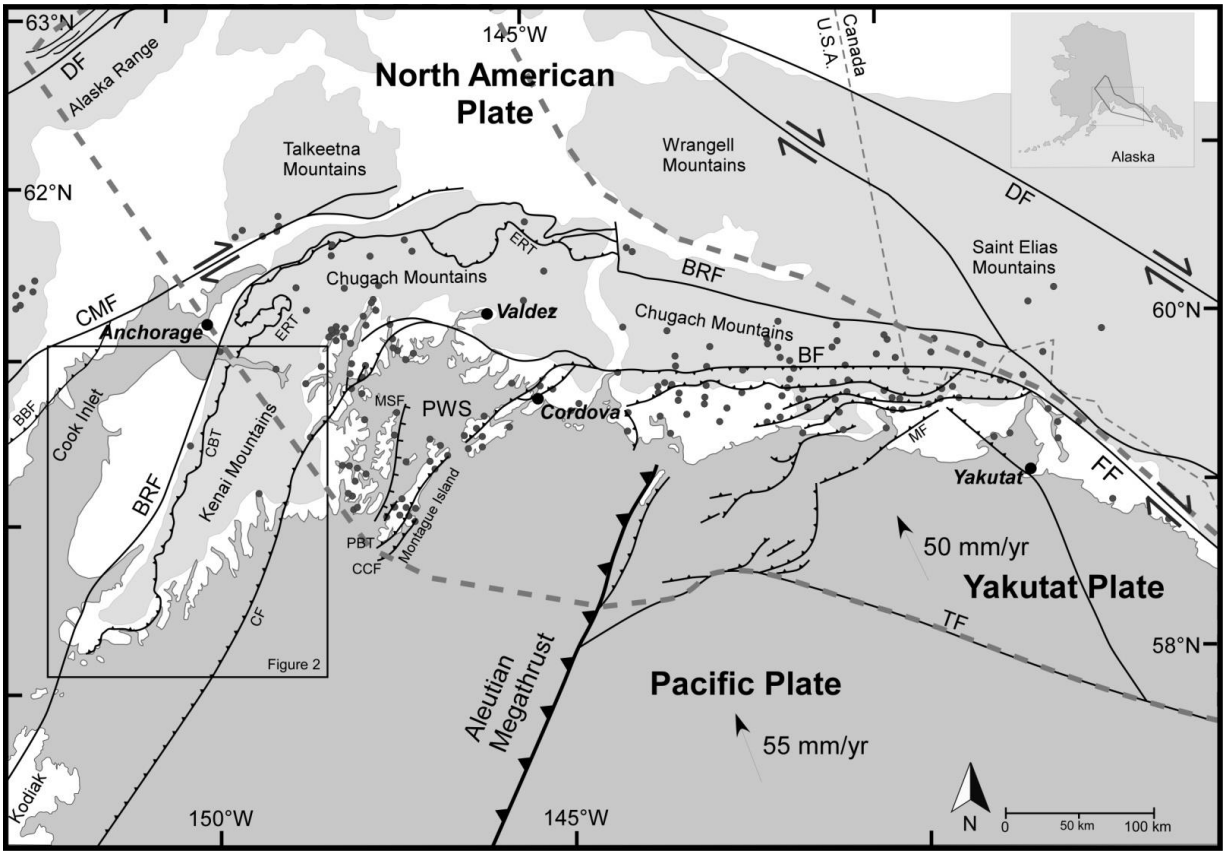

Figure 2.1. Generalized tectonic map of major orogens, faults and plate boundaries, and localities mentioned in text throughout south central Alaska. The grey dots depict the distribution of AHe ages from previous studies. Plate motion vectors are from Elliott et al. (2010) for Yakutat Plate and Plattner et al. (2007) for the Pacific Plate. The thick grey dashed line shows the limit of the underthrust Yakutat microplate (Eberhart-Phillips et al., 2006; Fuis et al., 2008). Fault line thicknesses indicate major (thick) to relatively more minor (thinner) activity. BF = Bagley Fault, BRF = Border Ranges Fault, CCF = Cape Cleare Fault, CMF = Castle Mountain Fault, CBT = Chugach Bay Thrust, CF = Contact Fault, DF = Denali Fault, ERT = Eagle River Thrust, FF = Fairweather Fault, MSF = Montague Strait Fault, PBT = Patton Bay Thrust, PWS = Prince William Sound.

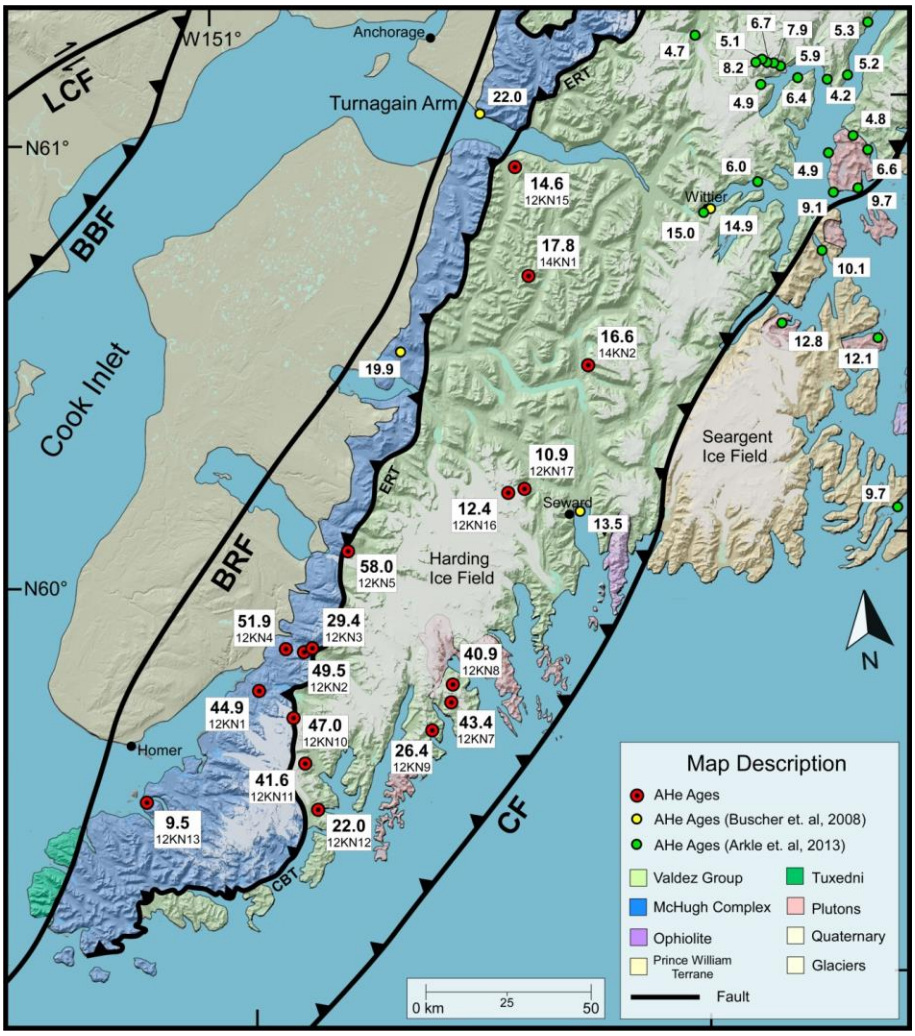

Figure 2.2. AHe ages for the Kenai Peninsula (in Ma). Previously completed ages (green and yellow circles) from other studies are included along with 17 new AHe ages (red circles).BBF = Bruin Bay Fault, CF = Contact Fault, LCF = Lake Clark Fault.

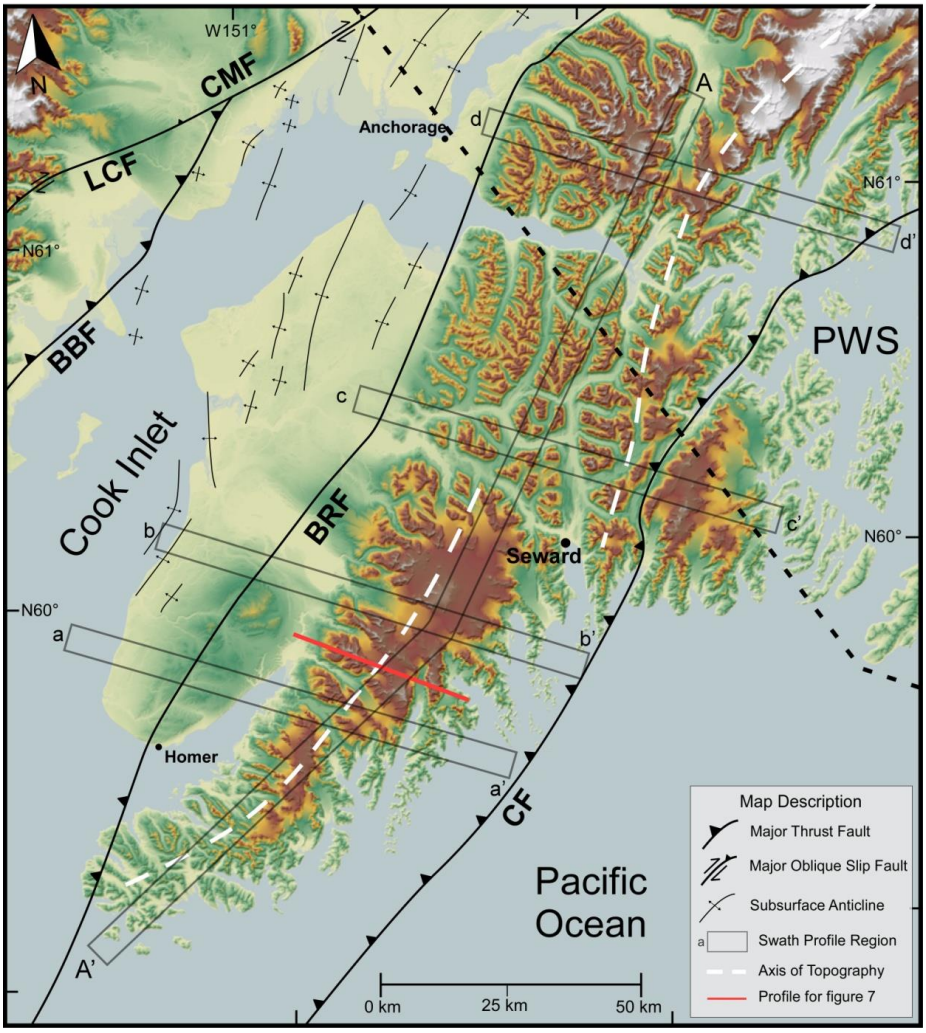

Figure 2.3. A 30-m digital elevation model overlain with major faults and subsurface anticlines. Topography is similar in ruggedness to the Chugach Mountains (see text for details). The axis of the mountain range shifts to the west south of Seward. The dashed line represents the location of the subducted Yakutat slab beneath the region. Rectangles represent locations of swath profiles depicted in figure 2.4. BRF = Border Ranges Fault, BBF = Bruin Bay Fault, CMF = Castle Mountain Fault, CF = Contact Fault, LCF = Lake Clark Fault.

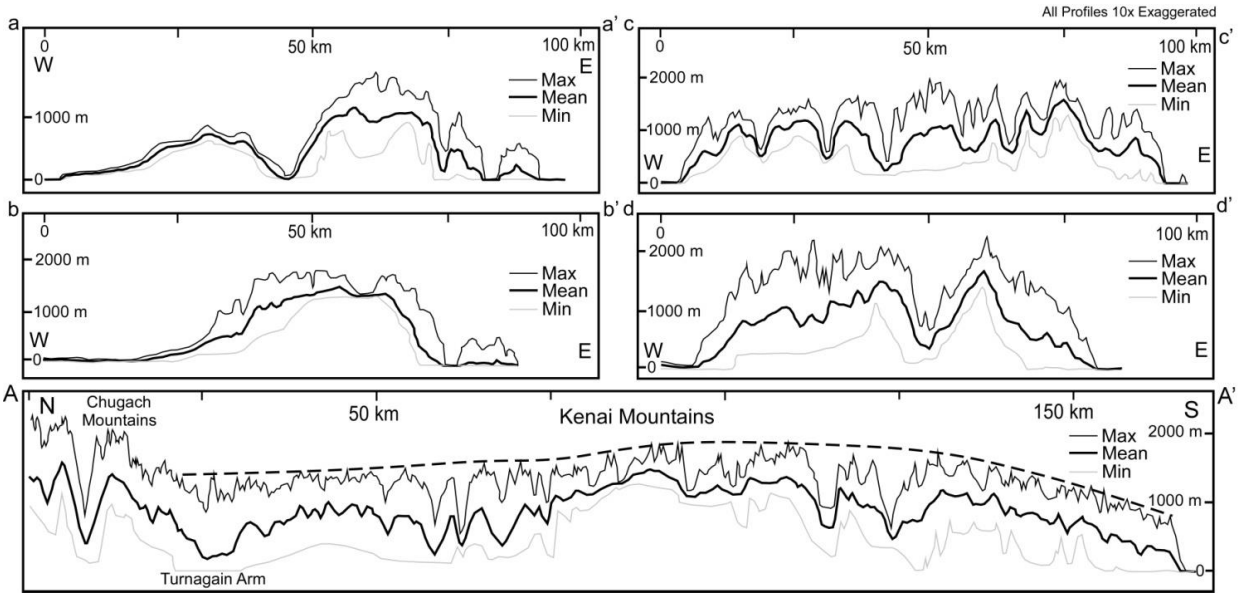

Figure 2.4. Swath profiles depicting topography across the Kenai Peninsula (a-d) and a long axis profile (A-A') down the Kenai Peninsula. See Figure 2.3 for the locations of the profiles. Profiles a-a' and b-b' show the dome like topography of the Harding Icefield and the southern half of the Kenai Peninsula. Profile c-c' shows the unglaciated portion of the northern Kenai Peninsula. Profile d-d' shows the higher and more deeply incised topography of the Chugach Mountains to the north. Profile A-A' shows the distinct topographic characteristics that separate the Kenai Mountains from the Chugach Mountains and the concordant elevation of peaks and ridges (black dashed line).

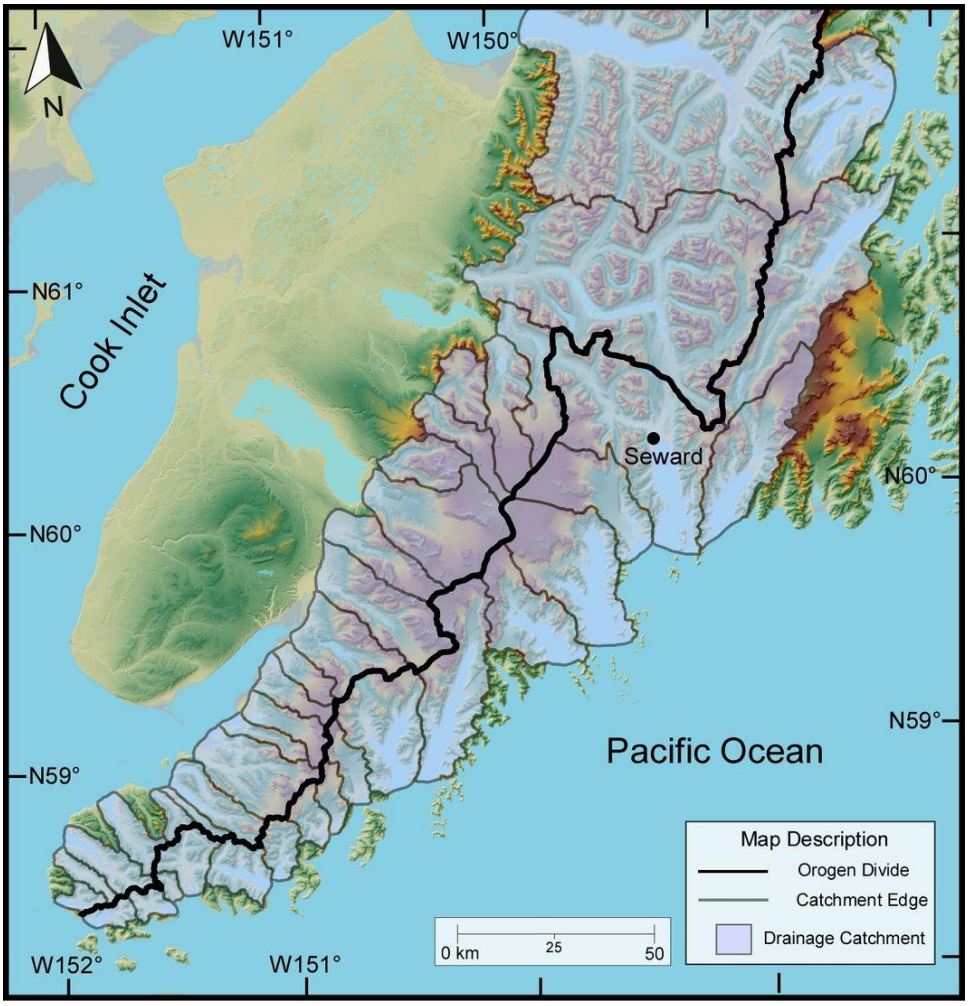

Figure 2.5. A 30-m digital elevation model of the Kenai Peninsula showing the main drainage divide and individual catchments. The drainage divide follows the coast to the north, but steps west south of Seward. Similarly, the drainage catchments are large (1,600 km^2) north of Seward and substantially smaller (300 km^2) to the south.

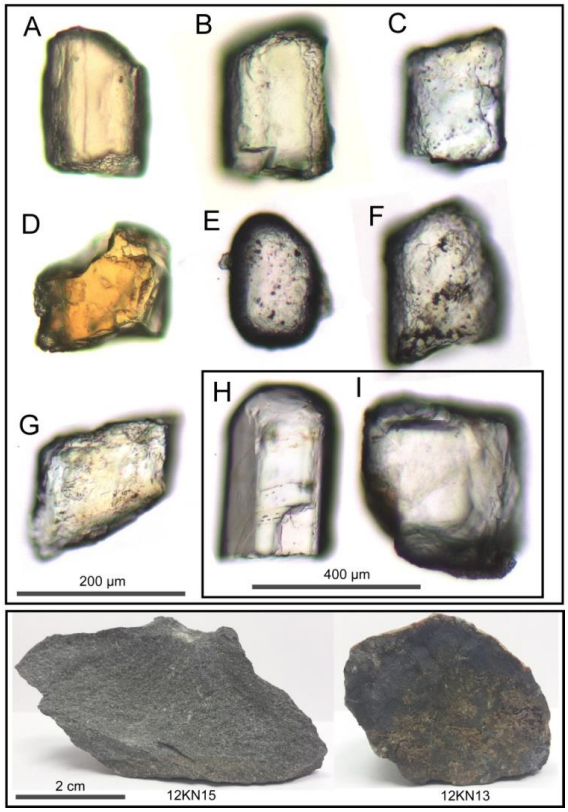

Figure 2.6. Apatite grains and hand samples depicting the range of samples used for analysis in this study. Apatite grain A is an example of some of the best quality grains used for the study, but this quality was rare. Apatites grains B and C are broken and have imperfections on their surfaces, but still preserve crystal habit and are inclusion free. Apatite grain D is good quality but fractured on many of the edges. Apatite grain E has worn edges and is frosted, suggesting that it may have undergone transport and alteration before deposition. Apatites grains F and G are examples of some of the lowest quality apatites used for this study. Apatite grains Hand I are decent quality grains which are larger than >100 µm and were used as single grain aliquots, but grains such as these often had internal flaws and non-birefringent microinclusions. Hand sample 12KN15 is an example of a coarser grained metasandstone that yielded apatite. Sample 12KN13 is an example of the majority of samples for the Kenai Mountains, which is fine grained and produced low quality apatite.

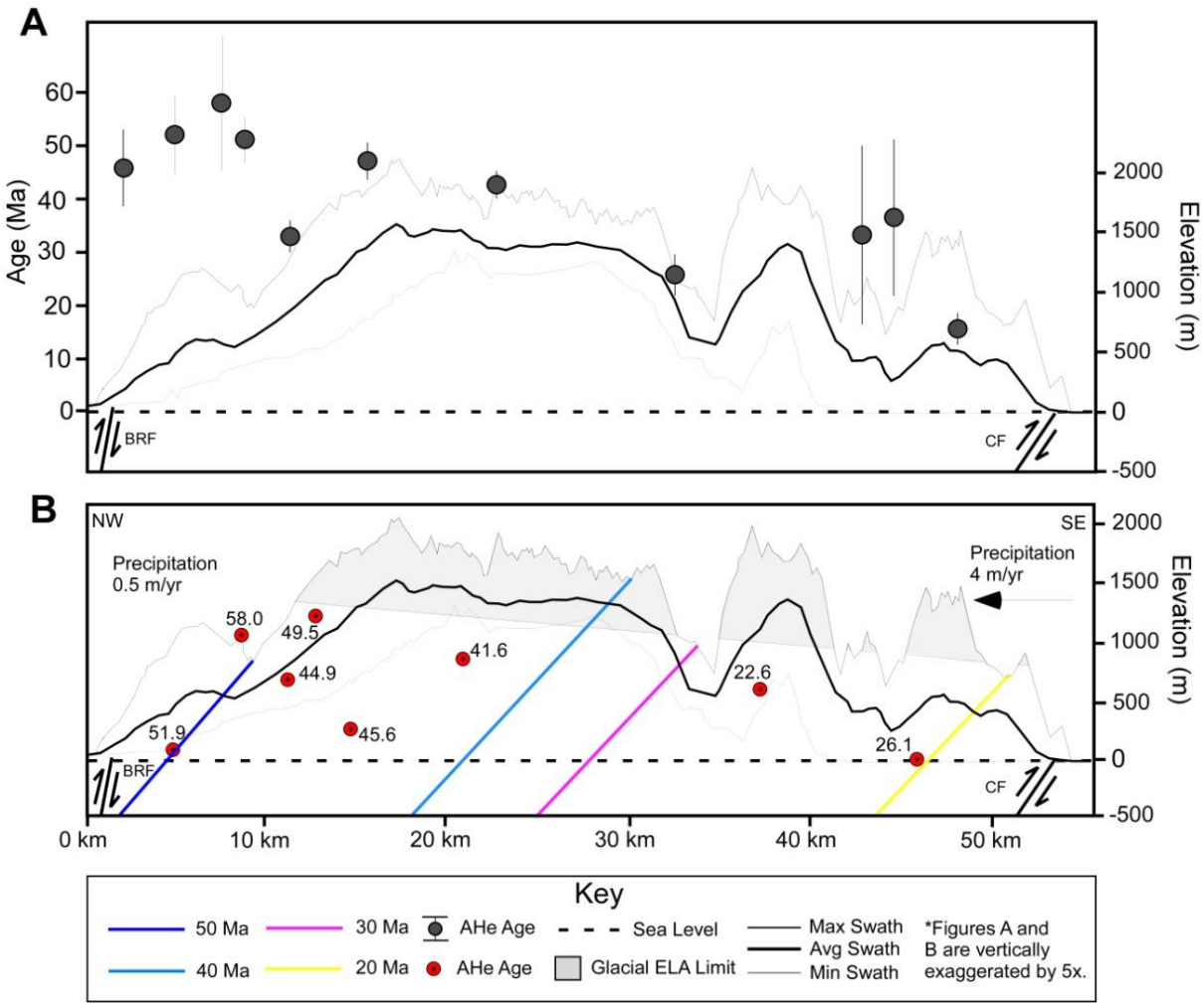

Figure 2.7. (A) AHe age vs. distance along swath topographic profiles along the Kenai Mountains. The general trend of AHe ages shows a decrease towards the east and windward flank of the mountains. (B) Age distance plot with approximate AHe isochrons illustrating a potential PRZ tilted down to the west. Glacial ELA (Mann & Peteet, 1994; Wiles et al., 1995) is shown lowering towards the east due to precipitation gradient. BRF = Border Ranges Fault, CF = Contact Fault.

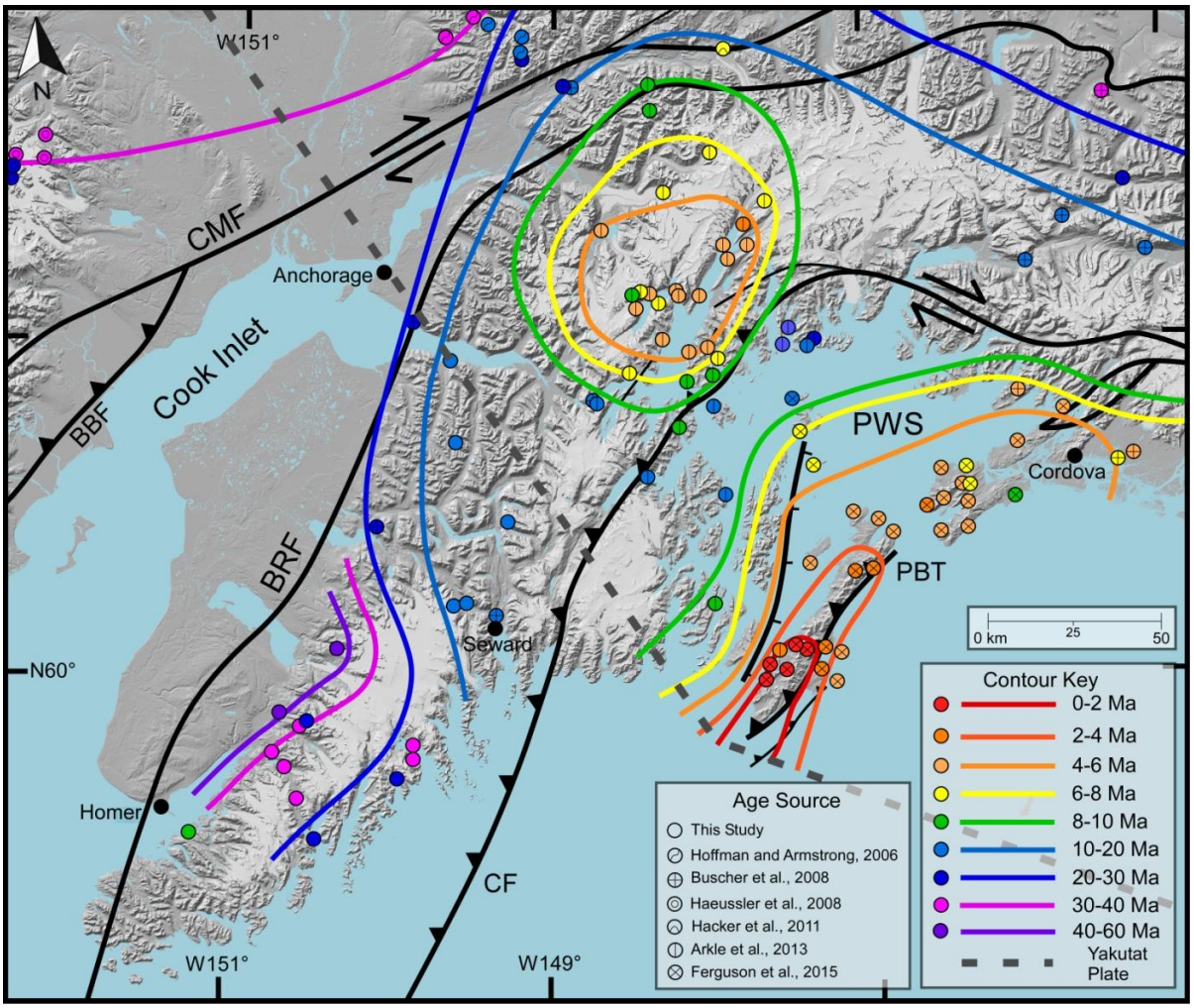

Figure 2.8. AHe age contour map for the Prince William Sound and surrounding coastal mountains. The new AHe ages are the oldest in the region and portray a zone of slow exhumation southwest of the edge of the Yakutat plate. The Chugach Core and the Patton Bay Thrust regions have much faster exhumation rates due to upper plate deformation related to the Yakutat plate. BRF= Border Ranges Fault, BBF= Bruin Bay Fault, CMF = Castle Mountain Fault, CBT = Chugach Bay Thrust, CF= Contact Fault (Bol and Roeske, 1993), ERT = Eagle River Thrust, PBT = Patton Bay Thrust

Sample	Elevation (m)	Latitude	Longitude	Rock type	Mass (mg)	mwar (µm)	He (pmol)	U (ppm)	Th (ppm)	Sm (ppm)	eU	Grains	F_T	Corr. Age (Ma)	Average Age (Ma)	Standard Deviation
12KN1	713	59.7295	-150.8627	meta. sand	0.0013	46.0	0.0022	8.3	16.4	141.6	12.8	1	0.68	40.1		
					0.0018	50.6	0.0010	3.3	6.3	60.0	5.1	1	0.79	28.1		
					0.0022	32.2	0.0033	5.3	14.6	127.2	9.4	3	0.63	50.5	**44.9**	8.5 Ma
					0.0137	47.2	0.0201	4.9	10.3	101.6	7.8	5	0.74	50.1	n=8**	19.0%
					0.0065	69.0	0.0097	5.1	7.8	115.8	7.5	1	0.82	48.2	N=8***	
					0.0044	55.2	0.0108	7.1	22.1	117.2	12.9	1	0.76	48.4		
					0.0111	46.4	0.0182	5.3	10.3	145.9	8.5	5	0.72	54.5		
					0.0113	38.0	0.0411	20.2	24.4	164.6	26.8	12	0.67	39.4		
12KN2	1227	59.8524	-150.6686	graywacke	0.0023	64.4	0.0034	5.1	9.3	121.4	7.9	1	0.81	45.6		
					0.0029	55.2	0.0037	4.1	9.3	115.7	6.9	1	0.81	46.6	**49.5**	3.8 Ma
					0.0052	59.8	0.0069	4.3	9.0	153.0	7.2	1	0.80	47.1	n=6	7.7%
					0.0066	69.0	0.0086	3.8	6.3	152.0	6.1	1	0.81	55.4	N=6	
					0.0042	53.0	0.0076	5.4	12.6	161.2	9.2	2	0.76	52.5		
					0.0033	48.5	0.0051	4.7	13.5	183.8	8.8	4	0.71	49.7		
12KN3	1568	59.8607	-150.6456	graywacke	0.0051	69.0	0.0274	29.7	43.3	107.8	40.4	1	0.82	31.1		
					0.0044	*52.2*	*0.0059*	*3.8*	*10.8*	*146.6*	*7.1*	*2*	*0.76*	*50.7*	**29.4**	2.3 Ma
					0.0080	*42.5*	*0.0366*	*14.7*	*8.0*	*279.5*	*18.0*	*7*	*0.69*	*74.3*	n=2	8.0%
					0.0077	35.9	0.0197	21.3	22.5	215.0	27.7	7	0.65	27.7	N=4	
					0.0138	*75.6*	*0.0352*	*2.1*	*6.1*	*118.2*	*4.1*	*2*	*0.83*	*223*		
12KN4	99	59.8524	-150.7424	graywacke	0.0055	34.7	0.0057	3.7	8.8	166.9	6.7	5	0.63	50.9		
					0.0057	36.8	0.0054	3.9	9.2	138.4	6.8	5	0.66	43.2	**51.9**	7.4 Ma
					0.0060	*37.7*	*0.0181*	*4.2*	*9.7*	*146.6*	*7.2*	*5*	*0.66*	*130*	n=5	14.3%
					0.0058	35.3	0.0070	4.4	10.8	162.4	7.7	6	0.63	50.6	N=6	
					0.0074	39.1	0.0112	4.3	9.6	169.3	7.4	6	0.66	63.8		
					0.0053	38.0	0.0094	6.2	14.8	197.0	10.6	5	0.67	50.7		
12KN5	1141	60.0678	-150.4240	meta. sand	0.0030	39.8	0.0246	22.8	42.3	120.1	33.3	3	0.68	70.0		
					0.0091	78.2	0.0698	24.1	20.2	34.1	29.0	1	0.84	59.8	**58.0**	13.0 Ma
					0.0102	*101.2*	*0.3968*	*24.0*	*7.4*	*210.2*	*26.8*	*1*	*0.90*	*312*	n=3	22.4%
					0.0039	70.1	0.0010	1.2	0.4	42.3	1.5	2	0.83	44.1	N=4	
12KN7	598	59.7393	-150.0264	meta.sand	0.0051	73.6	0.0128	5.6	12.6	219.1	9.6	1	0.86	62.5		
					0.0087	71.6	0.0292	8.7	17.1	183.7	13.6	2	0.82	59.6		
					0.0068	47.7	0.0210	41.1	22.6	194.5	47.4	3	0.77	16.4		
					0.0061	64.4	*0.0001	0.1	0.5	6.6	0.3	1	0.81	24.0	**43.4**	14.3 Ma
					0.0070	82.8	*0.0002	0.3	0.1	16.1	0.4	1	0.85	40.2	n=10	32.9%
					0.0077	87.4	0.0418	18.9	21.6	148.3	24.8	1	0.85	49.6	N=10	
					0.0128	101.2	0.0022	0.7	0.2	30.1	0.9	1	0.90	46.5		
					0.0079	52.8	0.0169	5.9	17.3	205.2	10.9	2	0.80	49.6		
					0.0035	55.4	0.0105	10.6	20.9	242.9	16.7	2	0.81	44.1		
					0.0044	68.8	0.0220	19.4	37.7	213.2	29.4	2	0.82	40.9		
12KN8	10	59.7685	-150.0314	meta. sand	*0.0152*	*105.8*	*0.0064*	*0.9*	*0.3*	*3.8*	*1.0*	*1*	*0.88*	*93.8*		
					0.0099	76.4	0.0810	45.7	17.1	135.9	50.4	2	0.82	38.0		
					0.0096	54.3	0.1408	73.7	8.4	197.5	76.6	3	0.78	47.4		
					0.0130	*49.6*	*0.2988*	*42.5*	*5.5*	*127.4*	*44.4*	*8*	*0.73*	*136*	**40.9**	11.7 Ma
					0.0059	37.8	0.0589	52.6	7.3	179.0	55.2	4	0.68	51.6	n=8	28.7%
					0.0137	51.3	0.0058	6.0	1.3	39.4	6.5	6	0.74	17.1	N=10	
					0.0209	147.2	0.0194	4.4	0.6	35.1	4.7	1	0.93	42.1		
					0.0054	51.4	0.0348	30.9	6.3	143.4	33.1	3	0.77	49.7		
					0.0125	80.1	0.0213	11.3	2.4	28.1	12.0	2	0.86	31.8		

					0.0130	70.1	0.1225	42.3	4.0	143.8	44.0	2	0.84	49.5		
12KN9	1	59.6333	-150.0969	schist	*0.0015*	*48.5*	*0.0151*	*47.6*	*47.4*	*186.2*	*59.6*	*3*	*0.74*	*45.3*		
					0.0087	72.8	0.0418	36.5	17.5	174.6	41.5	2	0.82	27.3		
					0.0027	*51.0*	*0.0099*	*6.8*	*16.6*	*184.3*	*11.6*	*2*	*0.75*	*85.5*	**26.4**	1.5 Ma
					0.0082	52.1	0.0281	24.7	33.3	168.5	33.4	2	0.80	24.8	n=4	5.7%
					0.0088	*92.0*	**0.0003*	*1.1*	*0.2*	*12.2*	*1.2*	*1*	*0.86*	*6.70*	N=7	
					0.0062	55.2	0.0254	31.5	34.1	103.1	40.1	2	0.78	25.4		
					0.0045	53.2	0.0198	27.3	49.2	196.3	39.8	2	0.77	28.0		
12KN10	375	59.7330	-150.7876	graywacke	0.0091	82.8	0.0059	1.6	6.0	191.1	4.0	1	0.87	43.1		
					0.0070	78.2	0.0236	11.5	25.9	183.4	18.5	1	0.85	42.0		
					0.0048	61.3	0.0090	5.2	16.8	175.5	10.0	2	0.80	46.8		
					0.0046	49.0	0.0069	5.1	12.3	150.4	8.7	2	0.75	46.1	**47.0**	3.1 Ma
					0.0051	73.6	0.0153	8.9	20.8	191.7	14.7	1	0.83	48.4	n=9	6.6%
					0.0046	55.2	0.0097	6.2	18.1	220.3	11.6	2	0.79	47.1	N=9	
					0.0086	67.6	0.0172	6.0	15.3	182.4	10.5	2	0.83	46.6		
					0.0072	59.8	0.0127	4.2	16.3	131.3	8.7	2	0.80	50.9		
					0.0055	57.8	0.0109	5.0	16.7	161.5	9.7	2	0.79	51.5		
12KN11	820	59.6727	-150.7210	meta. sand	0.0083	51.5	0.0271	11.6	35.4	280.1	21.3	5	0.76	40.4	**41.6**	1.6 Ma
					0.0058	43.7	0.0101	5.2	24.9	151.4	11.8	5	0.69	42.7	n=2/N=2	4.0%
12KN12	602	59.5215	-150.6630	meta. sand	0.0111	124.2	0.0353	12.6	51.2	296.3	26.1	1	0.88	27.0		
					0.0140	72.3	0.0185	10.0	14.6	201.8	14.5	4	0.83	21.9		
					0.0075	92.0	0.0155	53.8	1.5	242.8	55.4	1	0.86	8.41		
					0.0122	*56.7*	*0.4918*	*29.4*	*31.7*	*298.0*	*38.4*	*4*	*0.77*	*262*		
					0.0074	71.8	0.0209	18.4	28.1	242.0	26.2	3	0.83	25.7		
					0.0057	40.5	0.0027	4.2	17.3	209.0	9.3	4	0.68	15.6	**22.0**	5.8 Ma
					0.0042	69.0	0.0031	4.4	11.1	257.1	8.3	1	0.82	23.0	n=11	26.4%
					0.0061	*52.8*	*0.1312*	*5.0*	*13.4*	*234.4*	*9.3*	*4*	*0.77*	*611*	N=13	
					0.0017	39.7	0.0050	24.6	31.1	248.2	33.2	3	0.68	25.2		
					0.0046	50.4	0.0046	4.9	17.1	238.2	10.1	3	0.75	27.1		
					0.0090	72.8	0.0162	12.0	22.5	214.0	18.3	3	0.82	23.6		
					0.0015	39.4	0.0283	288.1	63.8	309.8	304.7	4	0.67	18.4		
					0.0052	78.2	0.0185	23.4	27.6	266.4	31.2	1	0.84	26.4		
12KN13	657	59.5260	-151.3715	graywacke	0.0093	82.8	0.0053	16.3	1.8	146.5	17.5	1	0.85	7.53		
					0.0084	78.2	0.0061	18.0	3.6	147.6	19.5	1	0.84	8.71	**9.5**	2.5 Ma
					0.0069	73.6	0.0066	18.0	1.4	154.8	19.1	1	0.80	12.3	n=3	26.4%
					0.0117	*39.9*	*0.0432*	*27.9*	*9.5*	*220.7*	*31.2*	*11*	*0.68*	*34.0*	N=3	
12KN15	94	60.9093	-149.6064	meta. sand	0.0057	64.4	0.0027	7.3	16.9	131.2	12.0	1	0.80	9.88		
					0.0068	69.0	0.0028	5.2	9.7	201.0	8.5	1	0.82	12.1		
					0.0067	78.2	0.0037	5.9	7.4	90.8	8.1	1	0.81	16.5	**14.6**	3.4 Ma
					0.0114	101.2	0.0202	15.4	25.7	239.9	22.6	1	0.87	17.7	n=5	23.3%
					0.0129	*52.3*	*0.0243*	*15.4*	*21.2*	*104.0*	*20.9*	*5*	*0.75*	*23.2*	N=6	
					0.0083	40.0	0.0206	30.8	45.2	154.4	42.2	6	0.68	16.6		
12KN16	1076	60.1800	-149.7063	meta.sand	0.0137	45.9	0.0283	41.4	36.3	207.3	51.0	6	0.72	10.8		
					0.0057	92.0	0.0117	21.2	55.2	245.7	35.4	1	0.86	13.2		
					0.0085	62.2	0.0106	13.8	33.7	231.4	22.9	2	0.80	13.4	**12.4**	1.1 Ma
					0.0052	55.2	0.0088	19.9	51.0	255.3	33.2	2	0.78	12.7	n=6	9.2%

					0.0073	47.4	0.0091	15.1	40.1	187.9	25.4	6	0.72	13.1	N=6	
					0.0132	41.2	0.0342	51.5	54.8	179.7	65.2	9	0.69	11.0		
12KN17	103	60.1947	-149.5880	meta. sand	0.0033	73.6	0.0074	21.9	43.8	237.5	33.4	1	0.83	15.8		
					0.0026	46.0	0.0040	22.0	45.8	68.9	33.1	1	0.74	12.1		
					0.0039	39.6	0.0044	23.2	39.2	262.7	33.7	2	0.74	8.96		
					0.0041	43.2	0.0058	24.8	47.4	136.8	36.6	3	0.71	10.4	**10.9**	2.4 Ma
					0.0066	87.4	0.0011	1.9	4.7	191.5	4.0	1	0.88	10.5	n=7	22.6%
					0.0029	59.8	0.0011	6.5	13.4	236.5	10.8	1	0.78	9.26	N=10	
					0.0033	47.1	0.0020	13.7	12.8	92.0	17.1	2	0.76	8.99		
					0.0030	*39.3*	*0.0096*	*6.0*	*10.7*	*154.2*	*9.3*	*2*	*0.69*	*99.3*		
					0.0032	*59.8*	*0.0093*	*16.8*	*31.5*	*175.9*	*25.1*	*1*	*0.82*	*27.0*		
14KN1	1249	60.6582	-149.5311	meta. sand	0.0062	62.3	0.0131	15.4	23.1	174.5	21.7	2	0.80	23.8	**17.8**	5.3 Ma
					0.0054	64.1	0.0139	34.5	33.8	153.2	43.2	2	0.82	13.9	n=3	29.9%
					0.0054	59.7	0.0037	7.1	15.0	94.1	11.1	2	0.79	15.4	N=3	
14KN2	1459	60.4523	-149.2947	schist	0.0222	147.2	0.0394	30.1	9.2	41.9	32.4	1	0.93	11.3	**16.6**	7.4 Ma
					0.0077	69.5	0.0163	13.9	33.7	73.7	22.2	2	0.83	21.8	n=2	44.8%
															N=2	

meta.=metamorphic rock
sand=sandstone
mwar = mass-weighted average radius
FT=alpha ejected correction factor
eU= U+(0.235*Th), effective uranium concentration
Standard deviation of ages used for average are as Ma and percent.

Ages in italics are excluded from averages (see text for explanation).
Latitude and Longitude datum is WGS84 and vertical datum is EGM96.
*** Measured ^{4}He was low and corresponds to higher uncertainty.**
**** "n" = number of replicates used in age**

***** "N" = total number of aliquots run for age**

Table 2.1. Summary of analyzed aliquots and averaged AHe ages.

CHAPTER 3

Timing and extent of Quaternary glaciation using ^{10}Be and ^{36}Cl terrestrial cosmogenic dating in the Chugach Mountains, Alaska

Joshua D. Valentino, James A. Spotila, Lewis A. Owen, Jason Cesta, Marc W. Caffee

Department of Geosciences, 4044 Derring Hall, Virginia Tech, Blacksburg, VA 24061, USA

Department of Geology, University of Cincinnati, Cincinnati, OH 45221, USA

Department of Physics, Purdue University, West Lafayette, IN, USA

Department of Earth, Atmospheric, and Planetary Science, Purdue University, West Lafayette, IN, USA

Submitted to the journal of Quaternary Research in January 2017

ABSTRACT

Geomorphic mapping, analysis of landforms and sediments, and cosmogenic ^{10}Be and ^{36}Cl dating of moraine boulders and glacially polished bedrock defines the timing of Wisconsin glaciations in the Chugach and Kenai mountains of South Central Alaska and refines the interpretations of previous chorological studies. The maximum extent of glaciation in this region during the last glacial occurred at ~50 ka, during marine oxygen isotope stage 3. Five valley glacial advances are recognized in the Williwaw Lakes Valley and Thompson Pass areas dating to ~ 23.8, 22.3, 17.1, 17.9, and 14.9 ka. Reconstructed equilibrium-line altitude depressions (ΔELAs) range from 298 to 314 m for late Wisconsin advances. The comparatively low temperature depression in the Chugach Mountains deduced from the ΔELAs suggests that the climate was warmer in Alaska than the average global temperatures during the gLGM. Previous studies across Alaska have observed similar ΔELAs and conclude that the region was more arid than other glaciated places during the late Wisconsin. Comparisons with other regions throughout Alaska show that glaciers advance and retreated later in southeast Alaska close to the main mass of the Laurentide ice sheet.

INTRODUCTION

Alaska is one of the world's best places to examine geomorphic and sedimentological evidence for late Cenozoic glaciation, particularly late Quaternary glaciation (Karlstrom, 1961; Pewe, 1975; Calkin et al, 2001; Briner and Kaufman, 2008). The Chugach Mountains, in south central Alaska, stretching for > 400 km, contains one of the most accessible and well-preserved glacial geologic records in Alaska; surprisingly the timing of past glaciations in this region is not well defined (Fig. 3.1). This mountain range was the locus of the western extent of the Cordilleran ice sheet during the last glacial (Karlstrom, 1964; Briner and Kaufman, 2008).

Today, glaciation is restricted to intermittent ice fields and valley glaciers that advance into Prince William Sound and adjacent lowlands (Fig. 3.1). Karlstrom (1961, 1964) was the first to develop a detailed relative glacial chronology for the Anchorage and Cook Inlet regions and showed that there are five late Wisconsin glaciations. Radiocarbon dating of the older moraines in this region was partially successful (Table 2.1), but complications with age calibration and less advanced analytical technologies available during the 1960s did not allow the timing of glaciation to be well defined (Karlstrom, 1964). Since then, the relative glacial history has been closely studied and outlined by Schmoll and Yehle (1986), Schmoll et al. (1999), Calkin et al. (2001) and Reger et al. (2007). A thorough study using modern techniques to date early and late Wisconsin glaciations in the Chugach Mountains has yet to be done.

Reconstructing the timing and extent of glaciation in Southern Alaska help test the synchronuity of glaciation between maritime and continental regions of the western margins of the Northern American ice sheets during the late Quaternary. This in turn help in understanding regional and global synchronuity of climate and glaciation that is essential for testing and developing models for past and future climate change. In addition, this study area provides new data on early-Wisconsin glaciation that is lacking for many regions of the world and tests the view that mountains glaciation was more extensive during the earlier part of the last glacial than during the global last glacial maximum (see definition below).

To provide the first Quaternary glacial chronostratigraphy for the Chugach Mountains we use remote sensing, geomorphic mapping, and cosmogenic ^{10}Be and ^{36}Cl to determine the timing of the deposition of glacial landforms. Our investigation covers two main regions: the Williwaw Lakes and Thompson Pass, both on the edges of the higher accessible portion of the Chugach Mountains. The Williwaw Lakes region, a deglaciated and low elevation valley located on the

western side of the Chugach Mountains (Fig. 3.1), contains a complete assemblage of presumed early Wisconsin glaciated surfaces and late Wisconsin moraines. The Thompson Pass region forms a plateau of high topography located on the eastern side of the Chugach Mountains (Fig. 3.1) and contains active glaciers and glacially polished bedrock benches, moraines, and erratics. We compare the new chronostratigraphy for these two regions with glaciation across Alaska to examine regional variations and possible forcing factors.

BACKGROUND

The Chugach Mountains are part of a 2000 km-long exhumed forearc-high along the southern margin of Alaska (Plafker et al., 1989; Plafker and Berg, 1994). The mountain range is a product of accretion in the Late Cretaceous, and oblique collision and subduction of the Yakutat microplate from the Oligocene to present (Plafker, 1987; Bruhn et al., 2004; Abers, 2008; Fuis et al., 2008; Haeussler et al., 2008; Finzel et al., 2011). The topography of the Chugach Mountains is rugged and rises to 4,016 m above sea level (asl) at Mount Marcus Baker, with valleys deeply incised by glaciers to below sea level (Buscher et al., 2008). Loci of high glaciated-topography correspond to zones of rapid exhumation in the core of the Chugach Mountains north of Prince William Sound (Arkle et al., 2013) and north of the Bagley Icefield in the Saint Elias Mountains (Berger and Spotila, 2008). The Chugach Mountains have been extensively glaciated throughout the Quaternary, fluctuating from complete coverage to valley glaciers that advanced from ice fields throughout the center region of the range (Fig 3.1). Today, the eastern Chugach Mountains are covered in ice fields and glaciers such as the Bagley icefield, and Bering and Malaspina glaciers. To the west, the ice fields and valley glaciers are much smaller and many of the valleys are unglaciated. The unglaciated valleys are rugged, ~ 3 km

deep and ~ 5 km wide, preserving numerous glacial landforms recording multiple former glacier fluctuations.

The first major glaciation in Alaska occurred in the Miocene as Earth's climate began to cool throughout the Cenozoic (Karlstrom, 1961; Péwe, 1975; Meigs and Sauber, 2000). Glacial chronologies dating back to ~ 30 ka can be dated using radiocarbon providing that dateable material is present (Reger et al., 2007; Briner and Kaufman, 2008). Cosmogenic nuclides allow glacial reconstructions on timescales from 10^2-10^5 years and has been applied in Alaska, including the northern Brooks Range, the Alaskan Range, the landward side of the St. Elias Mountains in the Yukon, and the Ahklun Mountains (Briner et al., 2005; Barclay et al., 2009; Dortch et al., 2010; Kaufman et al., 2011; Table 2.1). To date, no cosmogenic based chronostratigraphies have been obtained for south central Alaska and the interior of the northwest extension of the Cordilleran Ice Sheet (Schmoll et al., 1999; Reger et al., 2007).

Radiocarbon and cosmogenic nuclide ages for moraines in Alaska date to the early last glacial (early Wisconsin), late last glacial (late Wisconsin) and Holocene, and using lichenometry, to the late Holocene (Karlstrom, 1964; Briner et al., 2005; Briner and Kaufman, 2008; Solomina et al., 2015; Kaufman et al., 2016). Reconstructions and dating consistently indicate that glaciers in Alaska reached their maximum extent during the early Wisconsin (Ager et al., 2004; Briner and Kaufman, 2008; Kaufman et al., 2011). This contrasts with the maximum global ice volumes that occurred over the global last glacial maximum (gLGM) during the late Wisconsin, which Mix et al. (2001) defines between ~24–18 ka in Marine Oxygen Isotope Stage (MIS) 2. Like other mountain glacial systems across the globe (Thackray et al., 2008) regional climatic and tectonic factors in Alaska favored glacial growth during the early Wisconsin as compared to the late Wisconsin (Briner and Kaufman, 2008). The early Wisconsin glaciation is

dated to between ~ 70 and 30 ka (Dreimanis and Goldthwait, 1973; Eyles and Westgate, 1987) in MISs 3 and 4 (Railsback et al., 2015). In Alaska, it has been defined by a few numerical dating studies of glacial landforms and sediments from major mountain ranges at 60 to 50 ka (Briner et al., 2005; Ward et al., 2007; Briner and Kaufman, 2008; Kaufman et al., 2011). These glaciations should be referred to as the local last glacial maximum (lLGM), since the maximum extent of glaciation was not coincident with the gLGM. Late Wisconsin glacial advances in Alaska have been dated to between 24 and 14 ka (Schmoll et al., 1999; Briner et al., 2005), but their timing varies between mountain ranges, e.g., 24–17 ka in the Brooks Range (Pendleton et al., 2015), ~ 22 ka in the Ahklun Mountains (Briner et al., 2005), 22–19 ka in the Alaska Range (Briner and Kaufman, 2008, Dortch et al., 2010), and 23–21 ka in the Yukon Tana Upland (Briner et al., 2005). The average glacial equilibrium-line altitude depression (ΔELA) in Alaska during the late Wisconsin was 300–700 m (Hamilton and Porter, 1975; Briner and Kaufman, 2000; Balascio et al., 2005). Cosmogenic-based exposure ages of 11–12 ka on several moraines in the Brooks, Ahklun, and Alaska ranges led Briner et al. (2001) to suggest that there were glacial advances during the Younger Dryas Stade: whether there was a widespread glacial advance during the Younger Dryas throughout Alaska has yet to be adequately determined. Five main glacial advances are recognized throughout Alaska during the Holocene: i) 9.8–9.1 ka; ii) 4.5–4.0 ka; iii) 3.3–2.9 ka; iv) 2.2–2.0 ka; and v) broadly equivalent to the Little Ice Age with three minor oscillations at 0.8–0.7, 0.4–0.3, and 0.3–0.2 ka (Calkin, 1998; Calkin et al., 2001; Solomina and Calkin, 2003; Barclay et al., 2009; Solomina et al., 2015; Kaufman et al., 2016).

The Quaternary glaciation of south central Alaska and Cook Inlet is complex because of strong climatic gradients, extreme topographic changes, and active tectonism that have strong local influences on the style and timing of glaciation. The regional variation in the timing of late

Wisconsin glacial advances in mountain ranges is possibly related to changes in climate relating to orographically controlled precipitation gradients and atmospheric circulation, plus changes in the dominant regional pressure systems as the Laurentide ice sheet advanced and retreated (Otto-Bliesner et al., 2006; Briner and Kaufman, 2008; Pendleton et al., 2015).

South central Alaska and the Chugach Mountains are warmer and wetter today than elsewhere in Alaska because of their maritime climate. Annual precipitation for the windward flank of the Chugach Mountains is ~ 2.5 m (National Climate Data Center, 2007). In contrast, the landward side of the Chugach Mountains is characterized by a colder continental interior climate with an annual precipitation of ~ 0.5 m (National Climate Data Center, 2007). Northwesterly moving winds bring moisture from the Pacific Ocean to south central Alaska and produce heavy orographic precipitation in the windward flanks of the Kenai and Chugach mountains (Reger et al., 2007).

A complex assemblage of moraines, glaciated surfaces, and outwash deposits are present in the Chugach Mountains and their lowlands around Anchorage (Fig. 3.2; Schmoll et al., 1999). Karlstrom (1958, 1964) first characterized these moraines and correlated them with a series of pre-Wisconsin (Mount Susitna, Caribou Hills, Eklutna and Knik) and Wisconsin events (Naptowne) in the Kenai Peninsula to the south west of Anchorage. The pre-Wisconsin events are loosely preserved as a series of moraines and deposits, which roughly correlate with the Nebraskan, Kansan, and Illinoin chronologies (Miller and Dobrovolny, 1959). The Naptowne event is characterized by four stades; i) Moose Horn (32–19 ka); ii) Killey (18.5–17.5 ka); iii) Skilak (17.5–16.0 ka); iv) and Elmendorf (15.0–12.0 ka). These are loosely defined by radiocarbon dating and stratigraphic evidence (Kulp, 1951, 1952; Karlstrom, 1958, 1964; Schmoll and Dobrovolny, 1972; Schmoll and Yehle, 1986; Reger and Updike,1983; Mann and

Peteet, 1994; Reger et al., 1996; Stilwell and Kaufman, 1996; Reger and Pinney, 1997; Schmoll et al., 1999; Ager, 2000; Reger et al., 2007; Table 2.1). The ages of the stades for the Naptowne glaciation are rough approximations, poorly defined by radiocarbon dating, unpublished results, and crudely defined tephra correlation. Table 2.1 shows a summary of radiocarbon chronology for the stades of the Naptowne glaciation; only the Elmendorf stade is consistent and reproducible. Reger et al. (2007) made it clear that the current chronologic model for the Naptowne event is poorly defined by radiocarbon dating and further work is required.

Valley glaciers that advance from the mountain ranges into the Cook Inlet characterize the regional glacial chronology for the Anchorage lowlands (Fig. 3.2; Schmoll et al., 1999). The largest valley glaciers advanced from the Alaska Range and Talkeetna Mountains, progressing southwards and down the Susitna River valley into Cook Inlet (Fig. 3.1). These glaciations traveled further and deposited foreign granite boulders and clasts high on the ridges and saddles of the Chugach Mountains, signifying that their magnitude was larger than the locally derived late Wisconsin events. Smaller glacial advances originated from the Knik-Matanuska advance to the north and the Turnagain Arm advance to the south along the Chugach Mountain front in the Anchorage area (Fig. 3.2; Schmoll and Yehle, 1986; Schmoll et al., 1999). These glacier advances are responsible for the late Wisconsin and Holocene moraines in the Anchorage region (Schmoll et al., 1999). The elevated region of the Chugach Mountains between these glacial centers and outlets was not covered by any significant glacier throughout the Holocene, resulting in good preservation of glacial deposits ranging from early to late Wisconsin (Schmoll et al., 1999; Fig. 3.2).

Miller and Dobrovolny (1959) Schmoll and Yehle (1986), Reger and Updike (1983) and Schmoll et al. (1999) mapped moraines in the Anchorage region. Schmoll et al. (1999) presents

a detailed characterization and correlation of moraines and glaciated surfaces in the Chugach lowlands (Fig. 3.2), including three early Wisconsin surfaces, seven late Wisconsin moraines, and three Holocene moraines. Moffit (1935) and Pewe (1975) mapped moraines and glacial features in Thompson Pass. Detailed reconstructions are few.

Evidence for early Wisconsin glacial advances includes intermittent till deposits draped over glacially polished mountaintops and saddles above late Wisconsin glacial trimlines (Schmoll et al., 1999). The oldest glacial surface in this region is at an elevation of ~1070 m asl on Flattop Mountain and similar saddles, and polished surfaces in the surrounding mountains, which are coeval with the Susitna glaciation (Fig. 3.3; Schmoll et al., 1999). Three younger early Wisconsin glacial advances are characterized by till draped over glacially polished plateau steps along the side of Flattop Mountain (Fig 3.4A). These three plateau steps, from oldest to youngest, are named Mount Magnificent, Glen Alps, and Ski Bowl (Fig. 3.4A; Schmoll et al., 1999).

Evidence for late Wisconsin glacial advances in the Chugach Mountains adjacent to Anchorage comprises a complex sequence of well-developed end and lateral moraines, trimlines, striations, and p-forms (Schmoll et al., 1999). There are five late Wisconsin moraines in this region, which from oldest to youngest are called the Little Rabbit Creek, Rabbit Creek, Fort Richardson, Dishno Pond, and Elmendorf moraines (Schmoll et al., 1999; Table 2.1). The Little Rabbit Creek moraine is characterized by a discontinuous series of lateral moraines at the mouths of valleys adjacent to Flattop Mountain (Fig. 3.3). Four continuous terminal and lateral moraines are present higher up in the valley, which Schmoll et al. (1999) suggested correlate to the Naptowne glaciations of Karlstrom (1964). Lateral moraines that form 3–5 m high ridges along the sides of the valleys and a distinct end moraine characterize the Rabbit Creek moraine (Fig.

3.3). The Fort Richardson moraine forms 6-10 m high well-developed lateral moraines along valley walls in the westernmost Chugach Mountains adjacent to Anchorage (Fig. 3.3). The Dishno Pond moraine forms low relief end and lateral moraines, which are characterized by a series of paternoster lakes and swampy brush (Fig. 3.3). The Elmendorf moraine is a well-preserved end moraine with lateral moraines present in the upper reaches of the valley (Fig. 3.3). Holocene end moraines, 300–500 m long, are nested in the cirques at the headwaters of the valley. These moraines are the only Holocene glacial geomorphic evidence present in the Williwaw Lakes Valley.

The Thompson Pass is a partially glaciated saddle in the Chugach Mountains east of Valdez (Fig. 3.1). Deep U-shaped valleys and notch canyons are present on either side of the pass, suggesting that glaciers have advanced down these valleys numerous times throughout the Quaternary (Fig. 3.5). This region is one of the wettest in Alaska with an annual precipitation of ~ 3.3 m (Western Regional Climate Center, 2016). Active glaciers are present in the mountains and adjacent valleys surrounding Thompson Pass. Little previous work has been undertaken on the timing and extent of Wisconsin and Holocene glaciations in and around Thompson Pass. Moffit (1935) was the first to completely survey and characterize the glacial limits and features of Thompson Pass and concluded that a majority of the region was under ice during the gLGM. Pewe (1975) mapped the glacial limits using topographic maps and correlating cirque elevations, but a detailed glacial chronology has not been developed for this region. Several glacially polished benches covered in moraine and comparatively small sharp-crested end and lateral moraines originating from valleys with modern day glaciers on Thompson Pass (Fig. 3.5).

METHODS

Mapping

We remapped, using aerial photography and topographic maps, the moraines described by Schmoll et al. (1999), which comprise three early Wisconsin surfaces and five late Wisconsin moraines in Williwaw Lake Valley and the glacial landforms in and around Thompson Pass. The maps consist of 90-m digital elevation models (DEMs) and Google Earth imagery (Image © 2015 DigitalGlobe and U.S. Geological Survey). We recorded the surficial characteristics and spatial limits of moraines and glacial trimlines in the field.

A total of five moraines, three surfaces covered in glacial debris, and two series of benches of equal elevation were dated. We chose these sites because they were accessible and there were datable surfaces and objects, e.g., boulders and glacially polished bedrock. The Holocene end moraines are ~ 0.5–2 km away from the snouts of modern day glaciers, which indicates that the field areas were last covered in ice by pre-Holocene activity. The lack of Holocene glacial activity probably contributed the preservation of older glacial moraines, bedrock surfaces, and boulders from the early and late Wisconsin. From west to east, the five moraines are situated in the Williwaw Lakes Valley: Little Rabbit Creek, Rabbit Creek, Fort Richardson, Dishno Pond, and Elmendorf moraines (Fig. 3.3; Schmoll et al., 1999). We dated glacial boulders and ice polished surfaces from three flat surfaces situated on top of mountains and ridge saddles around the Williwaw Lakes Valley and adjacent ridges, which Schmoll et al. (1999) considered to be early Wisconsin. These surfaces are located on top of Flattop Mountain (Fig. 3.4A), on a saddle below Ptarmigan Peak (Fig. 3.2), and on a sloped surface below Wolverine Peak (Fig. 3.3). Boulders and glacially polished bedrock were dated at two elevated locations in Thompson Pass (Fig. 3.5). The two locations comprise glacially polished bedrock benches, and can be correlated across the pass and adjacent valleys.

Sampling approach

Thirty-nine ^{10}Be and ^{36}Cl exposure-age samples were collected from glacial boulders and glacially eroded bedrock surfaces throughout the Chugach Mountains. Approximately 500 g of rock was collected from the top each sampled surface using a hammer and chisel, recording the thickness (1–7cm) of each sample. We aimed to define the ages of moraines by collecting samples from five boulders on each moraine and one to three samples on the glacially eroded surfaces. Boulders were preferentially selected from high, flat locations and raised ridges or crests of moraines to help reduce shielding by snow and/or any former sediment cover. The size and shape of the boulders and the geometry of the resting surface were used to help assess whether the boulders have been stable since deposition. The larger and more angular boulders were chosen because they were least likely to have moved since deposition as compared to well-rounded and smaller boulders.

Thirty-four of the samples were composed of sandstone, shale, and metasedimentary rocks locally sourced from the Chugach Group (Plafker et al., 1989). The other six samples were composed of granite, sourced from the Talkeetna Mountains to the north of the field area (Fig. 3.1). Fifteen granitic or quartz rich samples were analyzed for ^{10}Be. The remaining samples that contained little quartz, which is necessary for ^{10}Be dating, were processed for ^{36}Cl.

^{10}Be dating

Mineral separation for quartz and isolation of ^{10}Be was completed in the geochronology laboratories at the University of Cincinnati. Each sample was crushed and sieved down to 250–500 μm. Quartz was separated from each sample following the methods of Kohl and Nishizumi (1992), and were spiked with low-background Be carrier. ^{10}Be was separated and purified by ion

exchange chromatography and precipitated as $Be(OH)_2$ at pH > 7. The $Be(OH)_2$ was combusted by ignition in quartz crucibles, producing BeO. The BeO was mixed with Nb metal prior to being loaded into steel carriers. The $^{10}Be/^{9}Be$ ratios were measured via accelerator mass spectrometry (AMS) at the Purdue Rare Isotope Measurement (PRIME) Laboratory at Purdue University.

Ages were calculated using CRONUScalc (Marrero et al., 2015a), a web calculator that incorporates the globally calibrated production rates of Marrero et al. (2015b; Table 3.2). We chose the scaling factors of Lal (1991)/Stone (2000) and Lifton et al. (2014) for comparison (Table 3.2). The Young et al. (2013) production rate calibration (3.96±0.15 atoms/g SiO_2/yr) was chosen for these calculations because it best represents high latitude environments and is most comparable to the field area (Baffin Island). The average $^{10}Be/^{9}Be$ ratio for eight blanks was $1.21\pm0.7 \times 10^{-15}$, and the average total percent uncertainty, including analytical and production rate/scaling model uncertainty, for individual surface exposure ages is 8.2%, (Table 3.2).

^{36}Cl dating

Sample processing and chemical analysis for ^{36}Cl was conducted in the geochronology laboratories at the University of Cincinnati. Methods for sample preparation and isolation of ^{36}Cl follow the procedures of Stone et al. (1996). Samples were crushed and sieved down to < 250 μm to obtain 250 g of sample. The sample was leached in HNO_3 to remove contaminants and eliminate meteoric ^{36}Cl. A ~ 10 g aliquot was separated from the sample and sent to Bureau Veritas Mineral Laboratories in Vancouver, Canada for major trace element analysis using ICP-MS and FUS-MS (Appendix A in data supplement). 30 g of sample were dissolved in a

HF/HNO_3 solution and spiked with ~ 1.0 mg enriched ^{35}Cl. After dissolution, fluoride compounds were isolated through centrifuging and adding $AgNO_3$ and HNO_3 precipitated AgCl. AgCl was collected and dissolved in NH_4OH and Cl was subsequently extracted through anion exchange chromatography. AgCl was finally precipitated with the addition of $AgNO_3$ and HNO_3 and loaded into Cu cathodes for AMS analysis at PRIME Laboratories at Purdue University.

Ages were calculated using CRONUScalc (Marrero et al., 2015a). We chose the scaling factors of Lal (1991)/Stone (2000) and Lifton et al. (2014) for comparison (Table 3.3), where the production rates were 51.7±4.9 atoms/g Ca/yr and 60.1±8.2 atoms/g Ca/yr, respectively. The two blanks have an average $^{36}Cl/^{37}Cl$ value of 7.88±0.98 x 10^{-15}, and the average total percent uncertainty, including analytical and production rate/scaling model uncertainty, for the surface ages is 6.5%

Equilibrium-line altitude reconstructions

The geometry of the glacier limits for each of the late Quaternary glacial events was used to calculate the former surface of the glacier and was part of the modeling of the equilibrium-line altitude (ELA; Fig. 3.6). The results from field mapping of the Rabbit Creek, Fort Richardson, Dishno Pond, and Elmendorf glacial events provide estimates of past glacier limits. The locations of moraine termini and laterals, glacial trimlines, and striations, chatter marks, and p-forms were used to geographically reconstruct the former glacial surfaces of each event. The perimeter of nine modern glaciers in closest proximity to Williwaw Lakes Valley were mapped and used to model the current ELA for comparison. These include Eagle River, Whiteout, Eklutna, Hunter Creek, and other subsidiary glaciers in the westernmost Chugach Mountains (Table 3.4).

The ELAs were reconstructed for each well-mapped moraine in the Williwaw Lakes Valley and modern glaciers. The ELAs were calculated from reconstructed glacial limits in ArcGIS using the methods and tools from the work of Pellitro et al. (2015). The contemporary ELA was calculated with the techniques of Pellitro et al. (2015) on the nearest modern glaciers (Fig. 3.1), and were used to calculate a ΔELA for each method in the Williwaw Lakes Valley (Table 3.4). The ArcGIS toolbox from Pellitro et al. (2015) calculates the ELA using the area altitude (AA), accumulation area ratio (AAR), and area altitude balance ratio (AABR) methods. The AA method calculates the ELA by summing the products of area and average altitude for each contour and dividing the sum by the total area of the glaciated basin (Osmaston, 2005). The AAR method calculates the ELA by forming a ratio of the accumulation area to the total area of the glacier, where values of <0.5, 0.5–0.8, and > 0.8 indicate negative mass balance, steady state, and positive mass balance, respectively (Osipov, 2004). The AABR method expands upon the AA method and calculates the ELA by iteratively calculating multiple former glacier mass balances for all possible ELAs (Osmaston, 2005; Pellitro et al., 2015).

Till pebble counts

The character and dimensions of deposits for each moraine provides information on the provenance and the distance the clasts traveled in the glacier before being deposited. The till from each moraine and glaciated surface were characterized using a variant of the Wolman's pebble count method (Wolman, 1954; Sampson and Smith, 2006). This technique involved laying out a measuring tape to 50 m across sections of the moraines that were not obscured by soil or vegetation and collecting clasts every 0.5 m. The intermediate axis, the angularity and composition of 100 clasts (1 clast per every 0.5 m) were recorded for the moraines and surfaces in this study (see Appendix B in data supplement).

Statistical analysis of exposure ages

Exposure ages for each moraine were averaged and statistically analyzed for scatter and outliers. Each data cluster associated with an event that had more than two ages was averaged using a weighted mean (Fig. 3.7). We calculated the reduced chi-square (X^2) statistic for each data set to determine the degree of scatter of the data sets using:

$$X_R^2 = \frac{1}{n-1} \sum_{i=n}^{n} \left[\frac{t_i - \bar{t}_i}{\sigma t_i} \right]^2 \quad (1)$$

where n = the number of ages, t_i = the exposure age, $\overline{t_i}$ = the average of ages, and σt_i = the age uncertainties (Balco, 2010: Fig. 3.7). The five moraines in Williwaw Lakes Valley and Bench 1 in Thompson Pass were analyzed in this way. In addition, the ages of each moraine were graphically depicted as a probability plot. The age mode, which corresponds with the peak of the probability plot, was reported and compared with the weighted mean age.

DESCRIPTION OF DETAILED STUDY AREAS

Early Wisconsin surfaces in the Chugach mountain front near Anchorage are present below Ptarmigan Peak (Fig. 3.2), on Flattop Mountain (Fig. 3.4A), and above Williwaw Lakes Valley (Fig. 3.3). Suitably sized and stable boulders were sampled from these surfaces. There are four early Wisconsin aged surfaces (Schmoll and Yehle, 1986) near Flattop Mountain, which form flat benches that are covered in moraine and boulders (Fig. 3.4A). The lowest surface is the Skibowl deposit, the second surface is Glen Alps, the third surface is Mount Magnificent, and the highest surface is the summit of Flattop Mountain (Fig. 3.4A). A saddle shaped bench at ~ 1100 m asl forms an indent in the mountain belt beneath the summit of Ptarmigan Peak. Hummocky

moraine and glacial boulders are present on this surface, which have been eroded during seasonal streams since deposition. Plateaus contain four early Wisconsin moraines above Williwaw Lakes Valley, which are located along the ridges of the valley and adjacent mountains (Fig. 3.3). These surfaces are sub-horizontal and lie ~ 200 m above the glacial trimlines of the late Wisconsin events, and are located on Wolverine Peak, the Ball Field, below O'Malley Peak, and below Williwaw Peak (Fig. 3.3). All the early Wisconsin moraine surfaces comprise mainly Chugach Group metasedimentary rocks mixed with a small portion (~ 3%) of granitic clasts (See Appendix B). The granitic clasts are well rounded and the Chugach Group clasts are very angular (Fig. 3.4B). Wolverine Peak has anomalously high (~ 16%) granitic content, and most of the boulders have intermediate axes lengths of > 5 m (Fig. 3.4C).

Discontinuous lengths of lateral moraine characterize the Little Rabbit Creek moraine that is in the lower reaches of the Williwaw Lakes Valley (Fig. 3.3). Pine trees, short shrubs, and tall grasses grow on the moraine and obscure any small-scale glacial features and the majority of the boulders (Fig. 3.4D, 3.8A). Significant erosion and the abundant vegetation have conspired to create smooth surface features and subdued moraine morphology. The middle of the moraine is at the mouth of the valley and is characterized by a ridge of glacial deposits that are ~ 500 m long and ~10 m high, with gravel and boulders on its surface (Fig. 3.8A).

The Rabbit Creek moraine is also located in the Williwaw Lakes Valley and is an end moraine and a discontinuous set of lateral moraines (Fig. 3.3). The moraine has ridges that raise some 5 m above the surrounding ground and are juxtaposed against the Little Rabbit Creek moraine (Fig. 3.4D, 3.8B). Short grass, moss, and pine trees grow on the moraine and obscure the majority of glacial landforms. The center of the moraine forms a ridge composed of bands of

gravel and boulders (Fig. 3.8B). The moraine is bisected on the northern and southern sides by meltwater channels, which has resulted in substantial erosion of the moraine.

The Fort Richardson moraine in the Williwaw Lakes Valley is composed of a discontinuous end and well-formed lateral moraines (Fig. 3.3, 3.4E). The two lateral ridges are ~ 5–8 m high and a kame terrace is present within the moraine. Pines and moss grow on the moraine, and the lateral moraines have gravel, boulders, and short shrubs on the surface (Fig. 3.8C).

An end and lateral moraines define the Dishno Pond moraine in Williwaw Lakes Valley (Fig. 3.3). The end moraine is ~ 2 m high that protrudes from the marsh-like interior of the Fort Richardson moraine. The moraine surface consists of hummocks and kame terraces, and is covered in shrubbery and flat gravel deposits (Figs. 3.3, 3.8D). There is also a series of paternoster lakes throughout the moraine (Fig. 3.3).

The Elmendorf moraine, located at the juncture of the main arms of the Williwaw Lakes Valley, is an end moraine with lateral moraines (Fig. 3.3). The headwaters of the valley are covered by a thin veneer of till and contains roche moutonnées ranging in height from ~ 1 to 3 m. Lower in the valley, there are thicker deposits and variably sized hummocks that range in height from ~ 2 to 6 m. The moraine surfaces include patches of exposed gravel, short grass, and moss (Fig. 3.8E).

The Thompson Pass has broad 1-10 km wide bedrock benches that have been eroded and shaped by valley glaciers (Fig. 3.5, 3.8F). There are three glacially carved benches at ~ 600, 800, and 1,200 m asl, which we refer to as B1, B2, and B3, respectively (Fig. 3.5). These benches are discontinuous throughout the valleys in this region. B1 is characterized by a series of east/west trending ridges. These ridges range in height from ~ 5–10 m and alternate between

raised bedrock ridges and low-lying swamps and vegetated terrain. The vegetated sections of the bench are covered in dense shrubs, conifers, and moss. B2 is characterized by ~ 3–15 m high east trending bedrock ridges alternating with swampy terrain. The bedrock has a well-developed glacial polish and ~ 2–4 m diameter boulders are present on its surfaces. The exposed bedrock on B1 and B2 exhibits well-preserved p-forms, striations, and chatter marks. B3 is characterized by exposed, polished bedrock paired with roche moutonnées, and small ponds and streams.

DATING RESULTS

Five ^{10}Be samples from the early Wisconsin boulders on glaciated benches yield ages ranging from 55 to 15 ka (Table 3.2). A granitic boulder on top of Flattop Mountain has an age of ~ 51.1 ± 4.5 ka and two granitic boulders from the saddle beneath Ptarmigan Peak yield ages of 55.8 ± 4.4 and 36.2 ± 2.9 ka (Fig. 3.4A, 3.9). Two granitic boulders from Wolverine Peak date to 26.0 ± 2.0 and 15.8 ± 1.2 ka (Fig. 3.3), and a single granitic boulder from Flattop Mountain dates to ~ 51.1 ± 4.5 ka. There is a wide range of ages on the early Wisconsin surfaces except for the age on Ptarmigan Peak and Flattop Mountain, which each have ages of ~ 50 ka.

Boulders in the Williwaw Lake Valley yield ^{36}Cl ages ranging from 28.5 to 13.7 ka (Table 3.3, Fig. 3.7). The Little Rabbit Creek (28.5–13.7 ka) has a weighted average of 23.8 ka with a X^2 value of 0.66 (Fig. 3.7) and 24.6 ka modal age from the probability plot (Fig. 3.9B). The Rabbit Creek (26.6 –18.5 ka) has a weighted average age of 22.3 ka with a X^2 value of 1.35 (Fig. 3.7), and 22.2 ka average age from the probability plot (Fig. 3.9C). The Fort Richardson (18.1–16.2 ka) has a weighted average age of 17.1 ka with a reduced X^2 value of 0.58 (Fig. 3.7), and 17.1 ka modal age from the probability plot (Fig. 3.9D). The Dishno Pond (19.1–16.9 ka) has a weighted age average of 17.9 ka (Fig. 3.7) with a reduced X^2 value of 0.7, and 17.8 ka modal age from the probability plot (Fig. 3.9E). The Elmendorf (19.4 –14.3ka) has a weighted

average age of 14.9 ka (Fig. 3.7) with a reduced X^2 value of 0.42, and 14.8 ka modal age from the probability plot (Fig. 3.9F).

On Thompson Pass, ^{10}Be dating of boulders and polished bedrock surfaces resulted in ages ranging from 22.3 to 0.7 ka (Table 3.2). The B2 (14.0–11.4 ka) weighted average age is 13.7 ka with a reduced X^2 value of 0.2, and 13.8 ka modal age from the probability plot (Fig. 3.9G). The B3 (18.5–17.8 ka) weighted average of two ages is 18.1 ka. A single sample from polished bedrock was collected to test for inheritance ~ 100 m downstream from the modern ice limit of Worthington Glacier, which yield in an age of ~ 0.7 ka.

ELA RESULTS

The average modern ELAs for the closest glaciers to Williwaw Lakes Valley are 1435 (AA), 1381 (AABR), and 1525 m asl (AAR) (Table 3.4). Dial et al. (2016) calculated the ELA for Eklutna glacier to be 1395 m asl, which closely correlates to our result of 1389 m obtained through the AABR method of Pelliterio et al. (2015). However, our ELA values calculated using the AA and AAR methods yielded results of 1417 and 1489 m asl, respectively, which do not compare favorably with the values of 1395 m from Dial et al. (2016). This relationship indicates that the AABR method is the most realistic ELA estimate for the western Chugach Mountains and that the AA and AAR techniques overestimate ELA. The ΔELA for the Williwaw Lakes moraines from the AABR technique are 314 (Rabbit Creek), 298 (Fort Richardson), 298 (Dishno Pond), and 309 m (Elmendorf) (Fig. 3.6A)

DISCUSSION

The new ages for the early Wisconsin surfaces span much of the last glacial at ~ 55–15 ka. The early Wisconsin ages recorded in the Ahklun Mountains show a maximum age of ~ 70 ka (Kaufman et al., 2001), a minimum age of ~ 39 ka (Manley et al., 2001) and a range of 56–53 ka (Briner et al., 2001). The ages on Ptarmigan Peak (55.8 ± 4.4 and 36.2 ± 2.7 ka) and age on Flattop Mountain (51.1 ± 4.5 ka) provide a minimum age for the timing for the local glacial maximum during of the early Wisconsin in the Chugach Mountains. The younger age is a product of settling post deposition or movement from stream erosion on the surface. The ages on boulders on Wolverine Mountain of 26.0 ± 2.0 and 15.8 ± 1.2 ka tentatively suggest that a glacier advanced across this area during the late Wisconsin. These granitic boulders have probably shifted since their deposition in the early Wisconsin and are not reliable representations of the age of the glaciation. The ages of these boulders, however, correlate with the timing of the Little Rabbit Creek/Rabbit Creek and Fort Richardson/Dishno Pond glaciations. The boulders may have been moved by surface creep in the till or seismic activity during those time periods. These mechanisms appear to be responsible for the large numbers of outliers in the early Wisconsin data set. The remaining ages that date to the early Wisconsin correlate with the ~ 50 ka ages of Briner et al. (2001).

The presence of granitic boulders and clasts on the early Wisconsin surfaces indicate that glaciers transported debris from ~ 80 km in the Talkeetna Mountains, where the nearest granite outcrops occur, to the Chugach Mountains (Fig. 3.1). Only very large glaciations could have transported the granite from these ranges and deposit them at over 1000 m on the ridges in the Chugach Mountains. The large contrast between the granitic clasts (well rounded) and the Chugach Group clasts (angular) implies that the granitic material was transported and mixed with the local material (see clast data in Appendix B). None of the sampled late Wisconsin

moraines contain granitic clasts and are composed of rock types present in the Chugach Mountains. This suggests that the glacial advances were smaller in the late Wisconsin as compared to early Wisconsin glacial.

The ^{36}Cl ages in Williwaw Lakes Valley range from 28.5 to 13.7 ka (Figs. 3.3 and 3.7). The ages of the moraines in the Williwaw Lakes Valley are oldest at the mouth of the valley and become sequentially younger up-valley. These ages conform to the general pattern of deglaciation across Alaska since the gLGM as described by Briner and Kaufman (2008). The ages of the moraines in the Williwaw Lakes Valley correlate with the Naptowne glaciation on the Kenai Peninsula. The new ages better define the ages of the Naptowne stades (Fig. 3.9A; Karlstrom, 1964; Reger et al., 2007).

The Little Rabbit Creek (average age of 23.8 ± 1.5 ka) and Rabbit Creek (average age of 22.3 ± 1.4 ka) moraines are both coeval with the Moosehorn stade (Fig. 3.9A; Reger et al., 2007). The broad age range, 32–19 ka, for the Moosehorn stade includes both the Little Rabbit and Rabbit Creek events. This inclusion of both Rabbit Creek moraines implies that there were either two advances in the Anchorage region during this period or that the range of the Moosehorn stade is not well defined (Reger et al., 2007). Schmoll et al. (1999) suggested that the Little Rabbit moraine formed during the early Wisconsin, yet our new ages suggest that it is much younger and has a similar age to the Rabbit Creek event. Although our ages suggest a younger deposition for the Little Rabbit Creek moraine, the high number of outliers, reduced X^2 values, and uncertainties discourage this notion without more ages (Table 3.3; Fig. 3.7).

Although the Fort Richardson moraine is geographically situated down stream of Dishno Pond moraine, the Fort Richardson moraine average age of 17.1 ± 1.2 ka is younger by 0.8 ka than Dishno Pond moraine (17.9 ± 1.1 ka). Relative dating and mapping of the Fort

Richardson and Dishno Pond moraines correlates them with the timing of the Killey and Skilak Naptowne stades, respectively (Schmoll et al., 1999; Reger et al., 2007). The details of the Fort Richardson moraine are discussed below, but since it is physically bracketed between Rabbit Creek and Dishno Pond, the age must be between 22.2 and 17.9 ka, which correlates with the Killey stade (18.5–17.5 ka; Fig. 3.9A). The Dishno Pond moraine morphostratigraphically correlates with the Skilak moraine by Schmoll et al. (1999). The age on Dishno Pond moraine is slightly older (17.9 ± 1.1 ka) than the age assigned to the Skilak stade (17.5–16.0 ka), implying that the Skilak stade should span the time of ~ 18.0–16.0 ka. Our new Elmendorf ages of 14.9 ± 0.9 ka correlate very well with the established age of the Elmendorf stade at 15.0–12.0 ka, and support the prior extensive radiocarbon dating (Fig. 3.9A; Reger et al., 2007).

The Fort Richardson moraine has the tightest cluster of ages and lowest reduced X^2 value of 0.58 (Fig. 3.7), yet these ages do not fall between those of Dishno Pond and Rabbit Creek moraines. This age anomaly was most likely caused by mass wasting that reorganized the moraine material after its original deposition (Fig. 3.3). Since all five ages reproduce well, it is likely that one event disturbed the moraine. The southern lateral moraine from which the samples were acquired does appear to have undergone erosion from a mass wasting event originating from the north-facing wall below the Ball Field (Fig. 3.3, 3.4E). Although the ridge crest of the lateral moraine does not appear to have been eroded, it is possible that the mass-wasting event pushed the material away from the wall, shifting the boulders at the surface and "resetting" the exposure ages.

The ΔELAs in Williwaw Lakes Valley ranged from 298 to 314 m for several advances during the late Wisconsin. These ΔELA are consistent with the lower limit ΔELA values of ~ 300–600 m of Briner and Kaufman (2000) in western Alaska and ΔELA of ~ 200–700 m of

Balascio et al. (2005) in the Brooks Range. Balascio et al. (2005) concluded that the Alaskan ΔELAs were ~ 600 m less than the global average (~ 1000 m) for the gLGM (Broecker and Denton, 1990), which was indicative of a precipitation deficit throughout the late Wisconsin (Porter et al., 1983; Kaufman and Manley, 2004). During the gLGM sea level was ~ 125 m lower (Fairbanks, 1989), and the coast of the Bering Sea retreated ~ 600 km exposing a continental shelf. This greater continentiality would have helped reduce precipitation in Alaska (Broecker, 1997). Our ΔELA values are substantially lower than the average ΔELA for Alaska during the lLGM (Balascio et al., 2005) of ~ 600 m. The lower ΔELA values suggest that either the western Chugach Mountain glaciers may have received less precipitation than the surrounding mountains or that temperatures were warmer.

The ΔELA and lapse rate for a region can be used to estimate the past temperature depressions (Porter, 2000). Determining temperature changes based on ΔELA is challenging because precipitation changes also affect ΔELA, but if we simply relate the change to temperature, this provides a maximum temperature depression (Seltzer, 1994). Assuming a mean alpine environmental lapse rate of -5.7 °C/km (Rolland, 2003; Kirchner et al., 2013), the ΔELA from each event in the Williwaw Lakes Valley results in temperature depressions ranging from 1.6 to 1.7 °C. This analysis provides us with a maximum temperature depression for the gLGM in the Chugach Mountains. With a likely reduction in precipitation over the gLGM it is possible that a drop in freezing elevation may have inhibited further glacial retreat. The average temperature depressions for the tropical glaciers during the gLGM was 5-6.4°C (Porter, 2000) and as high as 8.8-11°C in the central Andes (Stansell et al., 2007). The comparatively low temperature depression in the Chugach Mountains, imply that the climate was warmer in Alaska than the global temperatures during the gLGM. Previous studies across Alaska have observed

similar ΔELA depressions and conclude that the region was more arid than other glaciated places during the late Wisconsin (Briner and Kaufman, 2000; Briner et al., 2001; Kaufman and Manley, 2004; Briner and Kaufman, 2008)

The ^{10}Be exposure ages and glacial trimline locations in Thompson Pass area show that late Wisconsin glaciation advanced at least twice and completely covered the pass. These ages are the first for the region and show that the last two glacial advances where Thompson Pass was covered by ice was ~ 18.1 and ~ 13.7 ka (Fig. 3.5). The highest consistent glacial trimline on Thompson Pass is at ~ 1300 m asl (Fig. 3.5) suggesting an earlier than MIS 2 glacial advance in this region. The single age of 11.4 ka suggests a Younger Dryas advance, yet more ages are needed to substantiate this claim. The sample was obtained from polished bedrock ridge above a heavily glaciated region of the pass at an elevation of 1677 m asl. The fact that there is no other evidence for Younger Dryas ages except for a ridge sample directly above modern glaciers implies that if there was a Younger Dryas advance in Thompson Pass it was restricted to glaciers at high elevation that did not cover the pass.

The new ages provide the first glacial chronology for the Chugach Mountain, which in turn can be used to establish chronologies in adjacent regions throughout the Chugach Mountains and Prince William Sound. Comparison of the Chugach chronology with the timing of glaciation in adjacent mountain ranges depicts a broad pattern of uniform deglaciation in Alaska ranges with slightly younger ages (by 16 to 17 ka) towards the southeast and the main body of the Laurentide ice sheet (Fig. 3.10). Specifically, the pattern of deglaciation follows the topographically high mountain ranges of Alaska where precipitation gradients control the style and magnitude of glaciation. The former extent of glaciers, thickness of the ice, and temperature of the basal ice indicate the effect of erosion the glaciers had on the landscape and orogen

development through time. It seems likely that climate is changing again. Glacial activity in Cook Inlet and the surrounding mountains may behave asynchronously in the future relative to the global patterns, as it did during the lLGM and gLGM.

CONCLUSION

Geomorphic mapping, ^{10}Be and ^{36}Cl exposure age dating, and ELA reconstructions help define the timing and climatic environment since the lLGM in the western Chugach Mountains of Alaska. Correlation of ages on the early Wisconsin surfaces indicate that the Susitna glaciation and regional last glacial maximum may have reached its largest extent by ~ 50 ka. The presence of rounded granitic clasts (3-14 %) in the early Wisconsin moraines indicate an origin from either the Talkeetna Mountains or Alaska Range to the north, and support the current model that the lLGM glaciations were larger than the gLGM events since the boulders were transported and deposited ~ 1000 m above the current valley level. Exposure ages in Williwaw Lakes Valley establish a chronology for moraines that roughly correspond to the stades of the Naptowne chronology on the Kenai Peninsula to the south. The Little Rabbit (23.8 ka) and Rabbit Creek (22.3 ka) moraines have the widest age uncertainty yet still correlate with the Moosehorn stade. The Fort Richardson (17.1 ka) and Dishno Pond (17.9 ka) moraine ages are close to one another and correlate with the Killey and Skilak stades. The Elmendorf moraine ages cluster well around 14.9 ka and correspond very well with the prior work (Table 3.1) and dating on this event. Ages from Thompson Pass exhibit two age clusters at 13.7 ka and 18.1 ka, which correspond to B2 moraine (at ~ 800 m asl) and B3 moraine (at ~ 1200 m asl), respectively. A single age of 11.4 ka at an elevation of 1677 m suggest a Younger Dryas advance, which was limited to the highest cirques in Thompson Pass, but more dating is needed to confirm this view. Digital and field

based geomorphic mapping facilitated the reconstruction of the past ice extent in Williwaw Lakes Valley and calculation of ELAs during the late Wisconsin. The ΔELAs range from 298-314 m that correspond with the low average of ΔELAs from other mountain ranges in Alaska implying that the climate was dryer and warmer than the global average during the gLGM. The asynchronuity of glaciation across maritime and continental Alaska is controlled by steep orographic precipitation gradients which result from upper plate deformation pertaining to the active tectonics of the region.

REFERENCES

Abers, G.A., 2008. Orogenesis from subducting thick crust and evidence from Alaska. Active Tectonics and Seismic Potential of Alaska vol. 179. American Geophysical Union Monograph Series, 337–349.

Ager, T.A., 1983. Holocene vegetational history of Alaska, in Wright, H.E., Jr., ed., Late-Quaternary environments of the United States, v. 2, The Holocene: Minneapolis, University of Minnesota Press, 128–141.

Ager, T. A. 2000. Postglacial vegetation history of the Kachemak Bay area, Cook Inlet, south-central Alaska, in Kelley, K.D., and Gough, L.P., eds., Geologic Studies in Alaska by the U.S. Geological Survey, 1998: U.S. Geological Survey Professional Paper 1815, p. 147–165.

Ager, T. A., & Carrara, P. E. 2011. Latest Wisconsin Deglaciation and Postglacial Vegetation Development in the Turnagain Arm Area, Upper Cook Inlet, South-Central Alaska.

Ager, T. A., Axford, Y., Balascio, N. L., Begét, J. E., Brigham-Grette, J., Briner, J. P., ... & Reger, R. D. 2004. Pleistocene maximum and Late Wisconsinan glacier extents across Alaska, USA. *Quaternary Glaciations-Extent and Chronology: Part II: North America*, *2*, 9.

Arkle, J., Armstrong, P., Haeussler, P., Prior, M., Hartman, S., Sendziak, K., Brush, J., 2013. Focused exhumation in the syntaxis of the western Chugach Mountains and Prince William Sound, Alaska. Geol. Soc. Am. Bull. 125 (5–6), 776–793. http://dx.doi.org/10. 1130/b30738.1.

Badding, M. E., Briner, J. P., & Kaufman, D. S. (2013). 10Be ages of late Pleistocene deglaciation and Neoglaciation in the north-central Brooks Range, Arctic Alaska. *Journal of Quaternary Science*, *28*(1), 95-102.

Balascio, N. L., Kaufman, D. S., & Manley, W. F. 2005. Equilibrium-line altitudes during the last glacial maximum across the Brooks Range, Alaska. *Journal of Quaternary Science*, *20*(7), 821.

Balco, G. 2010. Contributions and unrealized potential contributions of cosmogenic-nuclide exposure dating to glacier chronology, 1990–2010.*Quaternary Science Reviews*, *30*(1), 3-27.

Barclay, D. J., Wiles, G. C., & Calkin, P. E. 2009. Holocene glacier fluctuations in Alaska. *Quaternary Science Reviews*, *28*(21), 2034-2048.

Berger, A.L., Spotila, J.A., Chapman, J.B., Pavlis, T.L., Enkelmann, E., Ruppert, N.A., Buscher, J.T., 2008. Architecture, kinematics, and exhumation of a convergent orogenic wedge: a thermochronological investigation of tectonic–climatic interactions within the central St. Elias Orogen, Alaska. Earth Planet. Sci. Lett. 270 (1–2), 13–24. http://dx.doi.org/10.1016/j.epsl.2008.02.034.

Briner, J. P., & Kaufman, D. S. 2000. Late Pleistocene glaciation of the southwestern Ahklun mountains, Alaska. *Quaternary Research*, *53*(1), 13-22.

Briner, Jason P., Darrell S. Kaufman, Al Werner, Marc Caffee, Laura Levy, William F. Manley, Michael R. Kaplan, and Robert C. Finkel. "Glacier readvance during the late glacial (Younger Dryas?) in the Ahklun Mountains, southwestern Alaska." *Geology* 30, no. 8 (2002): 679-682.

Briner, J. P., & Kaufman, D. S. 2008. Late Pleistocene mountain glaciation in Alaska: key chronologies. *Journal of Quaternary Science, 23*(6-7), 659-670.

Briner, J. P., Kaufman, D. S., Manley, W. F., Finkel, R. C., & Caffee, M. W. 2005. Cosmogenic exposure dating of late Pleistocene moraine stabilization in Alaska. *Geological Society of America Bulletin, 117*(7-8), 1108-1120.

Briner, J. P., Swanson, T. W., & Caffee, M. 2001. Late Pleistocene cosmogenic 36 Cl glacial chronology of the southwestern Ahklun Mountains, Alaska. *Quaternary Research, 56*(2), 148-154.

Broecker, W.S., 1997. Mountain glaciers: recorders of atmospheric water vapor content? Global Biogeochemical Cycles 11, 589-597.

Broecker, W. S., & Denton, G. H. (1990). The role of ocean-atmosphere reorganizations in glacial cycles. *Quaternary Science Reviews, 9*(4), 305-341.

Bruhn, R., Haeussler, P., 2006. Deformation driven by subduction and microplate collision: geodynamics of Cook Inlet basin, Alaska. Geol. Soc. Am. Bull. 118 (3–4), 289–303. http://dx.doi.org/10.1130/b25672.1.

Buscher, J.T., Berger, A.L., Spotila, J.A., 2008. Exhumation in the Chugach–Kenai Mountain Belt above the Aleutian Subduction Zone, Southern Alaska. Active Tectonics and Seismic Potential of Alaska vol. 179. American Geophysical Union Monograph Series, 151–166.

Calkin, P. E., Kaufman, D. S., Przybyl, B. J., Whitford, W. B., & Peck, B. J. 1998. Glacier regimes, periglacial landforms, and Holocene climate change in the Kigluaik Mountains, Seward Peninsula, Alaska, USA. *Arctic and Alpine Research*, 154-165.

Calkin, P. E., Wiles, G. C., & Barclay, D. J. 2001. Holocene coastal glaciation of Alaska. *Quaternary Science Reviews*, *20*(1), 449-461.

Dial, R. J., Becker, M., Hope, A. G., Dial, C. R., Thomas, J., Alexandrovna, K., Golden, T. S., Shain, D. H. 2016. The role of temperature in the distribution of the glacier ice worm Mesenchytraeus solifugus (Annelida: Oligochaeta: Enchytraeidae). *Arctic, Antarctic, and Alpine Research,* 48

Dortch, J. M., Owen, L. A., Caffee, M. W., Brease, P. 2010. Late Quaternary Glaciation and Equilibrium Line Altitude Variations of the McKinley River Region, Central Alaska Range. *Boreas*, *39*(2), 233-246.

Dortch, J. M., Owen, L. A., Caffee, M. W., Li, D., & Lowell, T. V. (2010). Beryllium-10 surface exposure dating of glacial successions in the Central Alaska Range. *Journal of Quaternary Science*, *25*(8), 1259-1269.

Dreimanis, A., & Goldthwait, R. P. (1973). Wisconsin glaciation in the Huron, Erie, and Ontario lobes. *Geological Society of America Memoirs*, *136*, 71-106.

Eyles, N., & Westgate, J. A. (1987). Restricted regional extent of the Laurentide Ice Sheet in the Great Lakes basins during early Wisconsin glaciation. *Geology*, *15*(6), 537-540.

Fairbanks, R.G., 1989. A 17,000-year glacio-eustatic sea level record: influence of glacial melting rates on the Younger Dryas event and deep-ocean circulation. Nature 342, 637-642.

Finzel, E.S., Trop, J.M., Ridgway, K.D., Enkelmann, E., 2011. Upper plate proxies for flat-slab subduction processes in southern Alaska. Earth Planet. Sci. Lett. 303 (3–4), 348–360. http://dx.doi.org/10.1016/j.epsl.2011.01.014.

Fuis, G., Moore, T., Plafker, G., Brocher, T., Fisher, M., Mooney, W., Nokleberg, W., Page, R., Beaudoin, B., Christensen, N., Levander, A., Lutter, W., Saltus, R., Ruppert, N., 2008. Trans-Alaska Crustal Transect and continental evolution involving subduction underplating and synchronous foreland thrusting. Geology 36 (3), 267–270. http://dx.doi. org/10.1130/g24257a.1.

Haeussler, P.J., 2008. An overview of the Neotectonics of interior Alaska: far-field deformation from the Yakutat microplate collision. Active Tectonics and Seismic Potential of Alaska. American Geophysical Union Geophysics Monograph Series 179, pp. 83–108.

Hamilton, T. D., & Porter, S. C. 1975. Itkillik glaciation in the Brooks Range, northern Alaska. *Quaternary Research, 5*(4), 471-497.

Kaufman, D. S., Manley, W. F., Forman, S. L., & Layer, P. W. (2001). Pre-Late-Wisconsin glacial history, coastal Ahklun Mountains, southwestern Alaska–new amino acid, thermoluminescence, and 40 Ar/39 Ar results. *Quaternary Science Reviews*, *20*(1), 337-352.

Kaufman, D.S., Manley, W.F., 2004. Pleistocene maximum and Late Wisconsinan glacier extents across Alaska, U.S.A. In: Ehlers, J., Gibbard, P.L. (Eds.), Quaternary Glaciations – Extent and Chronology, Part II: North America. Developments in Quaternary Science, vol. 2B. Elsevier, Amsterdam, pp. 9–27.

Kaufman DS, Young NE, Briner JP, and Manley WF 2011. Alaska PalaeoGlacier Atlas version 2. In: Ehlers J and Gibbard PL (eds.) Quaternary Glaciations Extent and Chronology, Part IV: A Closer Look. Developments in Quaternary Science, pp. 427–445. Amsterdam: Elsevier.

Karlstrom, T.N.V., 1958. Ground conditions and surficial geology of the Kenai–Kasilof area, Kenai Peninsula, south-central Alaska: U.S. Geological Survey Miscellaneous Geologic Investigations Map I-269, 1 sheet, scale 1:63,360.

Karlstrom, T. N. 1961. THE GLACIAL HISTORY OF ALASKA: ITS BEARING ON PALEOCLIMATIC THEORY*. *Annals of the New York Academy of Sciences, 95*(1), 290-340.

Karlstrom, T. N. 1964. *Quaternary geology of the Kenai lowland and glacial history of the Cook Inlet region, Alaska* (No. 443). US Govt. Print. Off.,.

Karlstrom, T. N. V. 1968. The Quaternary time scale-a current problem of correlation and radiometric dating. *Means of correlation of Quaternary successions: Internat. Assoc. Quaternary Research 7th Cong., USA, 1965, Proc, 8*, 121-150.

Kirchner, M., Faus-Kessler, T., Jakobi, G., Leuchner, M., Ries, L., Scheel, H. E., & Suppan, P. (2013). Altitudinal temperature lapse rates in an Alpine valley: trends and the influence of season and weather patterns. *International Journal of Climatology*, *33*(3), 539-555.

Kohl CP, Nishizumi K. 1992. Chemical isolation of quartz for measurement of in situ produced cosmogenic nuclides. Geochemica et Cosmochemica Acta 56: 3583–3587

Kulp, J. L., Feely, H. W., Tryon, L. E. 1951. Lamont natural radiocarbon measurements. Science, 114, 565-568.

Kulp, J. L., Tryon, L. E., Eckelman, W. R., Snell, W. A. 1952. Lamont natural radiocarbon measurements. Science, 16, 409-414.

Lal, D. 1991. Cosmic ray labeling of erosion surfaces: in situ nuclide production rates and erosion models. *Earth and Planetary Science Letters*,*104*(2-4), 424-439.

Lifton, N., Sato, T., & Dunai, T. J. 2014. Scaling in situ cosmogenic nuclide production rates using analytical approximations to atmospheric cosmic-ray fluxes. *Earth and Planetary Science Letters*, *386*, 149-160.

Mann, D. H., & Peteet, D. M. 1994. Extent and timing of the last glacial maximum in southwestern Alaska. *Quaternary Research*, *42*(2), 136-148.

Manley, W. F., Kaufman, D. S., & Briner, J. P. 2001. Pleistocene glacial history of the southern Ahklun Mountains, southwestern Alaska: Soil-development, morphometric, and radiocarbon constraints. *Quaternary Science Reviews*, *20*(1), 353-370.

Marrero, S. M., Phillips, F. M., Borchers, B., Lifton, N., Aumer, R., & Balco, G. 2015. Cosmogenic nuclide systematics and the CRONUScalc program. *Quaternary Geochronology*, *31*, 160-187.

Marrero, S. M., Phillips, F. M., Caffee, M. W., & Gosse, J. C. 2015. CRONUS-Earth cosmogenic 36 Cl calibration. *Quaternary Geochronology*,*31*, 199-219.

Matmon, A., Schwartz, D. P., Haeussler, P. J., Finkel, R., Lienkaemper, J. J., Stenner, H. D., & Dawson, T. E. (2006). Denali fault slip rates and Holocene–late Pleistocene kinematics of central Alaska. *Geology*, *34*(8), 645-648.

Meigs, A., & Sauber, J. 2000. Southern Alaska as an example of the long-term consequences of mountain building under the influence of glaciers. *Quaternary Science Reviews, 19*(14), 1543-1562.

Miller, R. D., & Dobrovolny, E. (1959). *Surficial geology of Anchorage and vicinity, Alaska* (Vol. 1093). USGPO.

Mix, A. C., Bard, E., & Schneider, R. 2001. Environmental processes of the ice age: land, oceans, glaciers (EPILOG). *Quaternary Science Reviews,20*(4), 627-657.

Moffit, F. H. 1935. *Geology of the Tonsina district, Alaska*: US Government Printing Office.

National Climate Data Center, 2007. Seward meteorological station. [online]. Available from http://www.ncdc.noaa.gov/cdo.web/quickdata ([cited 6 June 2016]).

Osipov, E. Y. 2004. Equilibrium-line altitudes on reconstructed LGM glaciers of the northwest Barguzinsky Ridge, Northern Baikal, Russia. *Palaeogeography, Palaeoclimatology, Palaeoecology, 209*(1), 219-226.

Osmaston, H. 2005. Estimates of glacier equilibrium line altitudes by the Area × Altitude, the Area× Altitude Balance Ratio and the Area × Altitude Balance Index methods and their validation. *Quaternary International, 138*, 22-31.

Otto-Bliesner, B. L., Brady, E. C., Clauzet, G., Tomas, R., Levis, S., & Kothavala, Z. 2006. Last glacial maximum and Holocene climate in CCSM3. *Journal of Climate*, *19*(11), 2526-2544.

Pendleton, S. L., Ceperley, E. G., Briner, J. P., Kaufman, D. S., & Zimmerman, S. 2015. Rapid and early deglaciation in the central Brooks Range, Arctic Alaska. *Geology*, *43*(5), 419-422.

Pellitero, R., Rea, B. R., Spagnolo, M., Bakke, J., Hughes, P., Ivy-Ochs, S., ... & Ribolini, A. 2015. A GIS tool for automatic calculation of glacier equilibrium-line altitudes. *Computers & Geosciences*, *82*, 55-62.

Péwé, T.L., 1975. Quaternary Geology of Alaska. U.S. Geological Survey Professional Paper 835, p. 145.

Pinney, D.S., 1993, Late Quaternary glacial and volcanic stratigraphy near Windy Creek, Katmai National Park, Alaska: Fairbanks, University of Alaska MS thesis, 185 p.

Pinney, D.S., and Begét, J.E., 1991, Late Pleistocene volcanic deposits near the Valley of Ten Thousand Smokes, Katmai National Park, Alaska, in Reger, R.D., ed., Short Notes on Alaska Geology 1991: Alaska Division of Geological & Geophysical Surveys Professional Report 111, p. 45–53.

Porter, S.C., Pierce, K.L., Hamilton, T.D., 1983. Late Wisconsin mountain glaciation in the western United States. In: Porter, S.C. (Ed.), Late Quaternary Environments of the United States: the Late Pleistocene. University of Minnesota Press, Minneapolis, pp. 71-111.

Porter, S. C. 2000. Snowline depression in the tropics during the Last Glaciation. *Quaternary Science Reviews, 20*(10), 1067-1091.

Plafker, G., Berg, H.C., 1994. Overview of the geology and tectonic evolution of Alaska. In: Plafker, G., Berg, H.C. (Eds.), The Geology of Alaska vol. G-1. Geological Society of America, Geology of North America, Boulder, Colorado, pp. 989–1021.

Plafker, G., 1987. Regional geology and petroleum potential of the northern Gulf of Alaska continental margin. In: Scholl, D.W., Grantz, A., Vedder, J.G. (Eds.), Geology and Resource Potential of the Continental Margin of Western North America and Adjacent Ocean Basins—Beaufort Sea to Baja California: Circum-Pacific Council for Energy and Mineral Resources. Earth Sciences Series, 6, 299–268.

Plafker, G., Nokleberg, W.J., &Lull, J.S. 1989. Bedrock geology and tectonic evolution of the Wrangellia, Peninsular, and Chugach Terranes along the Trans-Alaska Crustal Transect in the Chugach Mountains and Southern Copper River Basin, Alaska, *J. Geophys.*

Railsback, L. B., Gibbard, P. L., Head, M. J., Voarintsoa, N. R. G., & Toucanne, S. (2015). An optimized scheme of lettered marine isotope substages for the last 1.0 million years, and the

climatostratigraphic nature of isotope stages and substages. *Quaternary Science Reviews*, *111*, 94-106.

Reger, R. D., Pinney, D. S., Burke, R. M., & Wiltse, M. A. 1996. Catalog and initial analyses of geologic data related to middle to late Quaternary deposits, Cook Inlet region, Alaska. Alaska Division of Geological & Geophysical Surveys Report of Investigations 95-6, 188 p., 5 sheets, scale 1:250,000.

Reger, R. D., Berg, A. G., & EE Burns, P. A. C. 2007. A guide to the Late Quaternary history of northern and western Kenai Peninsula, Alaska. Published by State of Alaska, Department of Natural Resources, Division of Geological and Geophysical Surveys, Fairbanks.

Reger, R. D., & Pinney, D. S. 1997. Last major glaciation of Kenai Lowland.

Reger, R. D., & Updike, R. G. 1983. Upper Cook Inlet region and Matanuska Valley. *Quaternary Geology and Permafrost Along the Richardson and Glen Highways Between Fairbanks and Anchorage, Alaska: Fairbanks to Anchorage, Alaska July 1-7, 1989*, 1-10.

Rolland, C. (2003). Spatial and seasonal variations of air temperature lapse rates in Alpine regions. *Journal of Climate*, *16*(7), 1032-1046.

Sampson, K. M., & Smith, L. C. 2006. Relative Ages of Pleistocene Moraines Discerned from Pebble Counts: Eastern Sierra Nevada, California. *Physical Geography*, *27*(3), 223-235.

Schmoll, H.R., Yehle, L.A., Gardner, C.A., and Odum, J.K., 1984, Guide to surficial geology and glacial stratigraphy in the upper Cook Inlet basin: Anchorage, Alaska Geological Society guidebook, 89 p.

Schmoll, H. R., Szabo, B. J., Rubin, M., & Dobrovolny, E. 1972. Radiometric dating of marine shells from the Bootlegger Cove Clay, Anchorage area, Alaska. *Geological Society of America Bulletin*, *83*(4), 1107-1114.

Schmoll, H. R., & Yehle, L. A. 1986. Pleistocene glaciation of the upper Cook Inlet basin.

Schmoll, H. R., Yehle, L. A., & Updike, R. G. 1999. Summary of Quaternary geology of the Municipality of Anchorage, Alaska. *Quaternary International, 60*(1), 3-36.

Seltzer, G. O. 1994. Climatic interpretation of alpine snowline variations on millennial time scales. *Quaternary Research*, *41*(2), 154-159.

Solomina, O. N., Bradley, R. S., Hodgson, D. A., Ivy-Ochs, S., Jomelli, V., Mackintosh, A. N., ... & Young, N. E. 2015. Holocene glacier fluctuations. *Quaternary Science Reviews*, *111*, 9-34.

Solomina, O., & Calkin, P. E. 2003. Lichenometry as applied to moraines in Alaska, USA, and Kamchatka, Russia. *Arctic, Antarctic, and Alpine Research, 35*(2), 129-143.

Stansell, N. D., Polissar, P. J., & Abbott, M. B. 2007. Last glacial maximum equilibrium-line altitude and paleo-temperature reconstructions for the Cordillera de Mérida, Venezuelan Andes. *Quaternary Research*, *67*(1), 115-127.

Stilwell, K. B., & Kaufman, D. S. 1996. Late Wisconsin glacial history of the northern Alaska Peninsula, southwestern Alaska, USA. *Arctic and Alpine Research*, 475-487.

Stone, J. O., Allan, G. L., Fifield, L. K., & Cresswell, R. G. 1996. Cosmogenic chlorine-36 from calcium spallation. *Geochimica et Cosmochimica Acta*, *60*(4), 679-692.

Stone, J. O. 2000. Air pressure and cosmogenic isotope production. *Journal of Geophysical Research: Solid Earth*, *105*(B10), 23753-23759.

Thackray, G. D., Owen, L. A., & Yi, C. (2008). Timing and nature of late Quaternary mountain glaciation. *Journal of Quaternary Science*, *23*(6-7), 503-508.

Young, N. E., Schaefer, J. M., Briner, J. P., & Goehring, B. M. 2013. A 10Be production-rate calibration for the Arctic. *Journal of Quaternary Science*, *28*(5), 515-526.

Young, N. E., Briner, J. P., & Kaufman, D. S. (2009). Late Pleistocene and Holocene glaciation of the Fish Lake valley, northeastern Alaska Range, Alaska. *Journal of Quaternary Science*, *24*(7), 677-689.

Western Regional Climate Center. (2016). Period of Record Monthly Climate Summary. Retrieved from http://www.wrcc.dri.edu/cgi-bin/cliMAIN.pl?akthom

Wolman, M. G. 1954. A method of sampling coarse river-bed material. *EOS, Transactions American Geophysical Union*, *35*(6), 951-956.

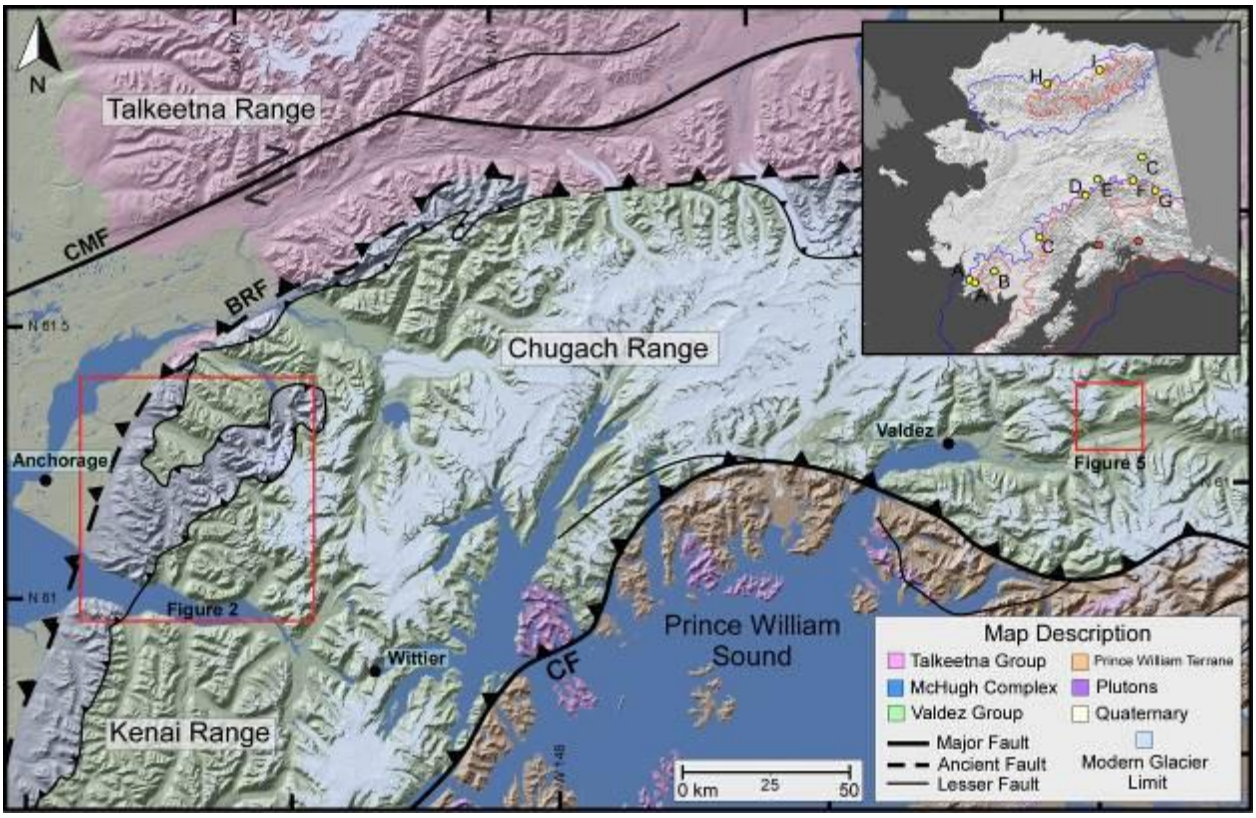

Figure 3.1. Elevation and land cover DEM map showing major faults and geologic terranes of south central Alaska. The red boxes outline the detailed field areas of this project. The inset map depicts a simplified glacial ice extent for the Pleistocene (blue) and the late Wisconsin (red) with locations of previous studies that use cosmogenic nuclide dating (yellow points). The orange points represent the locations of the field areas in this study. The base map for the inset is modified from Riehle et al. (1997). A = Briner et al. (2001), B = Briner et al. (2002), C = Briner et al. (2005), D = Dortch et al. (2010a), E = Dortch et al. (2010b), F = Matmon et al. (2006), G = Young et al. (2009), H = Badding et al. (2013), I = Pendleton et al. (2015). BRF = Border Ranges Fault, CF = Contact Fault, CMF = Castle Mountain Fault.

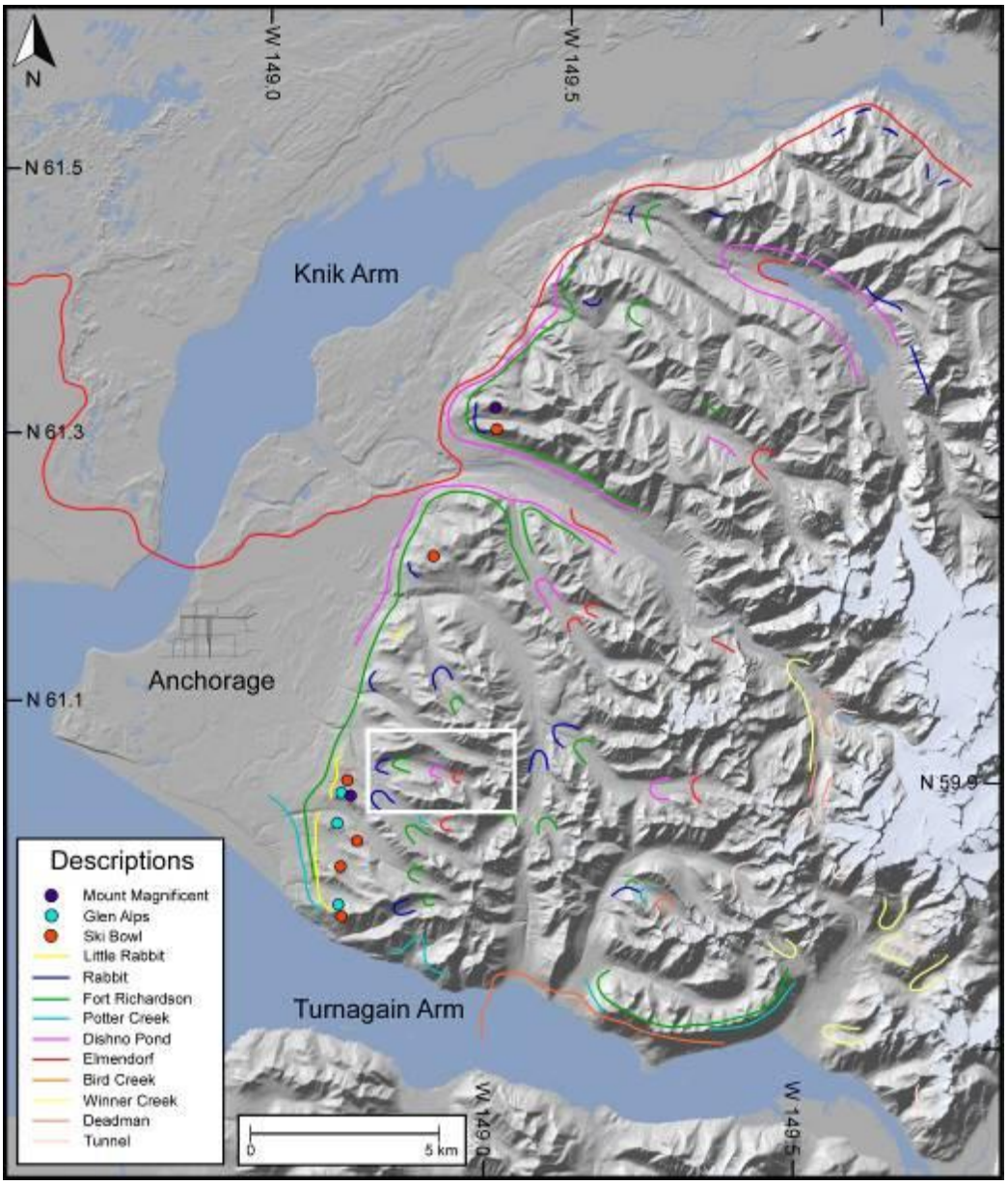

Figure 3.2. A shaded relief map (produced from an elevation DEM) showing the regional distribution and relative chronologies of moraines in the Anchorage and Chugach Mountain regions (adapted from Schmoll et al., 1999). Large dots represent Early Wisconsin glacial till, and colored lines represent late Wisconsin moraines, glacial trimlines, and former ice flow markers. White box refers to field area Figure 3.3. The major highways of Anchorage are shown as black lines.

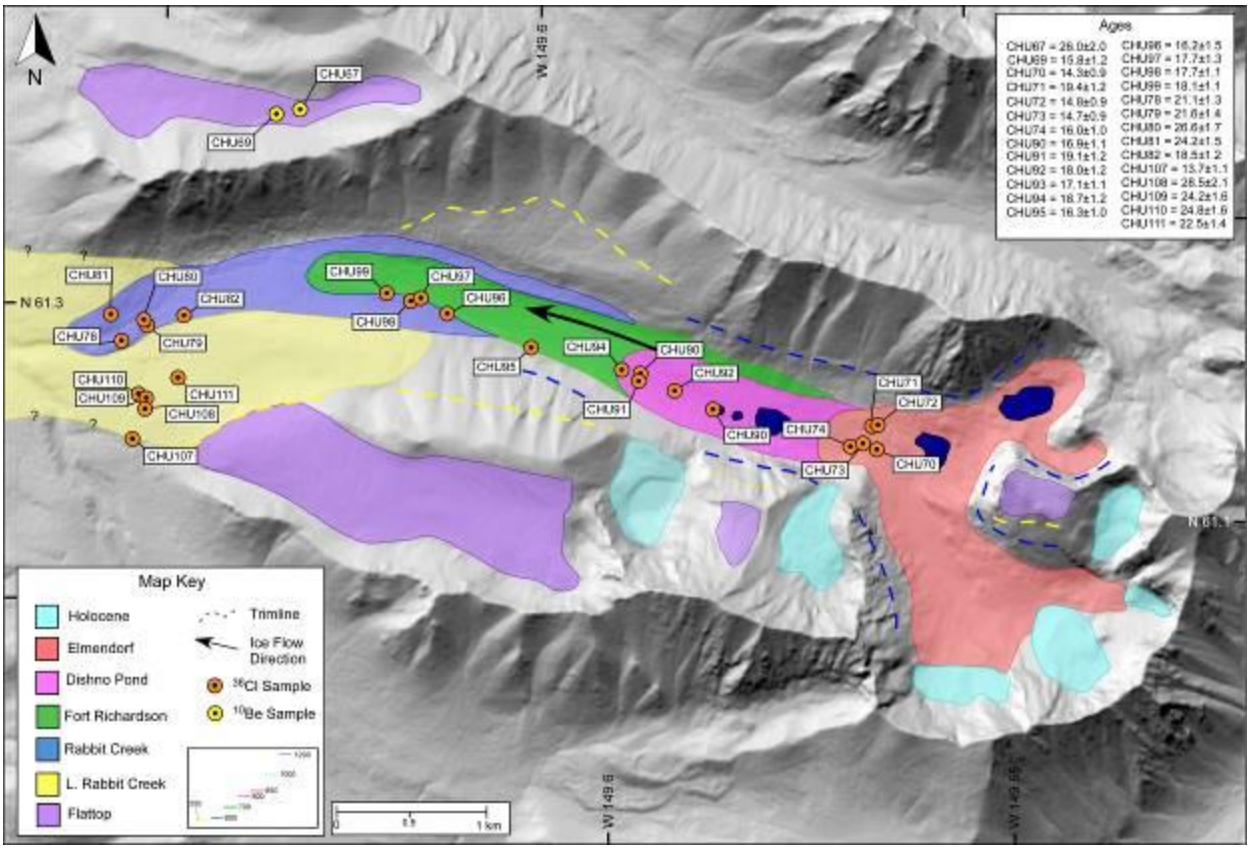

Figure 3.3. Glacial geomorphology of Williwaw Lakes Valley with the glacial chronology and sample locations. The completed chronology includes five sets of lateral moraines (red, pink, green, blue, yellow); pertaining to late Wisconsin activity, one higher bench of glacial till (purple); related to early Wisconsin activity, and presumed rock glacier deposits as pale green in the cirques. The large black arrows represent ice flow direction.

Figure 3.4. Views of significant geomorphic features in Williwaw Lakes Valley and Thompson Pass study areas. (A) A profile view of the Flattop Mountain and Early Wisconsin benches which from top to bottom correlate with the Mount Susitna, Mount Magnificent, Glen Alps, and Ski Bowl events (Schmoll et al., 1999). (B) A comparison of early Wisconsin clasts comprised of granite (left) and locally derived late Wisconsin moraine clast composed of metasedimentary volcaniclastics (right). (C) Granitic glacial boulder located below Wolverine Peak (CHU67). (D) View of the contact between the Rabbit Creek (right) and Little Rabbit Creek (left) moraines. (E) View of Williwaw Lakes Valley showing Fort Richardson lateral moraines and the flat glaciated benches above the valley.

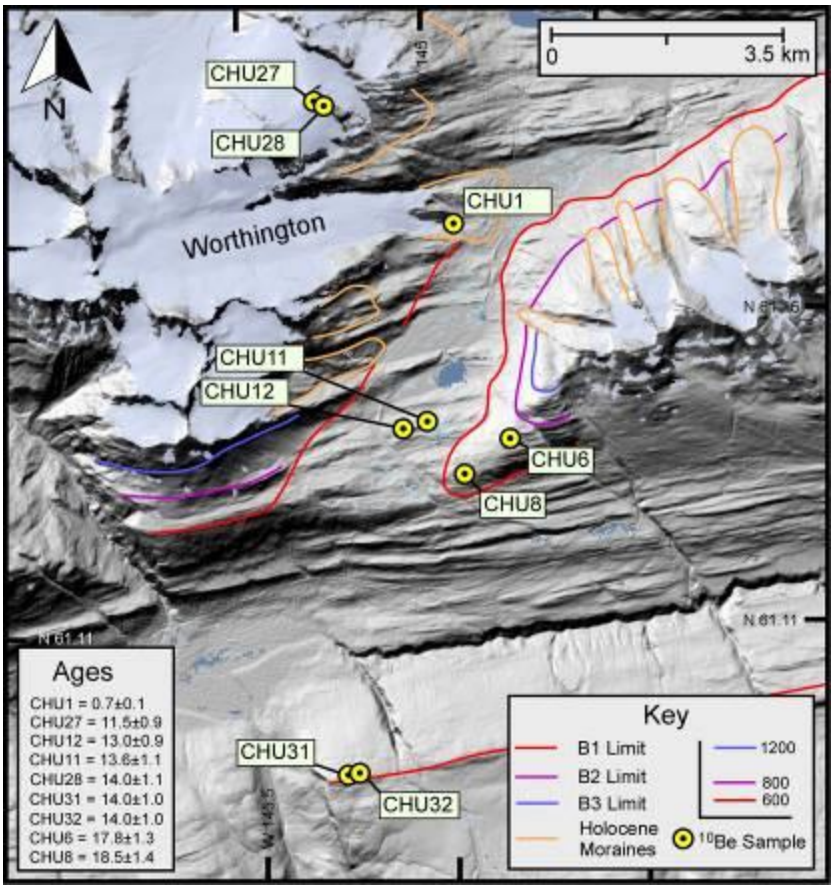

Figure 3.5. A shaded relief map of Thompson Pass showing glaciation trimlines and sampling locations. The red, purple, and blue lines represent the glacial trimlines for three Pleistocene aged glaciations. The orange lines represent the ice maximum during the Holocene. The blue color represents the modern ice extent.

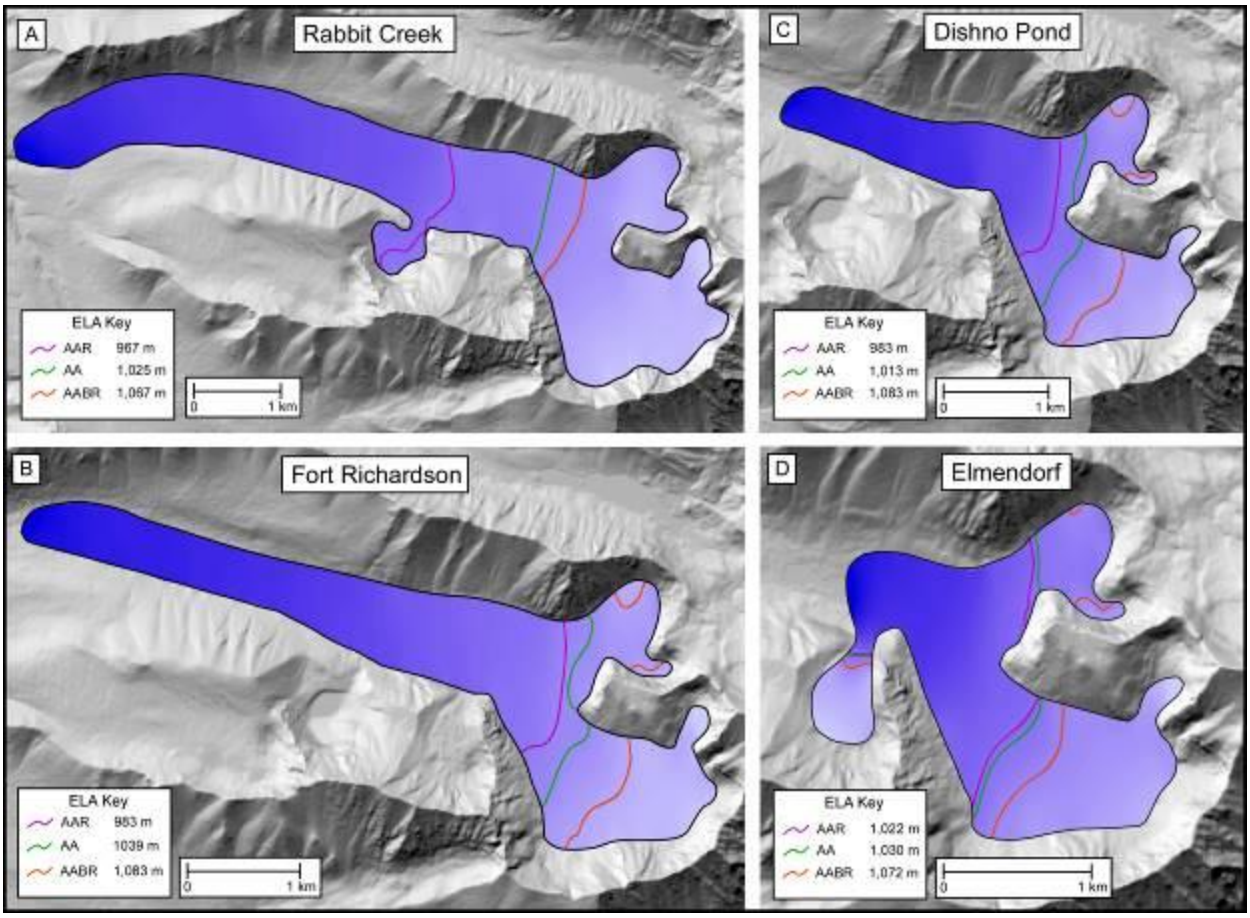

Figure 3.6. Reconstruction of glacier extent and calculated ELAs (lines) using different methods for the Late Pleistocene events in the Williwaw Lakes Valley study area. The ice limits were constructed using the locations of end and lateral moraines, glacial trimlines, and former flow markers. The ELAs were calculated in ArcGIS, using the tools and methods of Pelliterio et al. (2015).

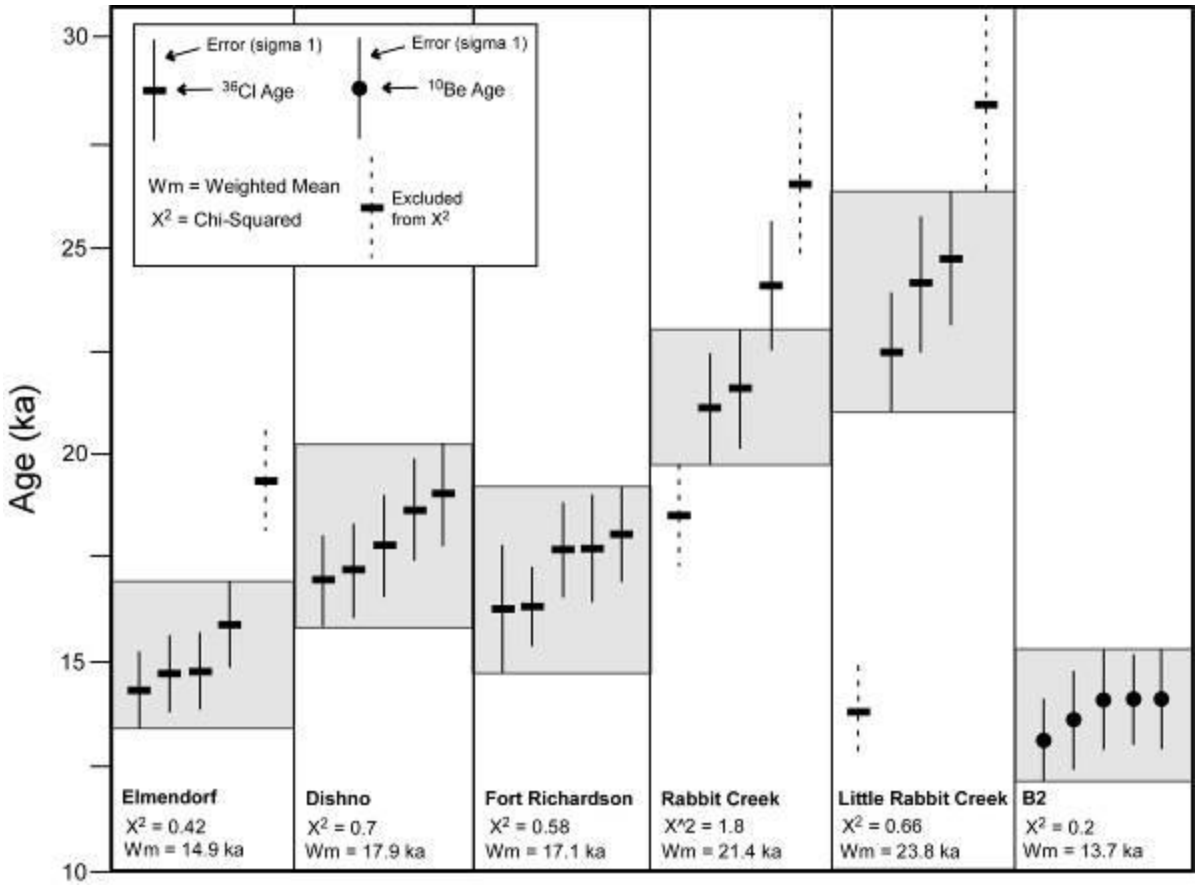

Figure 3.7. This diagram is showing the mean square weighted deviates (MSWD) and reduced X^2 values for each data set per moraine. The moraines are ordered chronologically from oldest to youngest from left to right, with the exception of B2. The dashed lines represent ages that were excluded from the MSWD calculation to produce a X^2 value of <1.

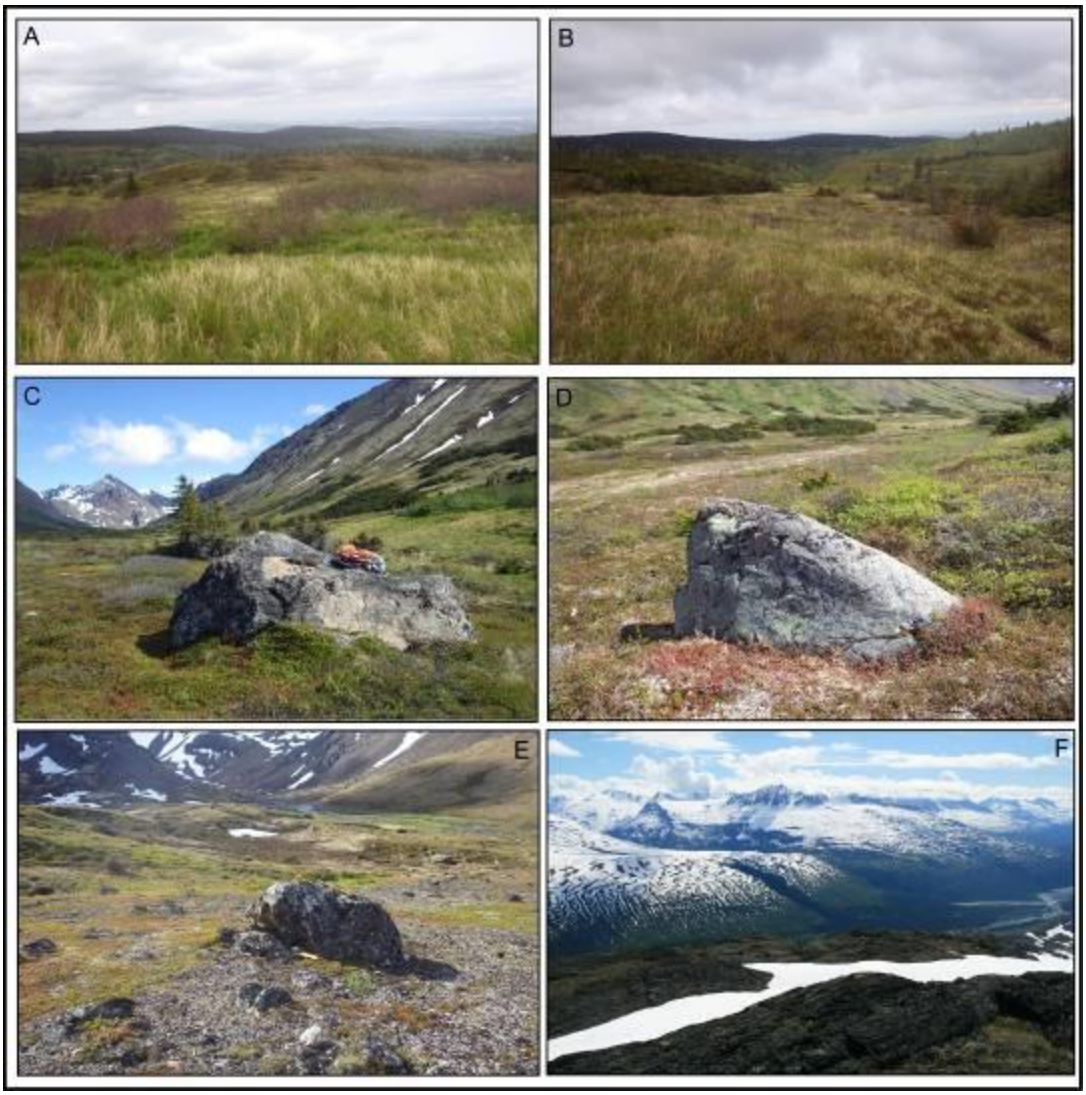

Figure 3.8. Views of the five moraines in Williwaw Lakes Valley and the incised benches of Thompson Pass study areas. The surface of Little Rabbit Creek (A), Little Rabbit (B), Fort Richardson (C), Dishno Pond (D), and Elmendorf (E) moraines. (F) View from Thompson Pass depicting the large glacial benches and the notch canyons.

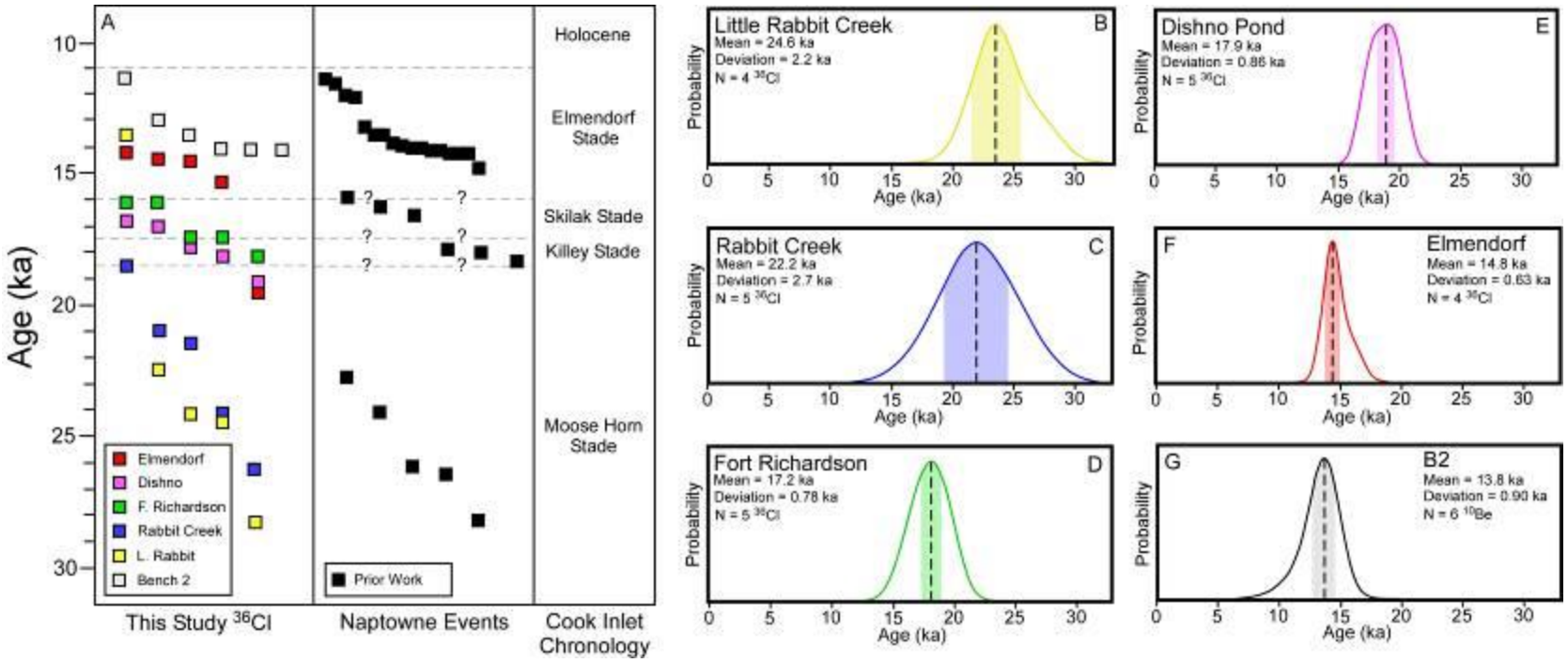

Figure 3.9. (A) A correlation of our new exposure ages with the radiocarbon ages and chronology of the Naptowne glaciation of Karlstrom (1964). The black square symbols represent previously completed radiocarbon ages in the region used to delineate the timing of the Naptowne event. (B–G) Probability plots for moraines and surfaces with a cluster of four or more ages. The 1 σ uncertainty is shown as the colored region beneath each curve and the mode is the dashed black line.

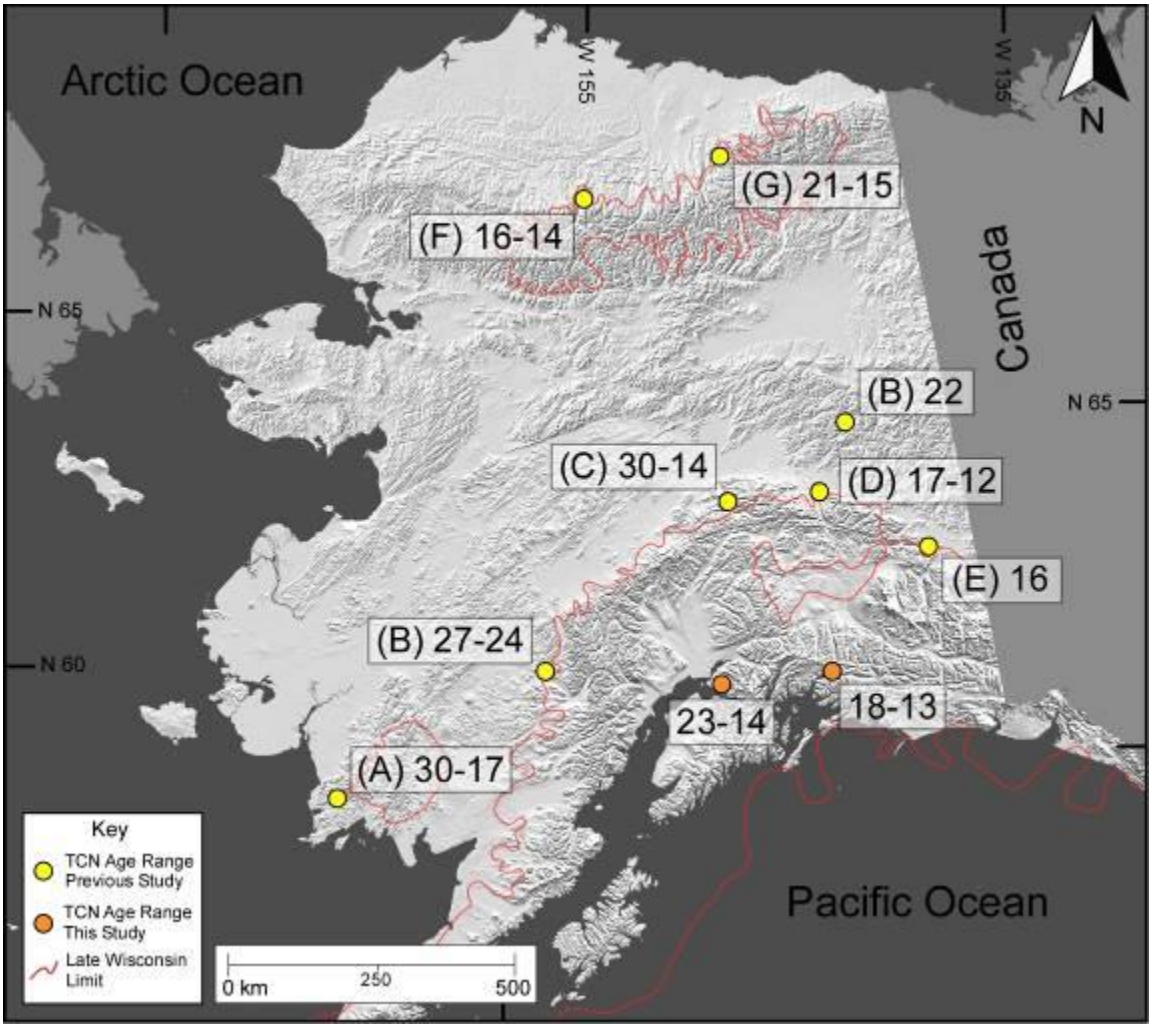

Figure 3.10. Exposure age ranges for the late Wisconsin glaciations in Alaska. The numbers in the rectangles are in ka. The yellow points represent previous studies and the orange locations are from the current study. The base map is modified from Riehle et al. (1997). The Late Wisconsin limits are from Briner and Kaufman (2008). A = Briner et al. (2001), B = Briner et al. (2005), C = Dortch et al. (2010b), D = Matmon et al. (2006), E = Young et al. (2009), F = Badding et al. (2013), G = Pendleton et al. (2015)

Kulp (1951, 1952)	**Karlstrom (1964, 1968)**	**Schmoll et al. (1972)**	**Rymer and Sims (1982); Reger and Updike (1983)**	**Schmoll et al. (1972, 1984); Schmoll and Yehle (1986)**	**Pinney (1993); Pinney and Beget (1991)**	**Mann and Peteet (1994)**	**Reger et al. (1995, 1996)**	**Stilwell and Kaufman (1996)**	**Ager (1983); Ager (2000); Ager and Carrara (2006)**	**^{10}Be Ages**
Naptowne (~ 8-14)	Elmendorf (~ 25-48)	Elmendorf (~ 14)	Elmendorf (~ 14)	Elmendorf (~ 14)	Elmendorf (~ 14)		Elmendorf (~ 11-14)		Elmendorf (~ 11-14)	Elmendorf (14.9±0.9)
Swan Lake (~ 14-19)			Skilak (~ 13-14)				Skilak (~ 16)			Dishno Pond (17.9±1.1)
							Killey (~ 18)			Fort Richardson (17.1+/-1.2)
						Moosehorn (~ 22-28)		Moosehorn (~ 26)		Rabbit Creek (22.3±1.4) Little Rabbit Creek (23.8±1.5)

Table 3.1. Radiocarbon ages for the four stades of the Naptowne glaciation as summarized by Reger et al. (2007)

Sample number	North latitude (DD)	East longitude (DD)	Altitude (m)	Qtz weight (g)	Be carrier weight (g)	Sample thickness (cm)	Feature	$^{10}Be/^{9}Be$ (10^{-12})	# of Be-10 atoms (10^{6})	Age (ka) Lifton	Age (ka) Lal/Stone
CHU1	61.16821	145.722	701	22.5766	0.3546	3	Bedrock	0.004±0.0007	0.006±0.001	0.7±0.1	0.8±0.2
CHU6	61.13702	145.703	1223	18.5511	0.3461	3	Bedrock	0.135±0.007	0.233±0.013	17.8±1.3	18.3±1.8
CHU8	61.13175	145.719	983	18.5095	0.3592	2	Boulder	0.108±0.085	0.199±0.157	18.5±1.4	19.0±1.5
CHU11	61.13815	145.727	865	16.2494	0.3572	4	Boulder	0.062±0.003	0.130±0.006	13.6±1.1	13.8±1.3
CHU12	61.13844	145.733	875	18.8066	0.3504	2	Boulder	0.072±0.005	0.127±0.009	13.0±0.9	13.3±1.4
CHU22	61.56061	146.024	1585	15.3616	0.36	4	Bedrock	0.177±0.014	0.393±0.032	22.3±1.7	23.2±2.6
CHU27	61.19592	145.759	1677	22.9428	0.3505	1	Boulder	0.154±0.006	0.223±0.008	11.5±0.9	12.0±1.0
CHU28	61.19592	145.759	1678	19.9958	0.3477	4	Bedrock	0.016±0.017	0.267±0.028	14.0±1.1	14.6±1.9
CHU31	61.08787	145.763	803	9.3258	0.3518	4	Bedrock	0.034±0.002	0.122±0.007	14.0±1.0	13.8±1.3
CHU32	61.08751	145.763	801	17.9106	0.3622	4	Bedrock	0.066±0.004	0.126±0.007	14.0±1.1	14.3±1.4
CHU67	61.13761	149.1381	1033	3.4674	0.3498	4	Boulder	0.042±0.004	0.282±0.027	26.0±2.0	25.0±2.0
CHU69	61.13749	149.6462	888	0.9149	0.3498	5	Boulder	0.059±0.002	0.150±0.049	15.8±1.2	15.5±1.2
CHU126	61.06258	149.6231	1109	3.324	0.3515	5	Boulder	0.059±0.003	0.415±0.019	36.2±2.9	35.3±2.7
CHU127	61.06251	149.6248	1108	4.718	0.3508	4	Boulder	0.129±0.005	0.642±0.026	55.8±4.4	54.4±4.2

Table 3.2. This table contains the results of ^{10}Be TCN dating. The ages were calculated with both Lifton et al., 2014 and Lal, 1991/ Stone, 2000 for comparison.

Sample	Moraine	Latitude °N	Longitude °W	Elevation	$^{36}Cl/Cl$ (10^{-15})	Cl (ppm)	Age (ka) Lifton	Age (ka) Lal/Stone
CHU-70	Elmendorf	61.10906	149.55737	844	170.20 ± 8.76	12.91 ± 2.05	14.3±0.9	14.7±0.9
CHU-71	Elmendorf	61.11004	149.55756	850	237.91 ± 9.68	2.02 ± 0.23	19.4±1.2	19.9±1.3
CHU-72	Elmendorf	61.11015	149.55733	853	170.58 ± 8.17	5.27 ± 0.30	14.8±0.9	15.4±0.9
CHU-73	Elmendorf	61.10957	149.55841	840	167.55 ± 12.42	8.89 ± 2.25	14.7±0.9	15±0.9
CHU-74	Elmendorf	61.11004	149.55902	836	158.48 ± 7.76	5.76 ± 0.13	16.0±1.0	17.0±1.0
CHU-78	Rabbit Creek	61.11858	149.66718	579	157.15 ± 5.77	2.05 ± 1.18	21.1±1.3	20.9±1.3
CHU-79	Rabbit Creek	61.11921	149.66411	595	155.99 ± 6.65	8.30 ± 0.20	21.6±1.4	21.4±1.3
CHU-80	Rabbit Creek	61.11902	149.66322	597	232.99 ± 8.85	3.93 ± 0.22	26.6±1.7	26.5±1.7
CHU-81	Rabbit Creek	61.1201	149.60782	596	179.99 ± 6.28	5.43 ± 0.55	24.2±1.5	24.0±1.5
CHU-82	Rabbit Creek	61.11836	149.65909	623	118.53 ± 7.58	8.95 ± 0.54	18.5±1.2	18.3±1.1
CHU-90	Dishno Pond	61.1163	149.59262	769	109.00 ± 3.78	15.36 ± 0.40	16.9±1.1	16.8±1.1
CHU-91	Dishno Pond	61.11602	149.59254	771	119.37 ± 4.28	12.55 ± 0.22	19.1±1.2	18.9±1.2
CHU-92	Dishno Pond	61.11529	149.59087	777	133.33 ± 4.41	4.31 ± 0.10	18±1.2	17.8±1.2
CHU-93	Dishno Pond	61.11472	149.59059	776	154.66 ± 5.79	4.77 ± 0.22	17.1±1.1	16.9±1.1
CHU-94	Dishno Pond	61.11628	149.59283	766	157.06 ± 6.52	5.05 ± 0.18	18.7±1.2	18.5±1.2
CHU-95	Fort Richardson	61.11824	149.61067	738	105.80 ± 4.94	10.37 ± 0.78	16.3±1.0	16.1±0.9
CHU-96	Fort Richardson	61.12097	149.61987	713	118.82 ± 6.38	38.38 ± 0.92	16.2±1.5	16.2±1.4
CHU-97	Fort Richardson	61.12125	149.6225	710	128.95 ± 4.63	18.57 ± 0.27	17.7±1.3	17.6±1.3
CHU-98	Fort Richardson	61.1207	149.62357	709	153.71 ± 5.91	8.68 ± 0.22	17.7±1.1	17.5±1.1
CHU-99	Fort Richardson	61.12048	149.62395	701	141.12 ± 5.89	9.93 ± 0.29	18.1±1.1	17.9±1.1
CHU-107	Little Rabbit Creek	61.11358	149.06629	568	89.13 ± 3.99	39.19 ± 0.90	13.7±1.1	12.3±1.2
CHU-108	Little Rabbit Creek	61.11483	149.66137	628	209.39 ± 9.05	27.40 ± 2.82	28.5±2.1	25.5±2.2
CHU-109	Little Rabbit Creek	61.11677	149.65822	637	155.01 ± 6.83	8.50 ±0.38	24.2±1.6	23.9±1.5
CHU-110	Little Rabbit Creek	61.11551	149.66243	616	248.72 ± 10.83	0.78 ± 0.33	24.8±1.6	24.1±1.5
CHU-111	Little Rabbit Creek	61.11359	149.66283	615	215.44 ± 7.24	0.98 ± 0.09	22.5±1.4	21.8±1.4

Table 3.3. This table contains the results of ^{36}Cl TCN dating. The ages were calculated with both Lifton et al., 2014 and Lal, 1991/ Stone, 2000 for comparison.

	Altitude (m asl)	Balance Ratio (m asl)	Area Ratio (m asl)
Raven Glacier	1348	1314	1414
Clear Glacier	1461	1449	1499
Eklutna Glacier	1417	1389	1489
61.11989, -148.87132	1425	1343	1593
Whiteout Glacier	1448	1388	1588
Eagle River Glacier	1465	1401	1551
61.25185, -148.74819	1433	1361	1511
Hunter Creek Glacier	1607	1528	1678
61.08906, -148.84006	1313	1258	1408
AVERAGE	1435	1381	1525
PALEO GLACIERS			
Elmendorf	1030	1072	1022
Dishno Pond	1013	1083	983
Fort Richardson	1039	1083	983
Rabbit Creek	1025	1067	967
ΔELA	(m)	(m)	(m)
Elmendorf	405	309	503
Dishno Pond	422	298	542
Fort Richardson	396	298	542
Rabbit Creek	410	314	558

Table 3.4. A summary of the ELA calculations in the Chugach Mountains. The ELAs for the modern glaciers were calculated with the tools of Pelliterio et al., 2015 to compare with the paleo ELAs from moraines.

DATA SUPPLEMENTS

The data supplements include additional information for the ^{36}Cl dating and a synopsis of the clasts analysis for each dated moraine. The table in appendix A shows the data used by the CRONUScalc web calculator to produce exposure ages. The total Cl was calculated from the results of the AMS measurements at PRIME lab at Purdue and the other constituents are from major trace element analysis using ICP-MS and FUS-MS at Bureau Veritas Mineral Laboratories in Vancouver, Canada. The table in appendix B shows the results of clasts analysis from each major moraine and glaciated surface in the Chugach Mountains. The data is presented as percentages of clasts characteristics including size, generalized composition, and angularity. Appendix C includes figures from this work which were not included in the published version due to figure number constraints.

APPENDIX A

^{36}Cl data

Sample	Latitude	Longitude	El	Depth	Total Cl	Al2O3	CaO	Fe2O3	K2O	MgO	MnO	Na2O	P2O5	SiO2	TiO2	B	Gd	Sm	Th	U
	°N	°W	m	cm	ppm	wt %	wt %	wt %	wt %	wt %	wt %	wt %	wt %	wt %	wt %	ppm	ppm	ppm	ppm	ppm
CHU-70	61.10906	149.55737	844	3	12.91566	14.93	4.34	5.4	1.84	2.38	0.11	2.96	0.02	64.11	0.64	236	2.25	2.46	2.1	1.1
CHU-71	61.11004	149.55756	850	5	2.024663	13.87	3.73	5.42	1.58	2.18	0.1	3.51	0.06	66.51	0.66	98	2.08	2.27	2.6	0.9
CHU-72	61.11015	149.55733	853	6	5.268932	15.06	4.72	5.07	1.34	2.21	0.1	3.58	0.03	64.63	0.59	417	2.08	2.18	1.7	0.8
CHU-73	61.10957	149.55841	840	3	8.889076	15.15	3.88	6.97	1.72	3.04	0.12	3.14	0.05	61.7	0.79	36	2.85	2.84	2.6	1.3
CHU-74	61.11004	149.55902	836	4	5.759422	11.65	3.27	4.82	1.45	1.96	0.12	2.3	0.04	70.61	0.61	40	2.21	2.08	2.5	1.3
CHU-78	61.11858	149.66718	579	4	2.053121	15.01	3.99	5.87	1.73	2.46	0.11	3.49	0.08	63.68	0.66	104	2.64	2.45	2.5	1.1
CHU-79	61.11921	149.66411	595	4	8.297021	13.89	3.17	6.04	1.5	2.5	0.11	3.69	0.05	64.97	0.72	261	2.24	2.24	2.3	1.1
CHU-80	61.11902	149.66322	597	4	3.930861	13.68	4.55	5.97	1.61	2.32	0.1	2.16	0.09	65.3	0.61	74	2.1	2.1	2.4	0.9
CHU-81	61.1201	149.60782	596	4	5.426959	14.22	3.88	5.45	1.56	2.22	0.1	3.37	0.03	65.26	0.65	48	2.33	2.29	2	1
CHU-82	61.11836	149.65909	623	4	8.9516	13.69	3.33	6.17	1.37	2.42	0.1	3.68	0.03	65.4	0.81	55	2.4	2.2	2	0.9
CHU-90	61.1163	149.59262	769	5	15.36366	12.33	4.54	7.28	1.04	2.95	0.13	2.86	0.03	64.42	0.98	40	2.66	2.29	2.2	1.2
CHU-91	61.11602	149.59254	771	5	12.54854	14	3.16	8.34	1.35	2.8	0.18	3.12	0.07	61.75	0.93	407	2.17	2.26	1.5	0.9
CHU-92	61.11529	149.59087	777	4	4.308323	14.99	2.25	5.59	1.55	2.46	0.11	4.4	0.02	65.01	0.68	55	2.2	2.25	1.8	0.8
CHU-93	61.11472	149.59059	776	4	4.774955	15.31	4.04	6.53	1.76	2.79	0.11	2.89	0.06	62.14	0.71	45	2.62	2.7	2.9	1.4
CHU-94	61.11628	149.59283	766	4	5.046526	15.27	4.57	5.94	1.69	2.54	0.11	3.25	0.04	62.42	0.63	467	2.31	2.28	2.3	1.1
CHU-95	61.11824	149.61067	738	7	10.36802	14.3	3.93	6.14	1.26	2.47	0.11	3.85	0.05	62.19	0.75	234	2.2	2.2	1.7	0.6
CHU-96	61.12097	149.61987	713	6	38.37738	12.82	2.26	5.48	2.08	2.07	0.11	2.99	0.05	67.82	0.53	58	2.09	2.1	2.3	0.8
CHU-97	61.12125	149.6225	710	4	18.57016	12.66	2.62	6.14	1.69	2.3	0.11	3.05	0.04	66.63	0.75	33	2.25	2.17	2.4	0.7
CHU-98	61.1207	149.62357	709	5	8.68109	14.75	4.72	5.66	1.53	2.3	0.11	3.05	0.08	63.62	0.6	35	3.03	2.99	2.9	1.4
CHU-99	61.12048	149.62395	701	4	9.926192	12.78	3.9	6.74	1.45	2.66	0.13	2.54	0.05	64.99	0.75	33	2.4	2.1	2.3	0.9
CHU-107	61.11358	149.06629	568	4	39.19432	13.48	5.43	8.07	0.72	2.67	0.12	2.9	0.04	61.87	0.85	27	2.58	2.6	2.4	1
CHU-108	61.11483	149.66137	628	5	27.40139	15.5	2.46	5.21	1.66	2.37	0.09	4.61	0.08	64.81	0.57	24	2.45	2.42	2.2	1.2
CHU-109	61.11677	149.65822	637	6	8.497765	12.97	3.19	6.14	0.91	2.24	0.12	3.5	0.08	67.27	0.65	20	2.07	2.08	1.8	0.8
CHU-110	61.11551	149.66243	616	6	0.788267	12.99	4.05	6.26	1.69	2.5	0.11	2.34	0.04	66.04	0.74	49	2.23	2.18	2.1	1
CHU-111	61.11359	149.66283	615	5	0.982656	14.42	4.26	5.62	1.57	2.36	0.1	2.9	0.04	64.59	0.67	40	2.49	2.53	2.2	1.2

APPENDIX B

Location	Percent Size (mm)										Percentage Composition		Percent Angularity			
	0.5 to 1	1 to 2	2 to 4	4 to 8	8 to 16	16 to 32	32 to 64	64 to 128	128 to 256	256 to 512	Chugach	Granite	Angular	M. Angular	M. Rounded	Rounded
Early Wisconsin																
Wolverine Peak	1	13	27	25	21	6	1	4	0	2	84	16	70	2	9	19
Ballfield (I)	15	16	20	17	13	9	7	1	2	0	97	3	72	17	5	6
Ballfield (II)	12	22	30	26	6	2	0	2	0	0	100	0	66	17	9	8
Ballfield (III)	0	3	6	69	21	1	0	0	0	0	100	0	80	14	6	0
Mount Magnificant	2	20	28	22	14	10	2	0	2	0	98	2	96	0	0	4
Glen Alps	14	33	36	14	3	0	0	0	0	0	97	3	98	2	0	0
Ski Bowl	19	32	30	16	1	1	1	0	0	0	94	6	91	4	3	2
Late Wisconsin																
Little Rabbit Creek	31	24	23	11	8	3	0	0	0	0	100	0	60	8	17	15
Rabbit Creek	21	24	30	11	11	1	2	0	0	0	100	0	82	9	8	1
Fort Richardson	17	27	18	14	12	7	5	0	0	0	100	0	81	13	4	2
Dishno Pond	13	33	28	11	5	5	3	0	1	0	100	0	81	9	8	2
Elmendorf	13	27	24	8	5	7	8	5	2	1	100	0	84	6	9	1

APPENDIX C

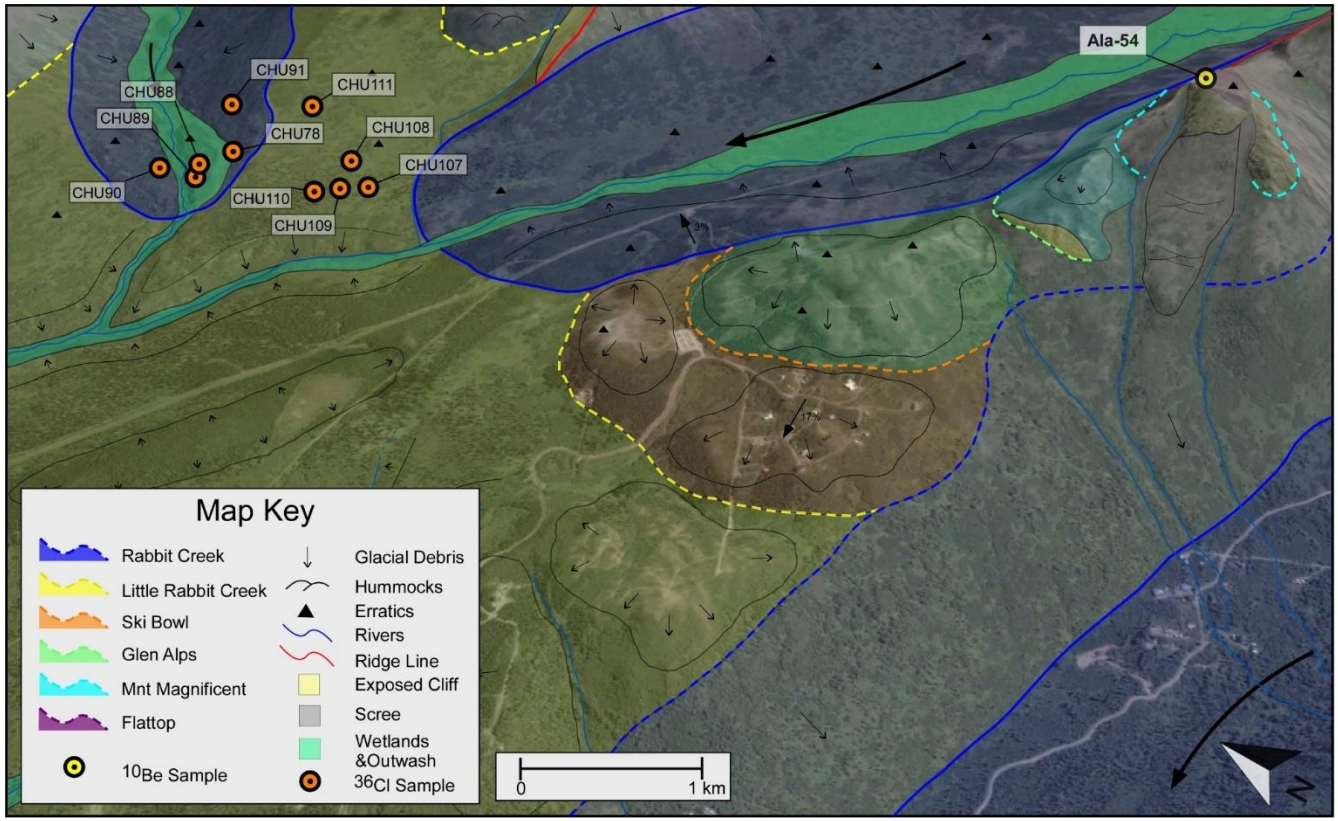

Figure C(1). Glacial geomorphology of Flattop Mountain depicting evidence of early Wisconsin glaciations. The western side of Flattop Mountain is characterized by three step-like plateaus, which are named Ski Bowl (orange), Glen Alps (green), and Mount Magnificent (light blue) (Schmoll et al., 1999).

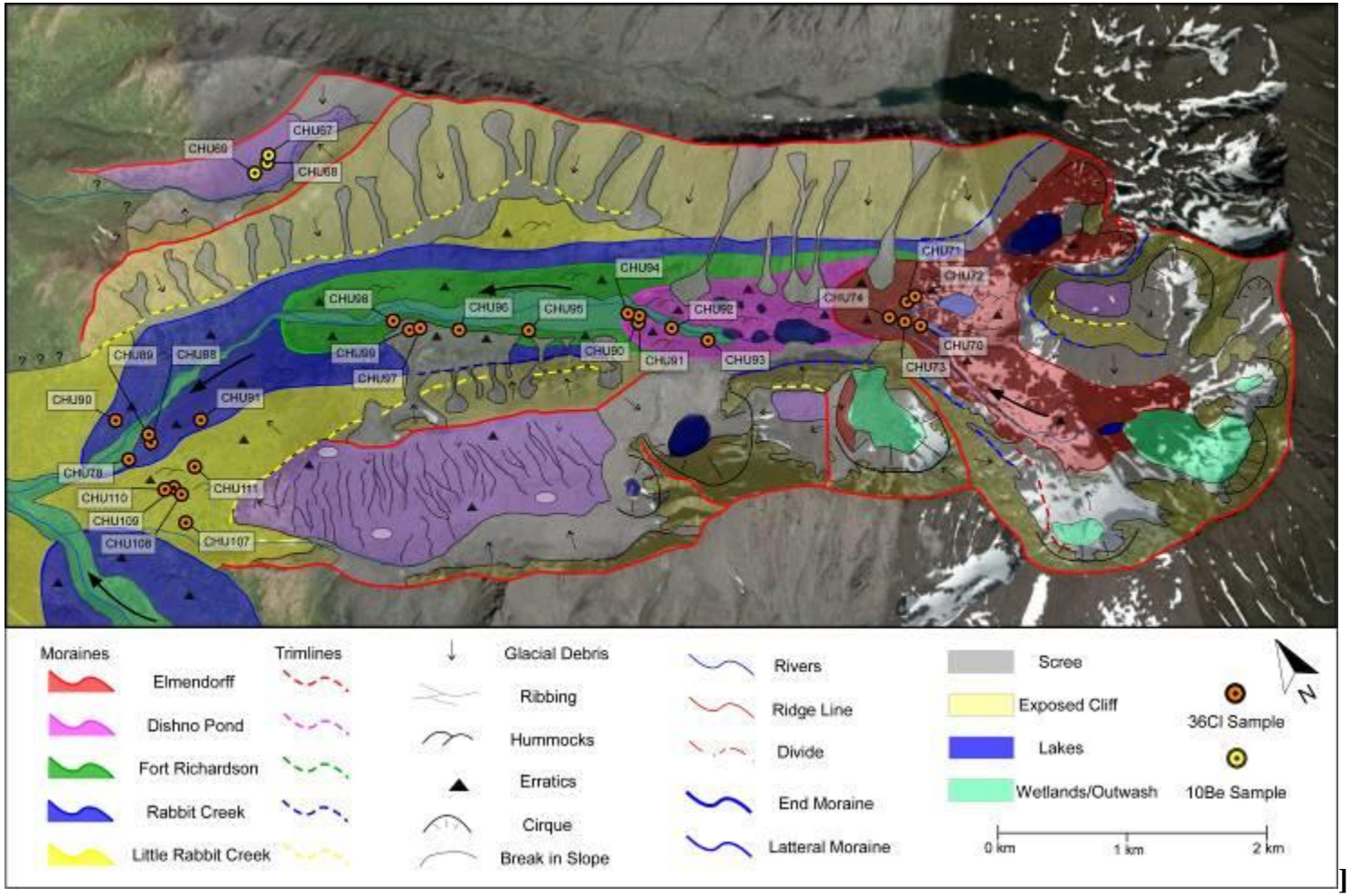

Figure C(2). Glacial geomorphology of Williwaw Lakes Valley with the glacial chronology and sample locations. The completed chronology includes five sets of lateral moraines (red, pink, green, blue, yellow); pertaining to late Wisconsin activity, one higher bench of glacial till (purple); related to early Wisconsin activity, and presumed rock glacier deposits as pale green in the cirques. The large black arrows represent ice flow direction. The base image is from Google Earth.

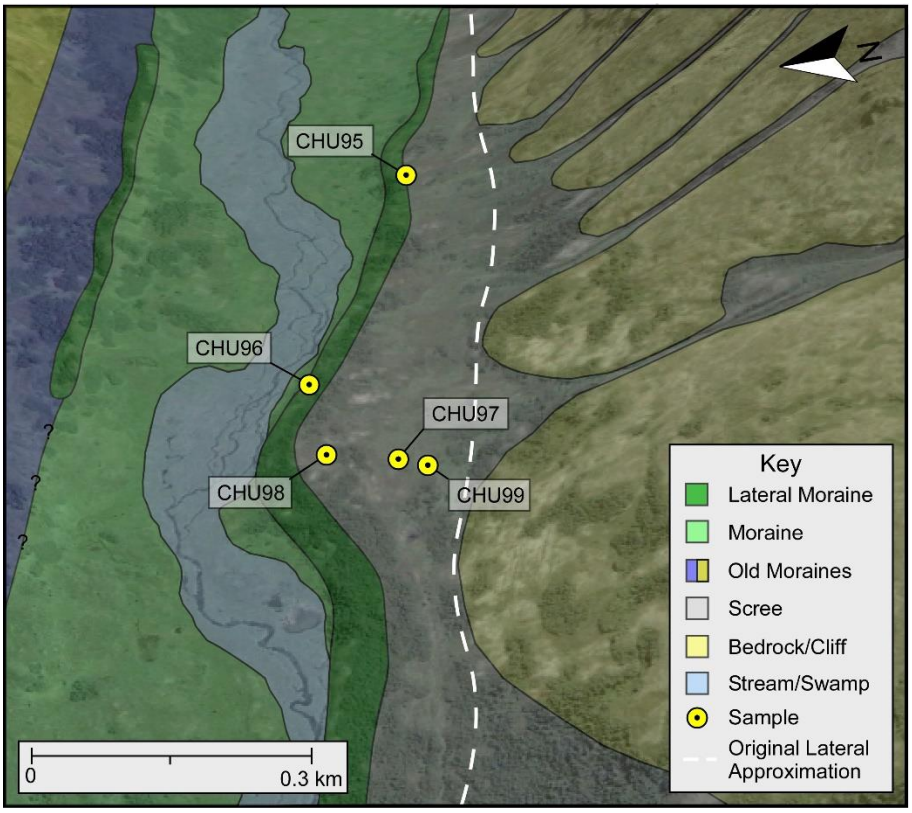

Figure C(3). Geomorphology of the Fort Richardson moraine in Williwaw Lakes valley. The white dashed line represents the estimated location of the lateral moraine, prior to movement from the debris slides. The elevation of the white line correlate with the height of the adjacent lateral moraine on the other wall of the valley.

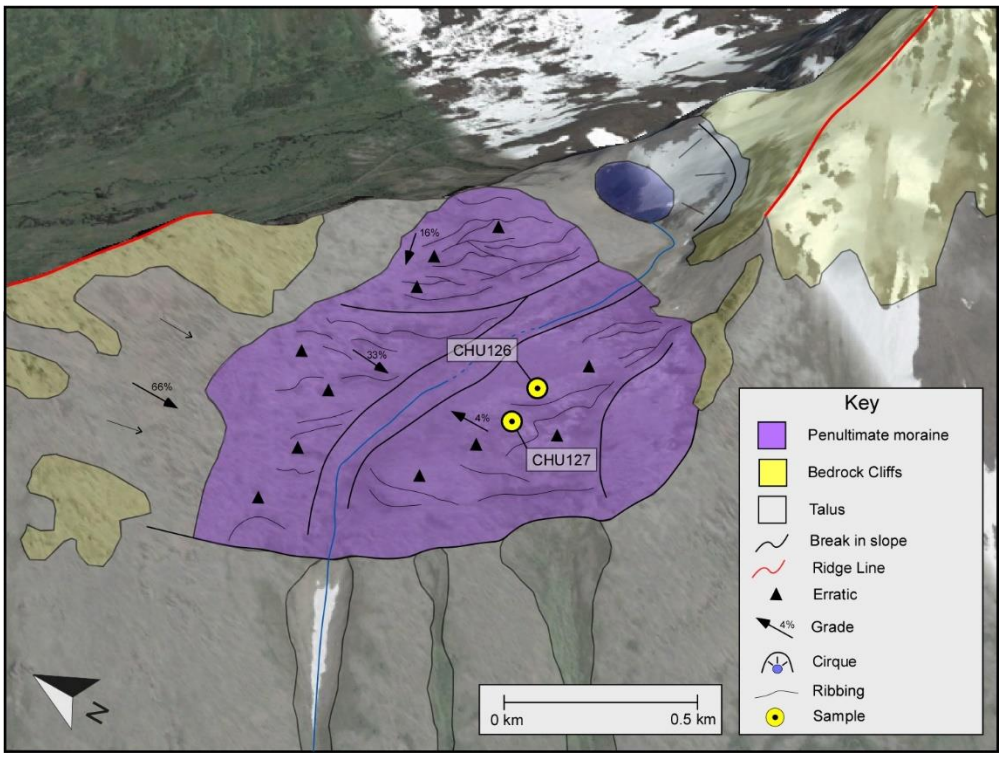

Figure C(4). A penultimate surface near Ptarmigan Peak, showing a carved-out saddle between the ridge and the mountain peak. The saddle is situated ~300 m above the adjacent valley base

CHAPTER 4

Multi-chronologic constraint on exhumation in the Chugach Mountains utilizing AHe and ^{10}Be Dating

Joshua D. Valentino[a]

[a] Department of Geosciences, 4044 Derring Hall, Virginia Tech, Blacksburg, VA 24061, USA

ABSTRACT

^{10}Be cosmogenic and (U-Th)/He thermochronology (AHe) dating were used to constrain erosion rates on average short and long term time frames in the Chugach Mountains of Alaska to determine whether the onset of climate driven accelerated glacial erosion occurs in regions with slow to moderate rock uplift. The majority of the new ^{10}Be cosmogenic (10^3-10^4 years) erosion rates range from 1-2 mm/yr and calculated erosion rates from the AHe dating (10^6-10^7 years) range from 0.08-0.17 mm/yr. Comparison of the short term to long term erosion rates show an increase in erosion occurring over the time of the onset of global glaciations through the late Cenozoic. The variations of area, glacial presence, and precipitation of each sampled cosmogenic catchment all depict a positive trend with erosion rate and climate controlled factors. These observations suggest that the presence of glaciers increases erosion and encourages the onset of effective glacial erosion in a region with slow to moderate rock uplift rates.

INTRODUCTION

Glaciation is considered to be a highly effective erosive force in orogens (Hallett et al., 1996; Brozovic et al., 1997; Anderson et al., 2006; Champagnac et al., 2014) and has been shown to match rock uplift (glacial buzz-saw) and limit topography growth (Mitchell and Montgomery, 2006; Egholm et al., 2009; Anders et al., 2010). Effective glacial erosion can dictate patterns of strain in an orogen through focused denudation (Meigs and Sauber, 2000; Montgomery et al., 2001; Thomson, 2002; Spotila et al., 2004; Tomkin and Roe, 2007; Berger and Spotila, 2008; Thomson et al., 2010), accelerated alpine erosion, increased rock uplift rate, and hastened sedimentation rates (Molnar and England, 1990; Small and Anderson, 1995; Whipple et al., 1999; Brocklehurst et al., 2008; van der Beek and Bourbon, 2008; Lease et al., 2016; Yu et al., 2016). Characterizing the comprehensive effect of glacial presence in an orogen is important to

understanding the development of an orogen through climate transitions. The onset of glaciations during the late Cenozoic resulted in a transient landscape response to climate change across the world (Raymo and Ruddiman, 1992; Farley et al., 2001; Shuster et al., 2005; Ehlers et al., 2006; Huntington et al., 2006; Haeuselmann et al., 2007; Densmore et al., 2007; Hebbeln et al., 2007; Berger et al., 2008; McAleer et al., 2009; Rahaman et al., 2009; Dowdeswell et al., 2010; Thomson et al., 2010; Ruddiman, 2010; Yu et al., 2016). A series of studies have focused on this climatic transition in regions experiencing high rock uplift by analyzing the glacially impacted topography of the orogens, creating numerical models (Brocklehurst and Whipple, 2002, 2004; Whipple and Meade, 2004; Tomkin and Roe, 2007), and delineating spatial variations in exhumation (Spotila et al., 2004; Whipple and Meade, 2004; Berger and Spotila, 2008; Enkelmann et al., 2015; Valentino et al., 2016; Lease et al., 2016; Enkelmann et al., 2017). However, very few studies have examined how active glaciation affects erosion in orogens with slow to moderate rock uplift rates.

The Chugach Mountains along the southern margin of Alaska comprise an uplifted forearc which is being uplifted and eroded at high exhumation rates (~ 2.0 mm/yr) in the east associated with the accretion of the Yakutat microplate (Plafker and Berg, 1994, Berger et al., 2008; Perry et al., 2009; Enkelmann et al., 2010), and slow to moderate rock uplift (~ 0.05 mm/yr) in the west where the microplate subducts (Buscher et al., 2008; Fuis et al., 2008; Finzel et al., 2011). The erosion in response to late Cenozoic glaciation and high exhumation rate has been well studied in the eastern Chugach Mountains (Spotila et al., 2004; Berger et al., 2008; Arkle et al., 2013; Falkowski et al., 2016). In contrast, this study focuses on the effect of glacial erosion in the western and central regions where the rock uplift is slower. The characterization of rock uplift, precipitation, and exhumation through time can shed light on whether erosion rates

increase with the presence of glaciers in orogens. We measured exhumation rates using catchment-wide cosmogenic (10^3-10^4 yr) dating and (U-Th)/He thermochronometry (10^6-10^7 years) and compared the results with the previously completed AHe ages in the region (Spotila et al., 2004; Berger et al., 2008; Buscher et al., 2008; Arkle et al., 2013; Ferguson et al., 2015; Valentino et al., 2016). A comparison of these two average exhumation rates allows for a description of the fluctuation in exhumation corresponding with the dramatic increase in glacial presence during the late Cenozoic. If the short-term erosion rates are greater than the long-term erosion rates, the implication is that where tectonic uplift is negligible, the presence of glaciers increases erosion rates. In contrast, if the short-term erosion rate is comparable in age or varied across the Chugach Mountains from basin to basin, then precipitation and rock uplift serve as thresholds for the onset of effective glacial erosion.

The approach of this study is to empirically measure the exhumation of the landscape on different time scales through the use of AHe and ^{10}Be cosmogenic dating. We used these two methods to determine if the presence of glaciers in orogens with slow to moderate rock uplift undergo effective glacial erosion. A sampling of catchment-wide cosmogenic apparent erosion rates and preliminary results are summarized below, but more data is necessary to provide a stronger conclusion to be published in a peer-reviewed paper.

BACKGROUND

The Chugach Mountains of Alaska comprise an uplifted forearc along the southern margin of Alaska, which is driven by the subduction of the Aleutian megathrust and the Yakutat microplate (Plafker, 1987; Bruhn et al., 2004; Abers, 2008; Fuis et al., 2008; Haeussler et al., 2008; Finzel et al., 2011). The forearc is dissected by ice sheets along the axis and syntaxes and is deeply

incised by valley glaciers emanating from the topographic high zones (Fig. 4.1). The region receives precipitation from the Pacific Ocean which is heavily controlled by the orographic effect of the Chugach Mountains. Annual precipitation for the windward flank of the Chugach Mountains is ~ 1.8 m (National Climate Data Center, 2007). In contrast, the landward side of the Chugach Mountains is characterized by a colder continental interior climate with annual precipitation of ~ 0.5 m (National Climate Data Center, 2007). This study constrains the apparent erosion rates of catchments in the western extent of the Chugach Mountains adjacent to Anchorage, and deeply incised basins in Thompson Pass east of Valdez (fig. 4.1).

Erosion rates and upper plate deformation in this region have been studied utilizing AHe dating which provides long term average erosion rates on the order of 10^6-10^7 years (Spotila et al., 2004; Whipple and Meade, 2004; Berger et al., 2008; Berger and Spotila, 2008; Buscher et al., 2008; Arkle et al., 2013; Enkelmann et al., 2015, 2017; Ferguson et al., 2015; Lease et al., 2016; Valentino et al., 2016). Completed AHe ages in the Chugach Mountains depict loci of high exhumation along the accretion front of the Yakutat microplate, within the Chugach core, and along faults in Prince William Sound (Fig. 4.2). Our study area avoids these exhumational high zones to examine the landscape response to glacial presence where rock uplift is slow. Specifically, ages obtained through the work of Buscher et al. (2008) are located near the catchments which have been sampled for catchment-wide cosmogenic dating and can be used to compare erosion on varying timescales. East of Valdez, two AHe ages at 17.9 and 11.5 Ma are located within the CHU4 and CHU29 catchments, respectively (Buscher et al., 2008; Arkle et al., 2013). There is an AHe age near CHU41 (22.0 Ma) and an age near CHU53 (4.7 Ma) (Arkle et al., 2013). The equivalent erosion rates for these AHe ages associated with the nearest catchment-wide catchments are CHU4 (0.23 mm/yr), CHU29 (0.15 mm/yr), CHU41 (0.12

mm/yr), and CHU53 (0.5 mm/yr). These long-term erosion rates are much slower than the short-term sediment accumulation erosion rates (Loso et al., 2004; Riihimaki et al., 2005).

Short term erosion rates have been constrained through a series of sediment accumulation rate studies throughout the Chugach Mountains (Hallet et al., 1996; Loso et al., 2004; Riihimaki et al., 2005; Koppes and Hallet, 2006). It was shown that sediment yields and erosion rates increase with glacial ice cover in Alaska where both rock uplift and glacial erosion are present (Hallet et al., 1996). The erosion rates of Hallet et al. (1996) ranged from 5-50 mm/yr in the most active parts of the Chugach and Saint Elias Mountains, and they noted that erosion rates varied by an order of magnitude between catchments with glaciers as compared to those without. These erosion estimates are very high and more modern studies have shown the rates to be slower in the western Chugach Mountains and away from the highest zone of rock uplift (Loso et al., 2004; MacGregor et al., 2005; Riihimaki et al., 2005). The work of Riihimaki et al. (2005) focused on Bench Glacier which is situated in the southern half of Thompson Pass, and demonstrated that the glacier erodes the landscape at a rate of 1-2 mm/yr. This erosion estimate was derived from the turbidity of the glacial outwash emanating from the Bench glacier over a long period. The concentration of turbidity was related to material sourced from bedrock erosion, which provides an estimate of decadal glacial erosion rate. Erosion rates inferred from glacial sediment yields of the Tana Glacier are approximated at 1.6 mm/yr (Loso et al., 2004). This erosion rate was derived from the analysis of four varve bound jökulhlaups deposits, which preserve both coarse and fine grained fraction of sediment.

^{10}Be catchment-wide cosmogenic dating was used for this project to constrain the apparent erosion rates of catchments located along the Kenai and Chugach Mountains. The underlying assumption in catchment-wide cosmogenic dating is that sediment collected at the

mouth of a catchment is a representative sample of material spanning the entirety of the catchment (Bierman and Steig, 1996; Portenga and Bierman, 2011). The bedrock in the reaches of the catchment undergo an increase in concentration of ^{10}Be with continuous exposure to cosmogenic radiation. The bedrock is eventually eroded, transported, and deposited at the mouth of the catchment where we collect quartz grains and measure the ^{10}Be concentration. The exposure age is directly related to the concentration of ^{10}Be in the sample and the erosion rate is conversely related to the concentration.

These assumptions and sediment transport architecture are sufficient for cases where there is extensive sediment mixing, large catchments, and the environment is fluvial. However, material in glaciated landscapes does not undergo extensive mixing and may not be representative of the entire catchment; complicating the process. Glaciers do not thoroughly mix sediment and create moraines which can store sediment to be remobilized in the future (Bierman and Steig, 1996). The glacier also inhibits accumulation of ^{10}Be through shielding, which results in an underestimate of average exposure age. It is common in glaciated environments for ^{10}Be concentrations to be comprised of a combination of current cosmogenic exposure and inheritance from sediment recycling. Fame et al. (2017) demonstrated that in the postglacial landscapes of Scotland, remobilized sediment was the dominant source of material as compared to fresh bedrock erosion. Fame et al. (2017) reported all of the cosmogenic catchment-wide results as concentrations of ^{10}Be instead of erosion rates due to the assumptions and complications related to a glacial or post-glacial landscape. For the sake of consistency and comparison with the AHe dating, the catchment-wide results will be reported as erosion rates, with the understanding that these rates are presented under complicating assumptions.

Contrary to the complications of catchment-wide cosmogenic dating in glaciated catchments it has been shown that sediment mixing in either steep mountainous regions with glaciers (Binnie et al., 2006) or large basins (Matmon et al., 2003; Bierman et al., 2005) can be sufficient to yield ^{10}Be concentrations that represent the entire catchment. Steep mountain basins consistently flush out old moraines and sediment banks, reducing the chance of sediment recycling. Partly glaciated large basins have enough transport distance to allow enough time for sediment to mix properly in the fluvial system below the glaciers. Many of the catchments from this study exhibit these characteristics, meaning that the problematic assumptions of catchment-wide cosmogenic analysis in a glacial landscape may not be as influential in this region.

METHODS

Sampling Strategy

A total of seventeen catchments were sampled for ^{10}Be, twenty-one samples were collected for AHe dating, and ^{4}He/^{3}He dating was attempted on two samples. Samples for catchment-wide ^{10}Be cosmogenic analysis were collected from streams and rivers at the mouths of catchments. Sampling included collecting ~ 1 kg of sand sized grains from the bottom of the river with a spade and eventually drying them out for analysis. Samples were obtained either directly from the flowing water or from sand banks as close to the center of the river as possible to reduce the likelihood of recycled, older material being collected. Areas adjacent to upstream tributaries or anthropogenic activity were avoided. During our field work where it was observed that quartz was scarce, individual grains < 0.25 cm were collected from the sand banks as close to the center of the river as possible (Fig. 4.3A).

Although a total of seventeen catchments were sampled for catchment-wide cosmogenic dating, only six of the catchments yielded successful results (Fig. 4.1 and Table 4.1). The region is underlain by the Chugach Terrane, which comprised metasedimentary and metavolcanic sequences (McHugh Complex) and deformed graywacke, argillite, and slates (Valdez Group) (Moffit, 1951; Plafker and Berg, 1994; Burns et al., 1991) (Fig. 4.1). We found that the quartz was generally restricted to the metamorphosed sandy units, which were uncommon in our field areas. Due to this fact, many of the samples collected at the base of catchments had very little quartz, which made processing for a suitable amount of quartz for analysis difficult or impossible. After processing twenty catchment-wide samples, only six samples contained enough quartz to go forward with the analysis. Four catchments east of Valdez (Fig. 4.4) and two catchments east of Anchorage were successfully measured (Fig. 4.5).

There was an original plan to sample bedrock above the glacial trimlines to obtain ridge erosion rates but the ridges were physically impossible to access. The ridges were oversteepened with average slopes greater than 60°, characterized by knife-edges ranging from 0.5 to 7 meters in width, and were composed of fragile and fractured rock (Fig. 4.3B). The unpredictable stability of the ridges and winds associated with the ridgelines made them dangerous to access with a helicopter. Due to these factors, no ridge samples were collected.

^{10}Be catchment-wide analysis

Mineral separation for quartz and isolation of ^{10}Be was completed in the cosmogenic dating laboratories at the University of Cincinnati. Each sample was crushed and sieved down to 250–500 μm. Quartz was separated from each sample following the methods of Kohl and Nishizumi

(1992), and were spiked with atomic absorption spectrometry low-background Be carrier ($^{10}Be/^{9}Be$ of ~ $1x10^{-15}$). ^{10}Be was separated and purified by ion exchange chromatography and precipitated as $Be(OH)_2$ at pH > 7. The $Be(OH)_2$ was combusted by ignition in quartz crucibles, producing BeO. The BeO was mixed with Nb metal prior to being targeted in steel carriers. The $^{10}Be/^{9}Be$ ratios were measured via accelerator mass spectrometry (AMS) at the Purdue Rare Isotope Measurement (PRIME) Laboratory at Purdue University.

The catchment-wide average erosion rates were calculated using the methods and equation of Seong et al (2009):

$$\varepsilon = \frac{\Lambda}{\rho}\left(\frac{P(0)}{N_i} - \lambda\right) \quad (1)$$

where Ni is inherited activity (atoms $^{10}Be\ g^{-1}$ quartz), P(0) is the production rate, ε is the erosion rate, ρ is the density of the material (g cm^{-3}), Λ is the attenuation depth (150 g cm^{-2}), and λ is the decay constant for ^{10}Be. The Matlab based code of Dortch et al. (2011) was used to calculate the production rate of each catchment, accounting for topographic shielding. The Young et al. (2013) production rate calibration was chosen for these calculations because it is most applicable to high latitude environments such as the field area (Baffin Island). The results are portrayed as the apparent average erosion rate and the concentration of ^{10}Be (Table 4.2).

AHe

Low temperature thermochronometry was used to constrain the exhumation history of the western limit of the Chugach Mountains. We obtained three new apatite AHe ages across the region, which corresponds with the edge of the exhumational high of Arkle et al. (2013).

Samples were collected via helicopter and where trail access was possible. AHe ages are based on the radiogenic production and thermal diffusion of ^{4}He and record cooling from closure temperatures of ~ 50–70 °C, or exhumation from ~ 2–3 km depth for typical geothermal gradient (i.e., 25 °C) (Farley, 2000 and Ehlers and Farley, 2003). Closure temperatures for AHe are dependent on multiple factors, however, including cooling history, crystal grain size, and radiation damage (Farley, 2000, Ehlers and Farley, 2003, Flowers et al., 2009 and Brown et al., 2013).

AHe ages were measured at Virginia Tech on both single and multigrain aliquots. Dated apatite grains were generally > 70 μm in diameter and were selected under 100 × magnification based on distinct crystal habit, birefringence, relief, and lack of obvious microinclusions or fractures. Aliquots were outgassed in Pt tubes in a resistance furnace at 950 °C for 20 min and analyzed for ^{4}He by ^{3}He spike and quadrupole mass spectrometry. Radiogenic parent isotopes were measured at the University of Arizona using isotope dilution and ICP mass spectrometry. Predicted age uncertainty is ~ 5% (1σ), based on instrument precision and *FT* calculations (Farley, 2000). However, average observed standard deviation of measured ages was 18.8% (1σ) (Table 4.2).

k_{sn}

Normalized channel steepness (k_{sn}) is defined as the slope-area regression (Flint's Law) normalized to the area of a location along the longitudinal profile (Wobus et al., 2006). The geomorphic response to tectonic activity in a fluvial environment is characterized by changes in the steepness and concavity of streams. Over steepened channels derived from tectonic forcing commonly exhibit high k_{sn} values (Safran et al., 2005; Kirby and Whipple, 2012; Castillo et al.,

2014). Lateral variations in channel steepness correlate with concentrations of upper plate deformation, e.g., fault activity, surface uplift, and focused erosion. The slope-area regression is defined as:

$$S = k_s A^{-\theta} \quad (2)$$

where S is the channel slope, k_s is the steepness index, A is the drainage area, and θ is the concavity index. A typical concavity value, based on regions that are not tectonically active (~ 0.45) was used as the reference for the slope area regression (Wobus et al., 2006). The resulting calculation along longitudinal profiles reveal regional variance in k_{sn} which is inferred to relate to or represent channel incision in response to tectonic forcing.

The geomorphic response to differential erosion and the presence of glaciers in the catchments was quantitatively characterized by comparing spatial k_{sn} patterns. The software packages Geomorphtools (Whipple et al., 2007), ArcGIS, and Matlab were used to calculate k_{sn} from 30 meter DEMs (National Map USGS) for each catchment. The program calculates the channel steepness and concavity for each pixel on the longitudinal profile of the catchment and normalizes the results to the area. The result is a colored set of shapefiles, which depict regional changes in k_{sn} throughout the catchment (fig 4.6A). This analysis was limited to basins, which had little presence of modern glaciers due to the fact that glaciers covered the underlying topography. Glacial cover inhibits the underlying topographic expression of the landscape and instead overestimates the elevation and smoothness on a DEM. The glacier characteristics on a DEM which homogenizes the k_{sn} analysis for those regions (Fig. fig 4.6B).

$^4He/^3He$

Apatite $^{4}He/^{3}He$ dating is a low temperature thermochronometer which effectively constrains the time-temperature path of the (U-Th)/He system (Shuster and Farley, 2005; Farley et al., 2010). This technique provides insight on the exhumation and temperature path of the apatite grain for ~ 1 km beneath the sampled surface. The alpha decay of U, Th, and Sm in the apatite produce ^{4}He, where the spatial distribution of ^{4}He relates to the grain time-temperature path (Shuster and Farley, 2005). A stepwise temperature degassing process is used to measure and map ^{4}He from the edge of the apatite grain to the center. The architecture of the resulting ^{4}He curve with ^{3}He varies with the time-temperature path and can provide meaningful exhumation information on the time scale of 10^{6}-10^{5} years.

We selected samples 06STP44 and 05STP7 from the earlier work of Aaron Berger for $^{4}He/^{3}He$ analysis because they had low elevations and were located within the Chugach Mountains. The mineral separates were sent to Berkeley University, CA where grains were picked under a microscope, irradiated, and sequentially degassed for ^{4}He. The results of this analysis were modeled for time-temperature paths but the results were inconclusive. Each degassing step of the ^{4}He curve had very large error margins, which could not be modeled with any statistical reliability. We believe that these complications were from badly deformed apatite grains with microinclusions and fractures, which produce an excess of ^{4}He and diffuse along the fractured boundaries, relatively.

RESULTS

A total of six catchment-wide cosmogenic average erosion rates were compiled and the results are presented in Table 4.1. The apparent erosion rates were separated into two sets, which varied by an order of magnitude. The first set of rates ranges from 0.93 to 1.94 mm yr^{-1} and includes

basins CHU3, CHU4, CHU29, and CHU53. The second set of rates ranges from 0.13 to 0.17 mm yr^{-1} and includes basins CHU30 and CHU41. The ksn map of CHU3 (fig. 4.5) shows very high values (>280) at the toes of glaciers where the outwash pours into the valley and at the mouth of the catchment where the river is forming a deep canyon.

The catchments exhibit steep topography with deeply incised valleys, with the exception of CHU41, which has broader valleys and moraine deposits throughout (fig. 4.4). Basins CHU29 and CHU53 are almost completely glaciated, CHU3, CHU4, and CHU30 are partially glaciated, and CHU41 is unglaciated. There is a correlation of catchment area and apparent erosion rate, where the largest basins have the highest erosion rates, and the smallest basins exhibit the slowest erosion rates (Table 4.1).

A total of three new AHe ages were calculated and are dated at 33.0 (12CH13), 26.6 (12CH11), and 15.2 (12CH17) Ma (Table 4.2). Our calculated closure temperature based on the cooling ages is ~ 58 °C, and the regional geothermal gradient of ~ 22 °C/km is estimated from the temperature logs of COST No. 1 well in Cook Inlet (Magoon, 1986). In this case, the closure temperature occurs at a depth of 2.6 km, resulting in erosion rates of 0.08, 0.09 and 0.17 mm/yr for 12CH13, 12CH11 and 12CH17, respectively.

DISCUSSION

The new catchment-wide cosmogenic erosion rates are high at ~ 1-2 mm/yr, with the exception of CHU41 and CHU29 which have slow rates at ~ 0.13 to 0.17 mm/yr. Our fast erosion rates are similar to the decadal scale rates of Riihimaki et al. (2005) at 1-2 mm/yr in Thompson Pass, Loso et al. (2004) at ~ 1.6 mm/yr in the Chugach Mountains, and Hallet et al. (1996) at 5–50 mm/yr across global alpine regions (Fig. 4.7). The new AHe ages ranged from

33.0 to 15.5 Ma and correlate with ages from previous work in the areas (Buscher et al., 2008; Arkle et al., 2013), all indicating slow erosion between 0.08–0.17 mm/yr (Fig. 4.7). A comparison of both average long term and short term erosion rates in figure 4.7 shows a shift from slow rates at ~ 0.1 mm/yr to higher rates at ~ 1–2 mm/yr, indicating that there has been an increase in erosion rates by an order of magnitude since the late Cenozoic.

The area, precipitation, glacial coverage, and slope were recorded in each cosmogenic catchment in order to compare with the erosion rates and spatial variations in long term rock uplift (Figs. 4.7, 4.8). Both precipitation and catchment area have positive correlations with the catchment-wide cosmogenic erosion rates (Fig. 4.8A, B). The percentage of glacial coverage compared with the erosion rate has a negative trend in the five catchments that are partially glaciated (Fig. 4.8C). The average slope for each catchment shows no distinct variation with erosion rate and range from 15 to 20^{o}. These trends all imply that climate controlled factors dictate the short-term erosion rates of these catchments in the Chugach Mountains.

Both CHU41 and CHU29 have slow erosion rates when compared with the rest of the basins. CHU41 has a slow erosion rate of 0.17 mm/yr but does not have any glacial coverage. Hallett et al. (1996) had suggested that it was possible for erosion rates to vary by an order of magnitude between glaciated and unglaciated catchments, which is what we observe in this case. An alternative reason for the slow rate is that this catchment is undergoing sediment recycling due to preexisting moraines that have not been successfully flushed from the catchment since the LGM. The catchment is characterized by older moraines, thick layers of sediment, and slow moving rivers. In contrast, the other basins with fast erosion rates are characterized by canyons where the sediment has been excavated via fast flowing water. CHU29 has a slow erosion rate of 0.13 mm/yr and has the most glacial coverage. It is possible that the slow erosion rate is due

to poor sediment mixing within the glacier, and incorporation of an excess of old ridge material from landslides.

Our new AHe ages and the regional map of AHe ages (Fig. 4.2) indicate that there has been an extended period of slow to moderate rock uplift on the timescale of 10^6-10^7 years in the field areas of this study. According to the catchment-wide cosmogenic and AHe data, the western limit of the Chugach Mountains and Thompson Pass have undergone slow to moderate rock uplift over the long-term timescale and have experienced a pulse of increased erosion on the short-term timescale. This relationship demonstrates that in regions with slow to moderate rock uplift rates, the presence of glaciers can increase erosion rates. In this case, fast rock uplift rate is not a fundamental component required for the onset of effective glacial erosion; therefore, climate change can drive accelerated erosion rates in an orogen.

It is possible that the variation in erosion rate is a reflection of the Sadler Effect, where process rates are a function of the measured time interval (Sadler, 1981; Gardner et al., 1987). The fluctuation of rates through time limit the reliability of measuring rate on varying timescales since the unsteadiness of rate increases with time (Sadler, 1981; Gardner et al., 1987; Willenbring and von Blanckenburg, 2010; Sadler and Jerolmack, 2015). The results of the AHe dating are on the order of $10^{6\text{-}7}$ years, which are typified by long periods of slow rock uplift and shorter pulses of fast rock uplift. The results of the cosmogenic dating are on the order of $10^{3\text{-}4}$ years which may capture one of the shorter pules, resulting in a comparatively high apparent erosion rate. In this case, the average of oscillating fast and slow erosion rates through time progressively become slower with time. Since our observations show this trend, it is possible that our results are reflecting the Sadler Effect and do not actually represent an increase in

erosion rate since the late Cenozoic. This phenomenon needs to be considered when conducting multi-chronologic research on rate fluctuations.

CONCLUSION

Comparison of six new ^{10}Be catchment-wide apparent erosion rates and three new AHe ages with the regional AHe long term exhumation rates shows that climate driven processes control the distribution of short term erosion in regions of slow to moderate rock uplift in the Chugach Mountains. The AHe long term average erosion rates range from 0.08–0.17 mm/yr and the short-term erosion rates range from 1–2 mm/yr. The dramatic difference between the erosion rates indicates that the presence of glaciers since global cooling in the late Cenozoic has increased erosion rates in the alpine regions of the Chugah Mountains. Analysis of precipitation and the area of each sampled catchment-wide cosmogenic catchment indicate that climate driven processes increase erosion rate in regions where rock uplift is slow to moderate. The net effect of glaciers on the alpine landscape of the Chugach Mountains is accelerated erosion due to an increase in precipitation and colder global temperatures during the late Cenozoic.

REFERENCES

Abers, G.A., 2008. Orogenesis from subducting thick crust and evidence from Alaska. Active Tectonics and Seismic Potential of Alaska vol. 179. American Geophysical Union Monograph Series, pp. 337–349.

Anderson, R.S., Molnar, P., and Kessler, M.A., 2006, Features of glacial valley profiles simply explained, J. Geophys. Res., 111, F01004, 14 p.

Arkle, J., Armstrong, P., Haeussler, P., Prior, M., Hartman, S., Sendziak, K., Brush, J., 2013. Focused exhumation in the syntaxis of the western Chugach Mountains and Prince William Sound, Alaska. Geol. Soc. Am. Bull. 125 (5–6), 776–793. http://dx.doi.org/10.1130/b30738.1.

Berger, A. L., & Spotila, J. A. (2008). Denudation and deformation in a glaciated orogenic wedge: The St. Elias orogen, Alaska. *Geology*, *36*(7), 523-526.

Berger, A.L., Spotila, J.A., Chapman, J.B., Pavlis, T.L., Enkelmann, E., Ruppert, N.A., Buscher, J.T., 2008. Architecture, kinematics, and exhumation of a convergent orogenic wedge: a thermochronological investigation of tectonic–climatic interactions within the central St. Elias Orogen, Alaska. Earth Planet. Sci. Lett. 270 (1–2), 13–24. http://dx.doi.org/10.1016/j.epsl.2008.02.034.

Binnie, S. A., Phillips, W. M., Summerfield, M. A., & Fifield, L. K. (2006). Sediment mixing and basin-wide cosmogenic nuclide analysis in rapidly eroding mountainous environments. *Quaternary Geochronology*, *1*(1), 4-14.

Bierman, P. R., Reuter, J. M., Pavich, M., Gellis, A. C., Caffee, M. W., & Larsen, J. (2005). Using cosmogenic nuclides to contrast rates of erosion and sediment yield in a semi-arid, arroyo-dominated landscape, Rio Puerco Basin, New Mexico. *Earth Surface Processes and Landforms*, *30*(8), 935-953.

Bierman, P., & Steig, E. J. (1996). Estimating rates of denudation using cosmogenic isotope abundances in sediment. *Earth surface processes and landforms*, *21*(2), 125-139.

Brocklehurst, S. H., & Whipple, K. X. (2002). Glacial erosion and relief production in the Eastern Sierra Nevada, California. *Geomorphology*, *42*(1), 1-24.

Brocklehurst, S. H., & Whipple, K. X. (2004). Hypsometry of glaciated landscapes. *Earth Surface Processes and Landforms*, *29*(7), 907-926.

Brocklehurst, S. H., Whipple, K. X., & Foster, D. (2008). Ice thickness and topographic relief in glaciated landscapes of the western USA. *Geomorphology*, *97*(1), 35-51.

Brozovic, N., Burbank, D.W., and Meigs, A.J., 1997, Climatic limits on landscape development in the northwestern Himalaya, Science, 276, 571-574.

Bruhn, R., Pavlis, T., Plafker, G., Serpa, L., 2004. Deformation during terrane accretion in the

Saint Elias orogen, Alaska. Geol. Soc. Am. Bull. 116 (7–8), 771–787. http://dx.doi.org/10.1130/b25182.1.

Burns, L. E., Pessel, G. H., Little, T. A., Pavlis, T. L., Newberry, R. J., Winkler, G. R., & Decker, J. (1991). Geology of the northern Chugach Mountains, southcentral Alaska. *Alaska Division of Geological and Geophysical Surveys Professional Report*, *94*, 63.

Buscher, J.T., Berger, A.L., Spotila, J.A., 2008. Exhumation in the Chugach–Kenai Mountain Belt above the Aleutian Subduction Zone, Southern Alaska. Active Tectonics and Seismic Potential of Alaska vol. 179. American Geophysical Union Monograph Series, pp. 151–166.

Castillo, M., Muñoz-Salinas, E., & Ferrari, L. (2014). Response of a landscape to tectonics using channel steepness indices (k sn) and OSL: a case of study from the Jalisco Block, Western Mexico. *Geomorphology*, *221*, 204-214.

Champagnac, J. D., Valla, P. G., & Herman, F. (2014). Late-Cenozoic relief evolution under evolving climate: A review. *Tectonophysics*, *614*, 44-65.

Densmore, M. S., Ehlers, T. A., & Woodsworth, G. J. (2007). Effect of Alpine glaciation on thermochronometer age-elevation profiles. *Geophysical research letters*, *34*(2).

Dowdeswell, J. A., Ottesen, D., & Rise, L. (2010). Rates of sediment delivery from the Fennoscandian Ice Sheet through an ice age. *Geology*, *38*(1), 3-6.

Ehlers, T. A., Farley, K. A., Rusmore, M. E., & Woodsworth, G. J. (2006). Apatite (U-Th)/He signal of large-magnitude accelerated glacial erosion, southwest British Columbia. *Geology*, *34*(9), 765-768.

Enkelmann, E., Piestrzeniewicz, A., Falkowski, S., Stübner, K., & Ehlers, T. A. (2017). Thermochronology in southeast Alaska and southwest Yukon: Implications for North American Plate response to terrane accretion. *Earth and Planetary Science Letters*, *457*, 348-358.

Falkowski, S., Enkelmann, E., Drost, K., Pfänder, J. A., Stübner, K., & Ehlers, T. A. (2016). Cooling history of the St. Elias syntaxis, southeast Alaska, revealed by geo-and thermochronology of cobble-sized glacial detritus. *Tectonics*.

Farley, K. A., Rusmore, M. E., & Bogue, S. W. (2001). Post–10 Ma uplift and exhumation of the northern Coast Mountains, British Columbia. *Geology*, *29*(2), 99-102.

Finzel, E.S., Trop, J.M., Ridgway, K.D., Enkelmann, E., 2011. Upper plate proxies for flat-slab subduction processes in southern Alaska. Earth Planet. Sci. Lett. 303 (3–4), 348–360. http://dx.doi.org/10.1016/j.epsl.2011.01.014.

Fuis, G., Moore, T., Plafker, G., Brocher, T., Fisher, M., Mooney, W., Nokleberg, W., Page, R.,Beaudoin, B., Christensen, N., Levander, A., Lutter, W., Saltus, R., Ruppert, N., 2008. Trans-Alaska Crustal Transect and continental evolution involving subduction underplating and synchronous foreland thrusting. Geology 36 (3), 267–270. http://dx.doi.org/10.1130/g24257a.1.

Gardner, T. W., Jorgensen, D. W., Shuman, C., & Lemieux, C. R. (1987). Geomorphic and tectonic process rates: Effects of measured time interval. *Geology*, *15*(3), 259-261.

Gosse, J. C., & Phillips, F. M. (2001). Terrestrial in situ cosmogenic nuclides: theory and application. *Quaternary Science Reviews*, *20*(14), 1475-1560.

Haeussler, P.J., 2008. An overview of the Neotectonics of interior Alaska: far-field deformation from the Yakutat microplate collision. Active Tectonics and Seismic Potential of Alaska. American Geophysical Union Geophysics Monograph Series 179, pp. 83–108.

Haeuselmann, P., Granger, D. E., Jeannin, P. Y., & Lauritzen, S. E. (2007). Abrupt glacial valley incision at 0.8 Ma dated from cave deposits in Switzerland. *Geology*, *35*(2), 143-146.

Hallet, B., Hunter, L., and Bogen, J., 1996, Rates of erosion and sediment evacuation by glaciers: A review of field data and their implications, Global and Planetary Change, 12, 213-255.

Hebbeln, D., Lamy, F., Mohtadi, M., & Echtler, H. (2007). Tracing the impact of glacial-interglacial climate variability on erosion of the southern Andes. *Geology*, *35*(2), 131-134.

Huntington, K. W., Blythe, A. E., & Hodges, K. V. (2006). Climate change and Late Pliocene acceleration of erosion in the Himalaya. *Earth and Planetary Science Letters*, *252*(1), 107-118.

Ivy-Ochs, S., & Kober, F. (2008). Surface exposure dating with cosmogenic nuclides. *Quaternary Science Journal*, *57*(1-2), 157-189.

Kirby, E., & Whipple, K. X. (2012). Expression of active tectonics in erosional landscapes. *Journal of Structural Geology*, *44*, 54-75.

Lease, R. O., Haeussler, P. J., & O'Sullivan, P. (2016). Changing exhumation patterns during Cenozoic growth and glaciation of the Alaska Range: Insights from detrital thermochronology and geochronology. *Tectonics*, *35*(4), 934-955.

Loso, M. G., Anderson, R. S., & Anderson, S. P. (2004). Post–Little Ice Age record of coarse and fine clastic sedimentation in an Alaskan proglacial lake. *Geology*, *32*(12), 1065-1068.

MacGregor, K. R., Riihimaki, C. A., & Anderson, R. S. (2005). Spatial and temporal evolution of sliding velocity on a small alpine glacier: Bench Glacier, Alaska 1999 and 2000. *J. Glaciol*.

Matmon, A., Bierman, P. R., Larsen, J., Southworth, S., Pavich, M., & Caffee, M. (2003). Temporally and spatially uniform rates of erosion in the southern Appalachian Great Smoky Mountains. *Geology*, *31*(2), 155-158.

McAleer, R. J., Spotila, J. A., Enkelmann, E., & Berger, A. L. (2009). Exhumation along the Fairweather fault, southeastern Alaska, based on low-temperature thermochronometry. *Tectonics*, *28*(1).

Mitchell, S.G., and Montgomery, D.R., 2006, Influence of a glacial buzzsaw on the height and morphology of the Cascade Range in central Washington State, USA, Quaternary Research, 65, 96-107.

Moffit, F. H. (1954). *Geology of the Prince William Sound region, Alaska* (No. 989-E).

Molnar, P., & England, P. (1990). Late Cenozoic uplift of mountain ranges and global climate change: chicken or egg?. *Nature*, *346*(6279), 29-34.

Plafker, G., 1987. Regional geology and petroleum potential of the northern Gulf of Alaska continental margin. In: Scholl, D.W., Grantz, A., Vedder, J.G. (Eds.), Geology and Resource Potential of the Continental Margin of Western North America and Adjacent Ocean Basins—Beaufort Sea to Baja California: Circum-Pacific Council for Energy and Mineral Resources. Earth Sciences Series, 6, 299–268.

Plafker, G., Berg, H.C., 1994. Overview of the geology and tectonic evolution of Alaska. In: Plafker, G., Berg, H.C. (Eds.), The Geology of Alaska vol. G-1. Geological Society of America, Geology of North America, Boulder, Colorado, pp. 989–1021.

Rahaman, W., Singh, S. K., Sinha, R., & Tandon, S. K. (2009). Climate control on erosion distribution over the Himalaya during the past~ 100 ka. *Geology*, *37*(6), 559-562.

Raymo, M. E., & Ruddiman, W. F. (1992). Tectonic forcing of late Cenozoic climate. *Nature*, *359*(6391), 117-122.

Riihimaki, C. A., MacGregor, K. R., Anderson, R. S., Anderson, S. P., & Loso, M. G. (2005). Sediment evacuation and glacial erosion rates at a small alpine glacier. *Journal of Geophysical Research: Earth Surface*, *110*(F3).

Ruddiman, W. F. (2010). A paleoclimatic enigma?. *Science*, *328*(5980), 838-839.

Sadler, P. M. (1981). Sediment accumulation rates and the completeness of stratigraphic sections. *The Journal of Geology*, *89*(5), 569-584.

Sadler, P. M., & Jerolmack, D. J. (2015). Scaling laws for aggradation, denudation and progradation rates: the case for time-scale invariance at sediment sources and sinks. *Geological Society, London, Special Publications*, *404*(1), 69-88.

Safran, E. B., Bierman, P. R., Aalto, R., Dunne, T., Whipple, K. X., & Caffee, M. (2005). Erosion rates driven by channel network incision in the Bolivian Andes. *Earth Surface Processes and Landforms*, *30*(8), 1007-1024.

Seong, Yeong Bae, Lewis A. Owen, Marc W. Caffee, Ulrich Kamp, Michael P. Bishop, Andrew Bush, Luke Copland, and John F. Shroder. "Rates of basin-wide rockwall retreat in the K2 region of the Central Karakoram defined by terrestrial cosmogenic nuclide 10 Be." *Geomorphology* 107, no. 3 (2009): 254-262.

Shuster, D. L., Ehlers, T. A., Rusmoren, M. E., & Farley, K. A. (2005). Rapid glacial erosion at 1.8 Ma revealed by 4He/3He thermochronometry. *Science*, *310*(5754), 1668-1670.

Small, E. E., & Anderson, R. S. (1995). Geomorphically driven late Cenozoic rock uplift in the Sierra Nevada, California. *Science*, *270*(5234), 277.

Spotila, J.A., Buscher, J.T., Meigs, A.J., Reiners, P.W., 2004. Long-term glacial erosion of active mountain belts: example of the Chugach–St. Elias Range, Alaska. Geology 32(6),501–504.

Thomson, S. N. (2002). Late Cenozoic geomorphic and tectonic evolution of the Patagonian Andes between latitudes 42 S and 46 S: An appraisal based on fission-track results from the

transpressional intra-arc Liquiñe-Ofqui fault zone. *Geological Society of America Bulletin*, *114*(9), 1159-1173.

Thomson, S. N., Brandon, M. T., Tomkin, J. H., Reiners, P. W., Vásquez, C., & Wilson, N. J. (2010). Glaciation as a destructive and constructive control on mountain building. *Nature*, *467*(7313), 313-317.

Tomkin, J. H., & Roe, G. H. (2007). Climate and tectonic controls on glaciated critical-taper orogens. *Earth and Planetary Science Letters*, *262*(3), 385-397.

Van Der Beek, P., & Bourbon, P. (2008). A quantification of the glacial imprint on relief development in the French western Alps. *Geomorphology*, *97*(1), 52-72.

Valentino, J. D., Spotila, J. A., Owen, L. A., & Buscher, J. T. (2016). Rock uplift at the transition from flat-slab to normal subduction: The Kenai Mountains, Southeast Alaska. *Tectonophysics*, *671*, 63-75.

Whipple, K. X., Kirby, E., & Brocklehurst, S. H. (1999). Geomorphic limits to climate-induced increases in topographic relief. *Nature*, *401*(6748), 39.

Whipple, K. X., & Meade, B. J. (2004). Controls on the strength of coupling among climate, erosion, and deformation in two-sided, frictional orogenic wedges at steady state. *Journal of Geophysical Research: Earth Surface*, *109*(F1).

Whipple, K. X., Wobus, C., Crosby, B., Kirby, E., & Sheehan, D. (2007). New tools for quantitative geomorphology: extraction and interpretation of stream profiles from digital topographic data. *GSA Short Course*, *506*.

Wobus, Cameron, Kelin X. Whipple, Eric Kirby, Noah Snyder, Joel Johnson, Katerina Spyropolou, Benjamin Crosby, and Daniel Sheehan. "Tectonics from topography: Procedures, promise, and pitfalls." *Geological Society of America Special Papers* 398 (2006): 55-74.

Young, N. E., Schaefer, J. M., Briner, J. P., & Goehring, B. M. (2013). A ^{10}Be production-rate calibration for the Arctic. *Journal of Quaternary Science*, *28*(5), 515-526.

Yu, X., Ji, J., Wang, F., & Zhong, D. (2016). Intensified Climate-Driven Exhumation along the South Himalayan Front since One Million Years ago. *Journal of Asian Earth Sciences*.

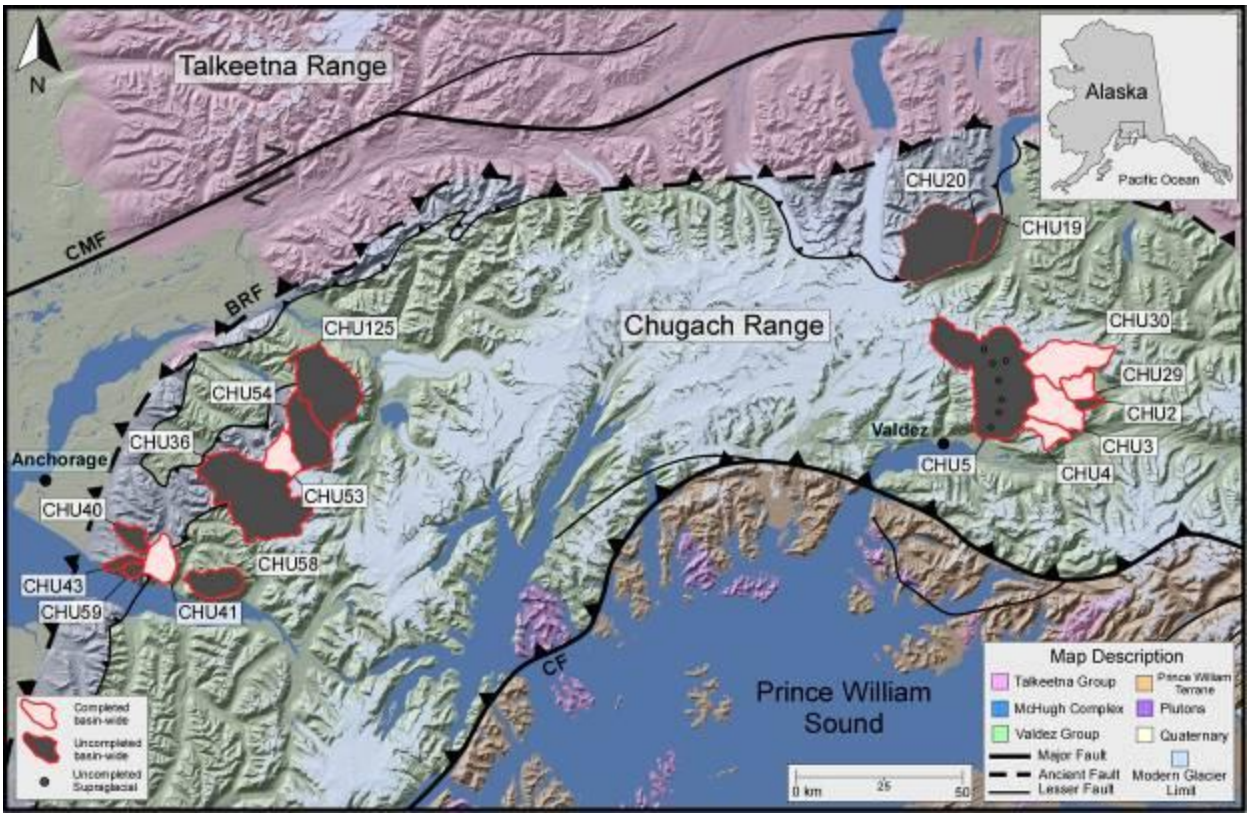

Figure 4.1. Elevation and land cover DEM map showing major faults and geologic terranes of south central Alaska. The catchments are outlined and labeled in red in the western Chugach Mountains and east of Valdez. BRF = Border Ranges Fault; CF = Contact Fault; CMF = Castle Mountain Fault

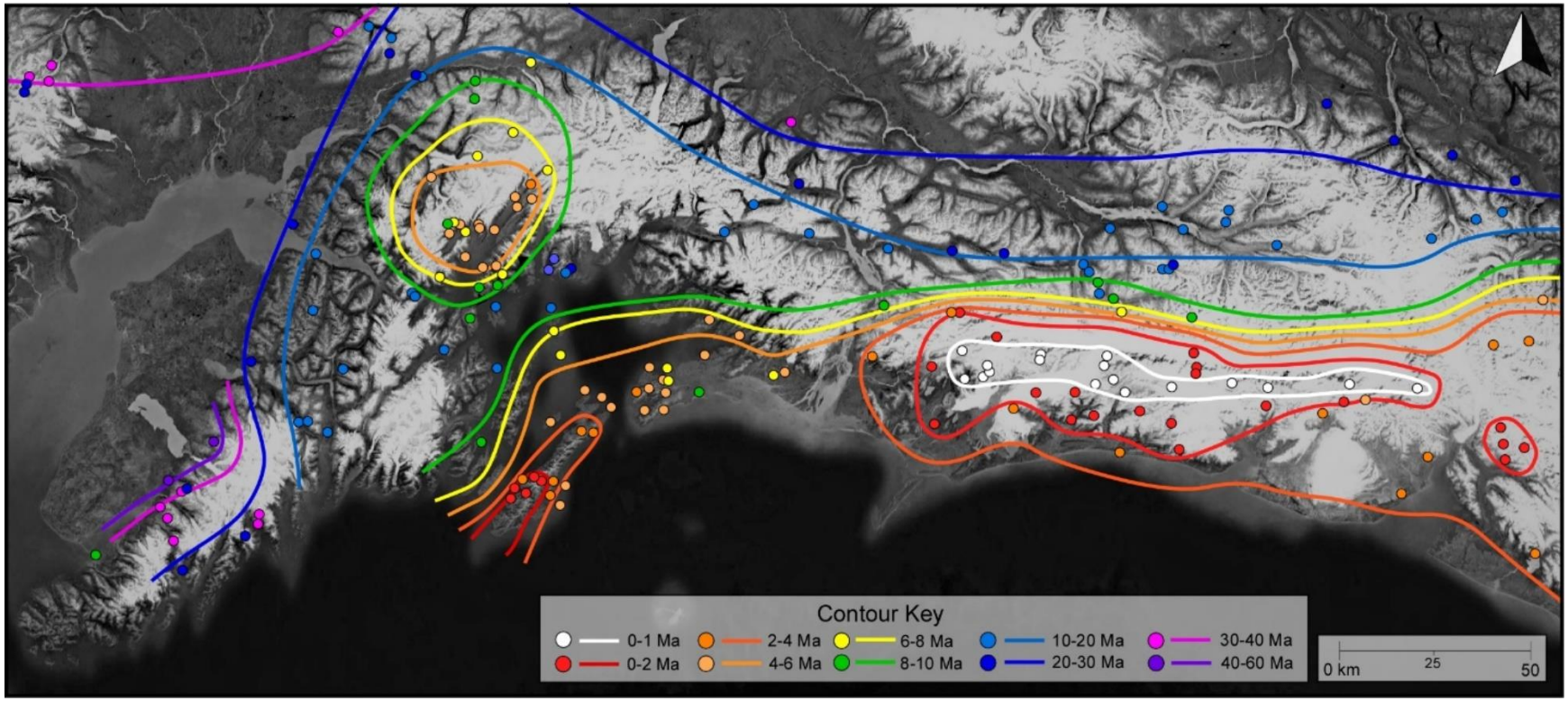

Figure 4.2. A summary contour map of AHe ages in southern Alaska. The majority of the high exhumation is in the eastern Chugach Mountains, associated with the accretion of the Yakutat microplate. High exhumation is also located along splay faults in Prince William Sound and above the Chugach core at the syntaxes in the forearc.

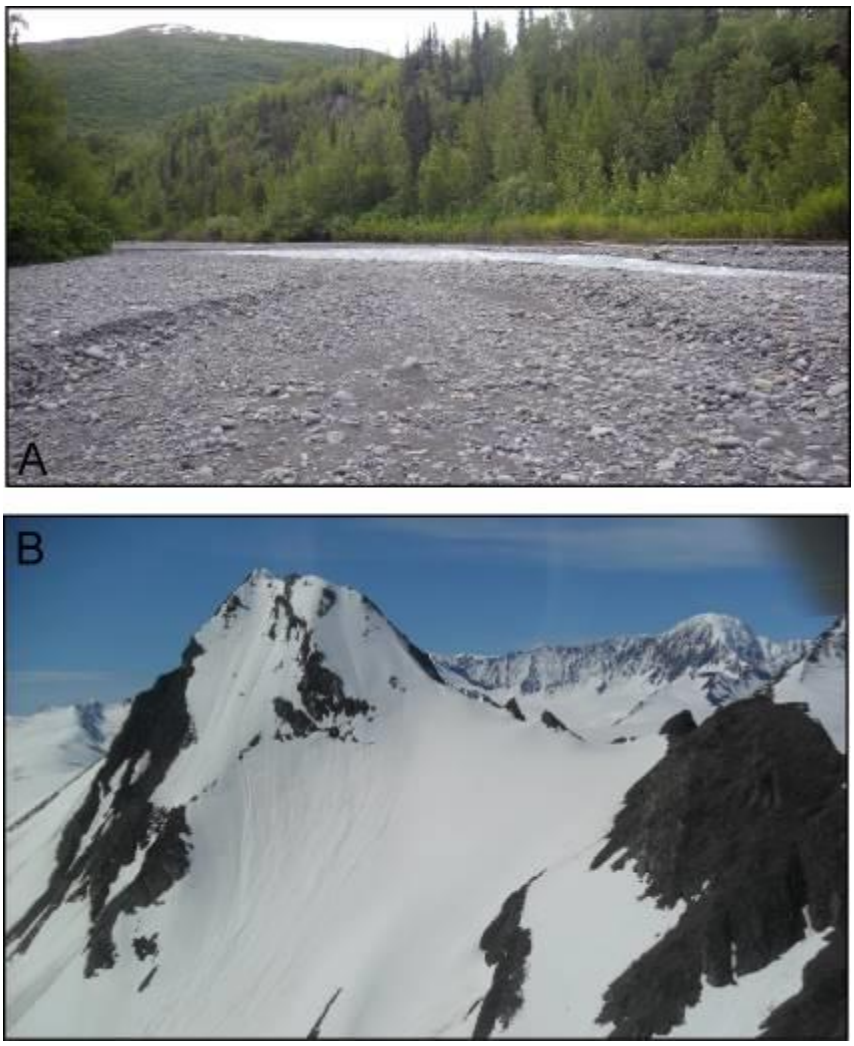

Figure 4.3. (A) Field location of one of the sampled catchment-wide cosmogenic catchments. Sediment was collected from the banks closest to the flowing water. (B) Example of the razor back ridges in the center of the Chugach Mountains which could not be accessed by helicopter.

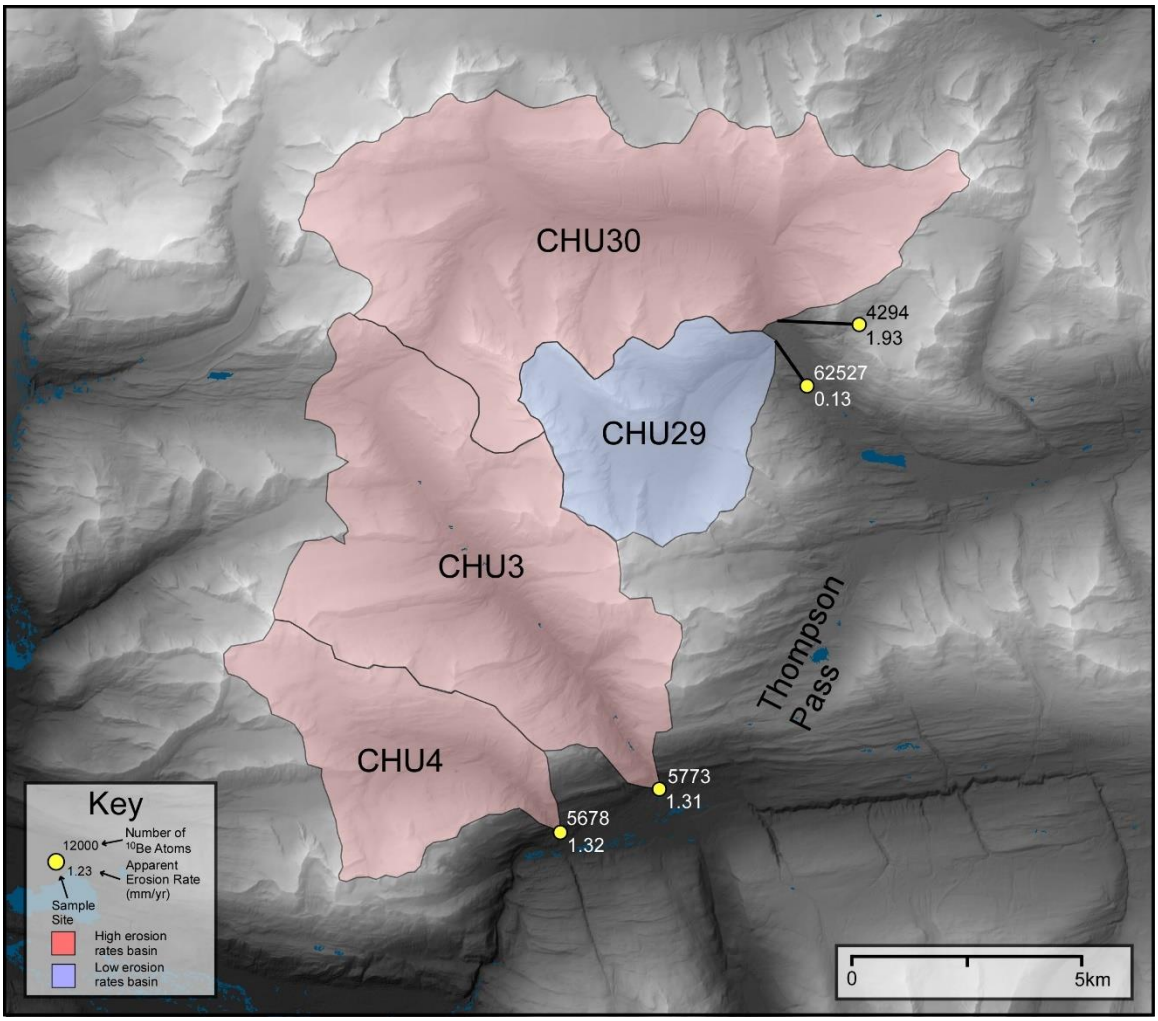

Figure 4.4. A shaded relief map of Thompson Pass and the surrounding mountains depicting catchment delineations of basins that were dated with catchment-wide cosmogenic dating. The red basins have comparably high apparent rates of erosion >1 mm/year while the blue basin has a slower rate <0.2 mm/year.

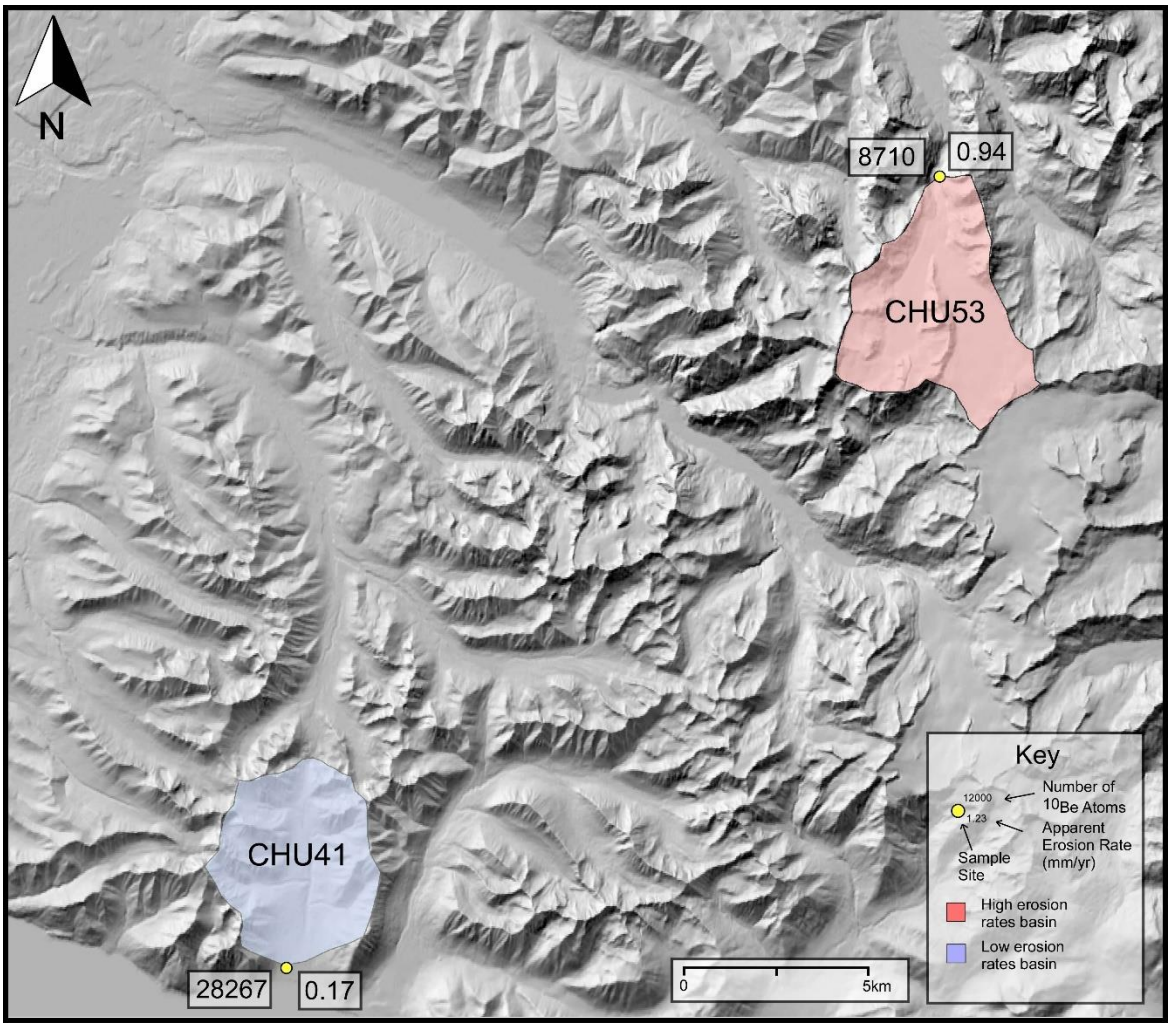

Figure 4.5. A shaded relief map of the westernmost Chugach Mountains east of Anchorage and the surrounding mountains depicting catchment delineations of basins that were dated with catchment-wide cosmogenic erosion rates. The red basins have comparably high apparent rates of erosion >1 mm/year while the blue basin has a slower rate <0.2 mm/year.

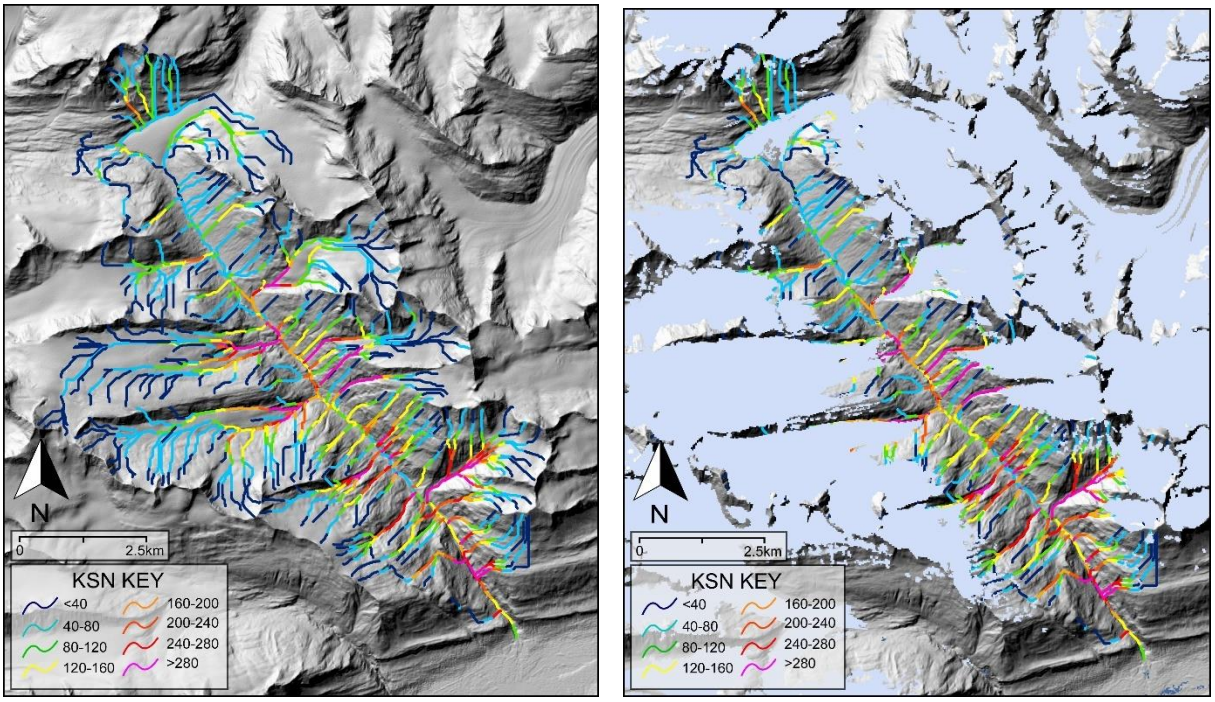

Figure 4.6. Shaded relief maps of the CHU3 catchment in Thompson Pass. k_{sn} is displayed as a series of colored lines showing focused erosion along the steep valley walls. The spatial distribution of k_{sn} in the glaciated portions of the catchment are oversimplified due to to the smooth and sub flat surface. (B) The current glacial coverage is superimposed.

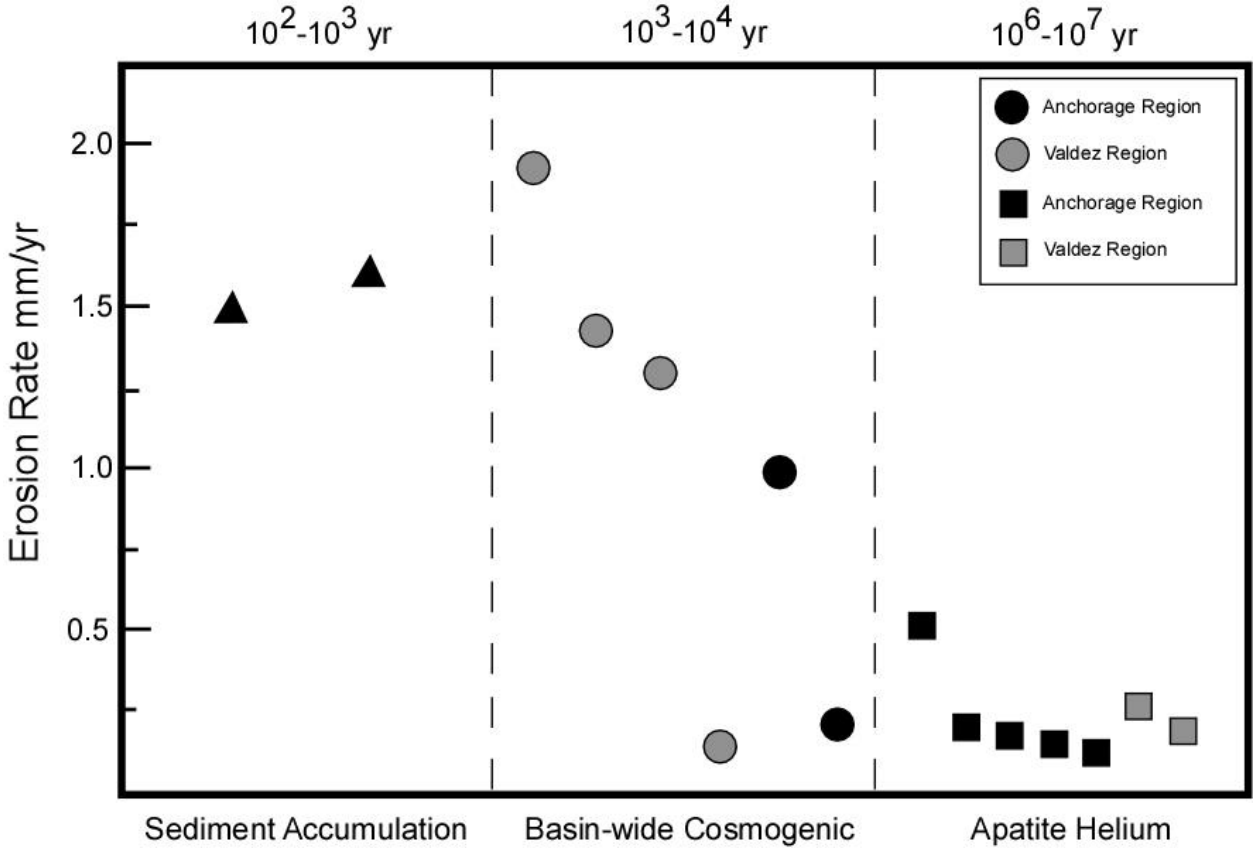

Figure 4.7. Summary graph of erosion rates on different timescales. The sediment accumulation erosion estimates are from the work of Loso et al., 2004 and Riihimaki et al., 2005 and the AHe ages are from Buscher et al., 2008 and Arkle et al., 2013. The plot clearly shows an order of magnitude difference between the short term and long term erosion rates.

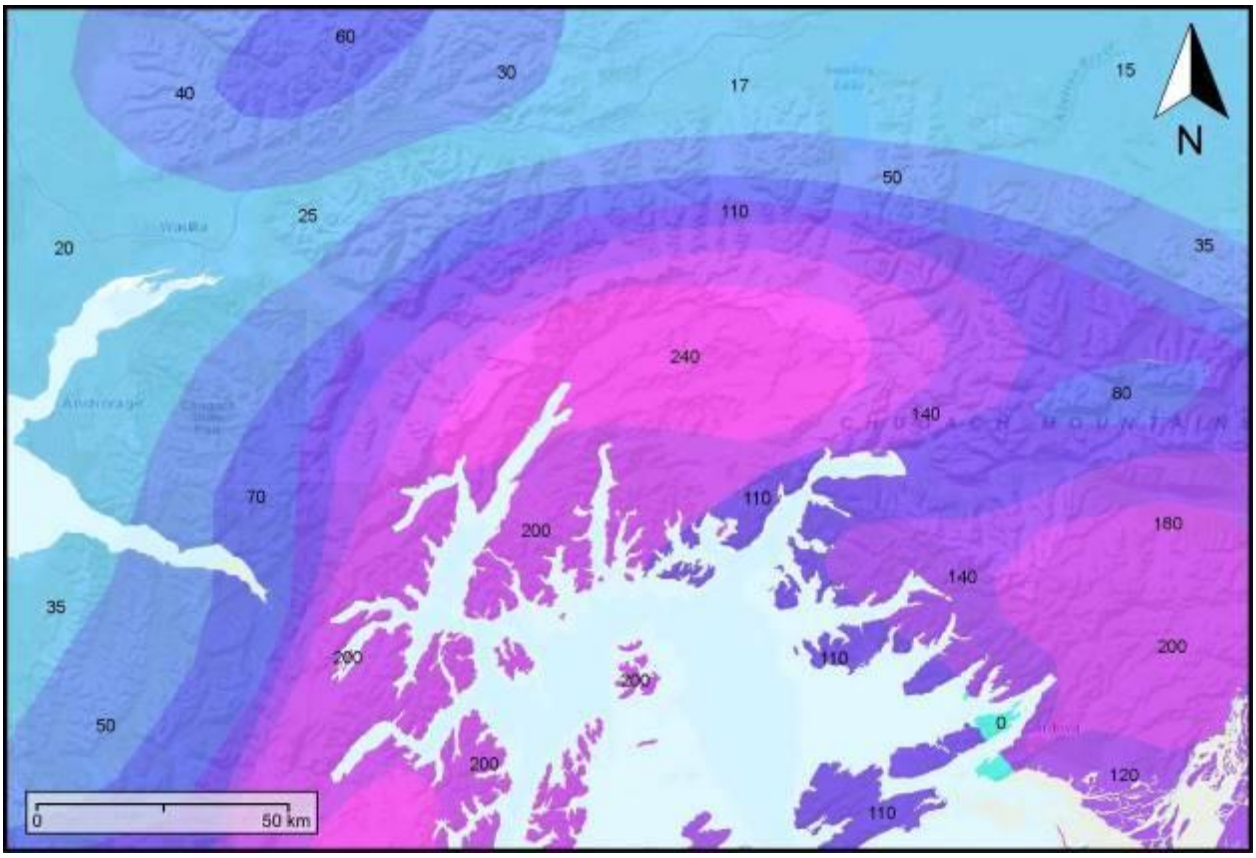

Figure 4.8. The regional precipitation map for the western Chugach Mountains and Prince William Sound. The labels are in inches per year. Data from USGS.

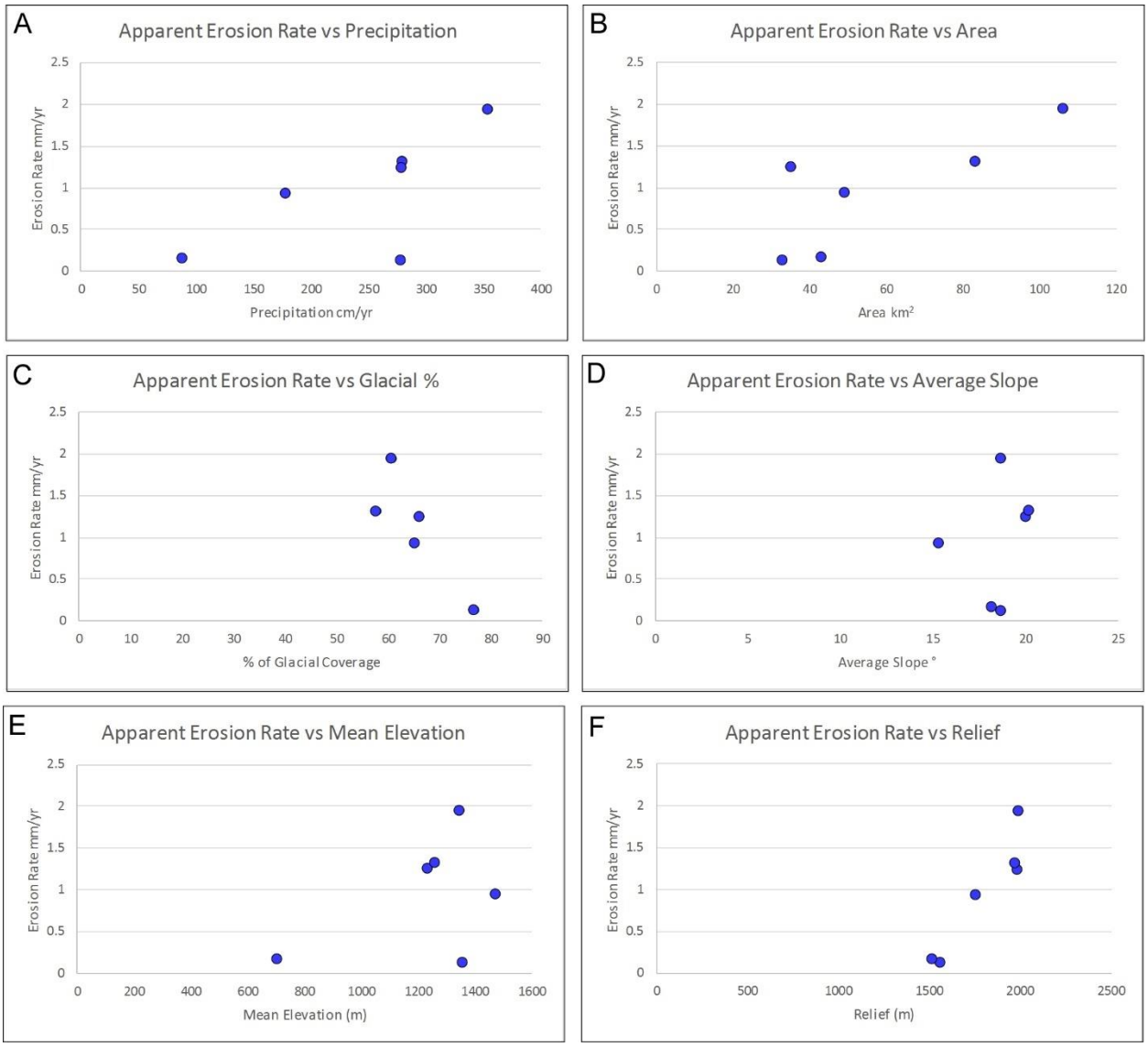

Figure 4.9. Comparative graphs of topographic and precipitation related characteristics of each basin-wide catchment. (A) Plot of precipitation against erosion rate shows positive trend. (B) Plot of catchment area with erosion rate shows positive trend. (C) Percentage of catchment covered in modern glacier against erosion rate shows a negative trend. (D) The average catchment slope with erosion rate does not have a trend but instead ranges from 15 to 20°. (E) The mean slope of each catchment compared with the erosion rates does not depict a trend but the overall relief (F) shows a very strong positive correlation.

Sample	Latitude	Longitude	Elevation (m)	Area Km^2	Quartz (g)	^{10}Be (atoms g-1 SiO2)	Standard erosion rate (mm yr-1)
CHU3	61.11233	145.81190	192	89	23.8	5773	1.32
CHU4	61.09993	145.86382	157	46	17.8	6023	1.25
CHU29	61.22705	145.73730	617	32	21.5	62527	0.13
CHU30	61.23606	145.74545	621	106	8.7	4294	1.94
CHU41	61.00291	149.49947	124	46	22.2	28267	0.17
CHU53	61.29461	148.97641	316	49	19.9	8710	0.94

***Erosion rate equation from Seong et al, 2009**

*** Average density for rock type average calculated by Barnes et al, 1966**

***^{10}Be Half Life, Attenuation Length, and Decay Constant from Gosse and Phillips, 2001**

Table 4.1: The results of the catchment-wide cosmogenic dating.

Sample	Elevation (m)	Latitude	Longitude	Rock type	Mass (mg)	mwar (μm)	He (pmol)	U (ppm)	Th (ppm)	Sm (ppm)	eU	Grains	F_T	Corr. Age (Ma)	Average Age (Ma)	Standard Deviation
12CH11	1127	61.23245	149.48279	meta. sand	0.0037	40.1	0.00152	8.2	19.8	177	13.7	3	0.708	25.8	**26.6**	6.5
					0.0041	39.3	0.00116	2.6	24.2	235	9.4	3	0.691	20.5	*n=3	
					0.0038	50.3	0.00206	5.1	16.7	110.4	9.6	2	0.743	33.4	**N=3	
12CH13	43	61.01744	149.73494	meta. sand	*0.0125*	*63.8*	*0.01396*	*4.5*	*13.5*	*140.8*	*8.4*	*2*	*0.81*	*50.5*	**33.0**	4.7
					0.008	58.7	0.00624	4.9	8.8	165.1	7.8	2	0.789	37.0	n=6	
					0.017	79.1	0.0079	4.2	6	116.5	6.1	2	0.839	34.5	N=8	
					0.0087	60.1	0.00256	3	10.7	97.1	6	2	0.799	23.9		
					0.0159	59.5	0.00643	4.1	6.9	104.9	6.3	4	0.778	34.7		
					0.0041	39.7	0.00441	5.5	14.8	218.3	10.1	3	0.68	35.0		
					0.0065	*41.2*	*0.00496*	*4.8*	*9*	*132.5*	*7.6*	*4*	*0.711*	*43.5*		
					0.0182	92	0.01399	6.5	5.1	116.2	8.2	1	0.851	33.0		
12CH17	61.04907	149.11095	963	meta. sand	0.0079	48.9	0.02944	24.3	157.6	381	14	2	0.785	14.0	**15.2**	2.7
					0.0088	*53.2*	*0.0236*	*25.3*	*154.4*	*420.2*	*23.2*	*2*	*0.792*	*23.2*	n=6	
					0.0107	57.3	0.02107	28.8	196.7	384.2	14.3	2	0.814	14.3	N=7	
					0.0119	60.9	0.01692	23.4	111.3	395.2	11.2	2	0.826	11.2		
					0.0058	40.7	0.00502	29	131.9	455.3	16.8	3	0.739	16.8		
					0.019	71.6	0.09256	21.9	181.1	357.3	18.2	2	0.849	18.2		
					0.0319	101.2	0.09807	25.1	130	435	16.4	1	0.895	16.4		

meta.=metamorphic rock
sand=sandstone
mwar = mass-weighted average radius
FT=alpha ejected correction factor
eU= U+(0.235*Th), effective uranium concentration
Standard deviation of ages used for average are as Ma and percent.

Ages in italics are excluded from averages (see text for explanation).
Latitude and Longitude datum is WGS84 and vertical datum is EGM96.
*** "n" = number of replicates used in age**

**** "N" = total number of aliquots run for age**

Table 4.2: The results of the AHe work in the Chugach Mountains.